4. SITE 921[1]

Shipboard Scientific Party[2]

HOLE 921A

Date occupied: 20 December 1993

Date departed: 21 December 1993

Time on hole: 1 day, 02 hr, 55 min

Position: 23°32.460′N, 45°1.866′W

Bottom felt (drill-pipe measurement from rig floor, m): 2488.0

Distance between rig floor and sea level (m): 10.50

Water depth (drill-pipe measurement from sea level, m): 2477.5

Total depth (from rig floor, m): 2505.10

Penetration (m): 17.10

Number of cores (including cores having no recovery): 2

Total length of cored section (m): 17.10

Total core recovered (m): 3.10

Core recovery (%): 18

Oldest sediment cored:
Depth (mbsf): 1.65
Nature: Foraminiferal ooze, igneous lithic breccia, and shell debris

Hard rock:
Depth (mbsf): 17.10
Nature: Gabbro, olivine gabbro
Measured velocity (km/s): 5.00

HOLE 921B

Date occupied: 21 December 1993

Date departed: 22 December 1993

Time on hole: 1 day, 08 hr, 40 min

Position: 23°32.478′N, 45°1.842′W

Bottom felt (drill-pipe measurement from rig floor, m): 2490.0

Distance between rig floor and sea level (m): 10.50

Water depth (drill-pipe measurement from sea level, m): 2479.5

Total depth (from rig floor, m): 2534.10

Penetration (m): 44.10

Number of cores (including cores having no recovery): 4

Total length of cored section (m): 44.10

Total core recovered (m): 10.19

Core recovery (%): 29

Oldest sediment cored: None

Hard rock:
Depth (mbsf): 44.10
Nature: Gabbro, olivine gabbro, gneissic gabbro, diabase
Measured velocity (km/s): 5.29–6.52

HOLE 921C

Date occupied: 22 December 1993

Date departed: 24 December 1993

Time on hole: 1 day, 17 hr, 55 min

Position: 23°32.472′N, 45°1.830′W

Bottom felt (drill-pipe measurement from rig floor, m): 2495.0

Distance between rig floor and sea level (m): 11.00

Water depth (drill-pipe measurement from sea level, m): 2484.0

Total depth (from rig floor, m): 2548.40

Penetration (m): 53.40

Number of cores (including cores having no recovery): 7

Total length of cored section (m): 53.40

Total core recovered (m): 6.09

Core recovery (%): 11

Oldest sediment cored: None

Hard rock:
Depth (mbsf): 53.40
Nature: Gabbro, olivine gabbro, diabase, trondhjemite
Measured velocity (km/s): 5.04–5.55

HOLE 921D

Date occupied: 24 December 1993

Date departed: 26 December 1993

Time on hole: 2 days, 0 hr, 45 min

Position: 23°32.442′N, 45°1.830′W

Bottom felt (drill-pipe measurement from rig floor, m): 2514.0

Distance between rig floor and sea level (m): 11.00

Water depth (drill-pipe measurement from sea level, m): 2503.0

Total depth (from rig floor, m): 2562.60

Penetration (m): 48.60

Number of cores (including cores having no recovery): 5

Total length of cored section (m): 48.60

Total core recovered (m): 6.16

Core recovery (%): 12

Oldest sediment cored:

Depth (mbsf): 1.58
Nature: Foraminiferal ooze, shell debris, siliciclastic sand, polygenic gravel

[1] Cannat, M., Karson, J.A., Miller, D.J., et al., 1995. *Proc. ODP, Init. Repts.,* 153: College Station, TX (Ocean Drilling Program).
[2] Shipboard Scientific Party is given in the list of participants preceding the contents.

Hard rock:
Depth (mbsf): 48.60
Nature: Gabbro, olivine gabbro, gabbronorite, diabase
Measured velocity (km/s): 5.07–6.01

HOLE 921E

Date occupied: 26 December 1993

Date departed: 29 December 1993

Time on hole: 3 days, 04 hr, 45 min

Position: 23°32.328′N, 45°1.878′W

Bottom felt (drill-pipe measurement from rig floor, m): 2456.0

Distance between rig floor and sea level (m): 11.10

Water depth (drill-pipe measurement from sea level, m): 2444.9

Total depth (from rig floor, m): 2538.60

Penetration (m): 82.60

Number of cores (including cores having no recovery): 9

Total length of cored section (m): 82.60

Total core recovered (m): 17.65

Core recovery (%): 21

Oldest sediment cored: None

Hard rock:
Depth (mbsf): 82.60
Nature: Olivine gabbro, gabbro, trondhjemite
Measured velocity (km/s): 5.25–6.33

Principal results: Site 921 (proposed Site MK-1) is located at approximately 23°32.40′N, 45°01.85′W, on the western median valley wall of the Mid-Atlantic Ridge about 10 km south of the Kane Transform (Fig. 4, "Introduction," this volume). During the first of a series of VIT surveys at this site, extensive outcrops of massive to tabular gabbroic rocks, studied in previous *Alvin* and *Nautile* dives, were observed. Several extensive outcrop surfaces sloping approximately 10° to 20° were mapped. These appear to be dip-slopes on prominent fault or foliation surfaces that are widely developed in the gabbroic rocks. These areas have sediment thicknesses ranging from nearly 0 to about 1 m and no visible rubble. They appeared to offer promising locations for deploying a hard-rock guide base (HRGB). The outcrops are separated by sediment covered terraces with somewhat thicker accumulations of pelagic ooze and sedimented talus ramps.

Four pilot holes (Holes 921A, 921B, 921C, and 921D) were spudded within 50 m of the marker beacon. These four holes penetrated 17.1 to 53.4 mbsf into gabbroic basement rocks, with a cumulative core recovery between 11.4% and 29.0%. Drilling at each one of these holes was impeded by high and erratic torque, suggesting irregular borehole walls. Rubble near Hole 921A may have caved-in and adversely affected drilling. An interval of rapid penetration, low recovery, and abundant open fractures in the cored material is interpreted as a cataclastic fault zone. This interval was encountered at about the same depth (2514–2533 mbsl) in Holes 921B, 921C, and 921D, indicating that the top of this interval is subhorizontal. Each of the three holes that penetrated it was abandoned due to increasing torque and decreasing core recovery before reaching the bottom of the interval.

A fifth pilot hole (Hole 921E) was spudded approximately 200 m to the south of the marker beacon, on a sparsely sedimented bench surrounded by steep outcrops of massive gabbroic rock displaying gently dipping joints and fault surfaces. This hole did not encounter the inferred fault interval drilled at Holes 921B, 921C, and 921D, but was drilled with similarly high levels of torque. Increasing pump pressures with depth of penetration and overpull indicated generally unstable borehole walls. Due to these unfavorable drilling conditions, Hole 921E was abandoned after penetrating 82.6 mbsf into a diverse suite of gabbroic rocks with a cumulative recovery of 21.4%.

A total of 43 m of gabbroic rocks were recovered from the 246 m cored at Holes 921A, 921B, 921C, 921D, and 921E, with a cumulative recovery of 17.6%. The gabbroic rocks display large variations in composition, grain size, texture, degree of deformation, and extent of alteration. The textural variations, commonly occurring over length scales of a few centimeters to tens of centimeters, suggest crystallization in an environment characterized by high thermal gradients and syn- to post-magmatic deformation. Generally, the rocks include meter-scale layers of gabbro and olivine gabbro, with lesser troctolite and iron-titanium oxide gabbro. These rocks are cut by millimeter to decimeter sized veins of highly altered leucogabbro, quartz diorite, and trondhjemite, that represent products of more extensive melt fractionation. Meter-scale diabase dikes with chilled margins were also encountered.

Alteration of the igneous mineralogy is generally low and non-uniform at the decimeter to meter scale. Variable development of alteration coronas around olivine consisting of chlorite, tremolite-actinolite, and talc is common. High-temperature minerals such as brown amphibole and talc are widely preserved. Minor actinolite and actinolite + chlorite veins are also widely developed.

Plagioclase in the gabbroic rocks has commonly experienced crystal-plastic deformation, resulting in a weak shape fabric defined by elongated mafic phases. In discrete, strongly foliated shear zones, plagioclase is highly strained and extensively recrystallized. Irregular stringers of iron-titanium oxide minerals occur in many of these shear zones. In some samples, limited dynamic recrystallization of plagioclase overprints an earlier shape preferred orientation produced by magmatic processes. Cataclastic domains occur in the upper sections of Holes 921B and 921C. These domains are typically a few centimeters to decimeters thick and have a subhorizontal orientation. They are likely to be associated with the east-dipping fault surfaces seen in the surrounding outcrops.

Gabbroic rocks cored at Site 921 have complex remanent magnetizations, including components of both normal and reverse polarity. This complex magnetization history may preclude restoration to geographic coordinates of structural features in the cores from paleomagnetic constraints. Reverse polarities are dominant, suggesting an age of 0.78–0.9 Ma. This inference is consistent with the location of Site 921 on the median valley wall some 13 km west of the MAR axis and spreading rates deduced from regional magnetic anomaly studies (Purdy et al., 1979; Schouten et al., 1985; Schulz et al., 1988).

Despite the limited number of samples and the heterogeneous nature of the rock units in Holes 921A, 921B, 921C, 921D, and 921E, variations in physical properties appear to correlate, at least in a general way, with the units. Physical properties variations also locally occur within units, for example at the bottom of Unit 4 in Hole 921C. This is accounted for by a difference in alteration within that unit. Considering the entire data set, the relationships between V_p and porosity and between V_p and density are apparently not systematic, possibly due to compositional variations in, for example, iron to magnesium ratios. Resistivity and porosity measurements appear to show a moderate correlation.

OPERATIONS

Site 920 to Site 921 (MK-1) Transit

The 13.6 mile transit to Site 921 (MK-1) was made in dynamic positioning (DP) mode while the drill string was being retrieved from Hole 920D. A positioning beacon was deployed from the *JOIDES Resolution* at 0620 hr, 20 December, initiating Site 921. A 16 hr seafloor survey was performed to locate level terrain for coring operations. A back-up positioning beacon was deployed from the VIT frame at 2235 hr, 20 December.

Hole 921A

A rotary coring barrel bottom-hole assembly (RCB BHA) was constructed and lowered to the seafloor and Hole 921A was spudded at 0200 hr, 21 December. Water depth was determined by drill-pipe measurement to be 2488 mbrf (2477 mbsl). Two cores were cut to a depth of 2505.1 mbrf (17.1 mbsf) recovering 3.1 m (Table 1). Constant hole fill and high erratic torque caused the hole to be abandoned at 0900 hr, 21 December, when the bit was pulled clear of the seafloor.

Table 1. Coring summary, Holes 921A–E.

Core	Date (Dec. 1993)	Time (UTC)	Depth (mbsf)	Cored (m)	Recovered (m)	Recovery (%)
153-921A-						
1R	21	0720	0.0–7.7	7.7	1.65	21.4
2R	21	1220	7.7–17.1	9.4	1.45	15.4
Coring totals				17.1	3.10	18.1
153-921B-						
1W	21	2040	0.0–14.6	14.6	1.63	
2R	22	0340	14.6–24.5	9.9	2.25	22.7
3R	22	1135	24.5–34.1	9.6	2.01	20.9
4R	22	2045	34.1–44.1	10.0	4.30	43.0
Coring totals				29.5	8.56	29.0
Washing totals				14.6	1.63	
Combined totals				44.1	10.19	
153-921C-						
1R	23	0545	0.0–10.0	10.0	0.31	3.1
2R	23	1045	10.0–19.6	9.6	2.77	28.8
3R	23	1945	19.6–29.3	9.7	3.01	31.0
4R	24	0135	29.3–38.9	9.6	0.00	0.0
5R	24	0450	38.9–43.9	5.0	0.00	0.0
6R	24	0925	43.9–48.5	4.6	0.00	0.0
7R	24	1410	48.5–53.4	4.9	0.00	0.0
Coring totals				53.4	6.09	11.4
153-921D-						
1R	25	1955	0.0–9.8	9.8	1.58	16.1
2R	26	0305	9.8–19.5	9.7	0.95	9.8
3R	26	0610	19.5–29.3	9.8	0.84	8.6
4R	26	0930	29.3–38.9	9.6	0.61	6.4
5R	26	1500	38.9–48.6	9.7	2.18	22.5
Coring totals				48.6	6.16	12.7
153-921E-						
1R	27	2115	0.0–9.9	9.9	0.35	3.5
2R	28	0415	9.9–19.8	9.9	2.01	20.3
3R	28	0740	19.8–29.7	9.9	1.33	13.4
4R	28	1335	29.7–39.6	9.9	1.50	15.1
5R	28	1830	39.6–49.5	9.9	2.91	29.4
6R	29	0115	49.5–59.4	9.9	2.01	20.3
7R	29	0655	59.4–69.0	9.6	5.14	53.5
8R	29	1055	69.0–78.6	9.6	1.68	17.5
9R	29	1440	78.6–82.6	4.0	0.72	18.0
Coring totals				82.6	17.65	21.4

Hole 921B

The vessel was offset 30 m southeast of Hole 921A where Hole 921B was spudded at 0915 hr, 21 December. Drill-pipe measurement indicated the water depth to be 2490 mbrf (2479 mbsl). While coring Hole 921A an apparent fault zone was penetrated at 2514.5 mbrf (24.5 mbsf). The penetration rate doubled through the fault zone. Although high erratic torque and hole fill were constantly present, both increased in the fault zone.

Hole 921B was cored four times to a depth of 2534.1 mbrf (44.1 mbsf) recovering 8.56 m. High erratic torque with hole fill eventually caused the hole to be abandoned. The bit was pulled clear of the seafloor at 1755 hr, 22 December, ending Hole 921B.

Hole 921C

The VIT was lowered to survey the immediate area around Hole 921B. The vessel was then offset 15 m southeast of Hole 921B and Hole 921C was spudded at 2235 hr, 22 December. The seafloor depth was determined by drill-pipe measurement to be 2495 mbrf (2484 mbsl).

The first 6 m of Hole 921C cored at the rate of 3.5 m/hr. The penetration rate then dropped to less than 2 m/hr to a depth of 2534 m (39 mbsf) where a drilling break occurred. The penetration rate increased to 3.6 m/hr and the hole began to take fluid as evidenced by low fluid levels in the drill string. High erratic torque and hole fill were observed to TD at 2548.4 mbrf (53.4 mbsf).

Hole 921C ended when the bit was pulled clear of the seafloor at 1150 hr, 24 December. Hole 921C was cored seven times penetrating 53.4 mbsf of fractured gabbroic material; 6.09 m of core were recovered for an 11.4% recovery rate.

Hole 921D

The BHA was round-tripped for a bit change. Once the BHA was back on bottom the VIT was deployed for a seafloor survey. After a 9 hr TV seafloor survey Hole 921D was spudded at 0900 hr, 25 December, approximately 48 m east of Hole 921C. Drill-pipe measurement indicated the water depth to be 2514 mbrf (2503 mbsl).

Hole 921D cored similarly to Hole 921C. The same apparent fault zone was encountered at 2534 mbrf (29.3 mbsf). As in Hole 921C the penetration rate doubled, fluid was lost to the formation and high erratic torque with hole fill was encountered.

After cutting five RCB cores to a depth 2562.6 mbrf (48.6 mbsf) and recovering 6.16 m of core for a recovery rate of 12.7%, the decision was made to abandon the hole. Hole 921D ended at 1235 hr, 26 December, when the bit was pulled clear of the seafloor.

Hole 921E

The VIT was deployed once again for a seafloor survey. After 20 hr of surveying, the bit was placed in a small sediment pond on top of what appeared to be a large outcrop. The VIT was recovered and Hole 921E was spudded at 1201 hr 27 December. Hole 921E is located approximately 200 m southwest of Hole 921D. The water depth was determined by drill-pipe measurement to be 2456 mbrf (2444.9 mbsl).

The entire hole was cored with high erratic torque. Pump pressures slowly increased throughout the hole occasionally dropping back to near normal levels. Frequent mud sweeps were used with only marginal success in reducing the pressure fluctuations and torquing.

The decision was made to abandon Hole 921E and move to another site. Hole 921E ended at 1827 hr, 29 December, as the bit cleared the seafloor. Nine cores were cut in Hole 921E to a depth of 2538.6 mbrf (82.6 mbsf) recovering 17.65 m.

Camera Surveys

Three VIT and sonar surveys were devoted to the exploration of extensive outcrops of gabbroic rocks in the area surrounding Site 921. This area (Fig. 4, "Introduction," this volume) was previously surveyed by *Alvin* dive 1014 (Karson and Dick, 1983) and *Nautile* dive KN 2 (Auzende et al., 1993) and selected as a potential location to drill gabbroic rocks using the HRGB.

The first VIT and sonar survey was started about 100 m northwest of a positioning beacon located at 23°32.35′N, 45°01.77′W (Beacon 1; Fig. 1). The survey continued for 6 hr, 30 min on 21 December, documenting outcrops at depths between 2420 and 2526 mbsl (estimated from drill-pipe measurements). The first leg of the survey traversed parallel to contours in a northerly direction, then upslope toward the west, then southward and along slope again, and finally back northward to return to the most promising outcrops observed. A back-up beacon was dropped to mark the location and a pilot hole (Hole 921A) was spudded.

Outcrops of slabby to massive rocks, inferred to be gabbroic on the basis of samples collected during submersible operations, were encountered repeatedly below 2480 mbsl. Above 2480 mbsl, outcrops are concealed under a nearly continuous blanket of sediment and rubble. Typically, the outcrops form dip-slope slabs interrupted by cliffs less than 10 m high protruding from the muddy gently east-dipping slope. Local seafloor topography associated with these outcrops was estimated to have a slope on the order of 15° to 20° (from repeated "tagging" of the bottom with the end of the drill pipe and estimates of the total drill-string length). More chaotic slopes are associated with talus, commonly comprising blocks a few meters in size.

A second VIT survey, which lasted 10 hr, 20 min, 25 December, was started after poor drilling conditions had led to the abandonment

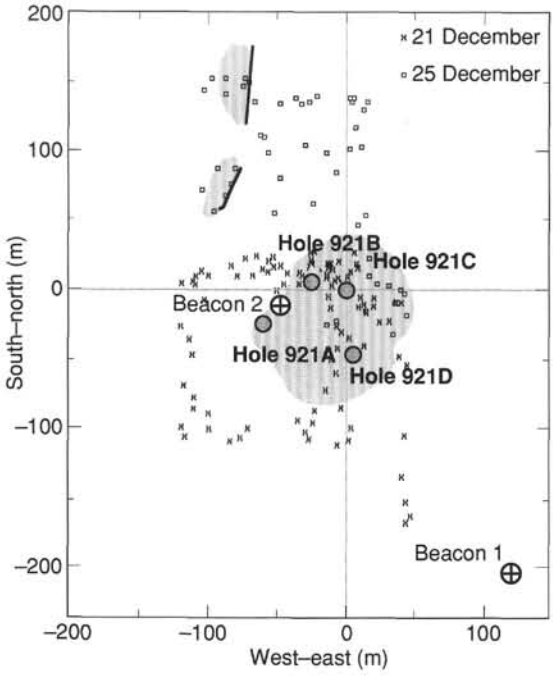

Figure 1. Map of camera survey for Holes 921A, 921B, 921C (23°32.474′N, 45°01.832′W), and 921D. Shaded areas mark outcrop. Thick lines represent inferred faults bounding these outcrops. Open boxes and x's are positioning points along survey track.

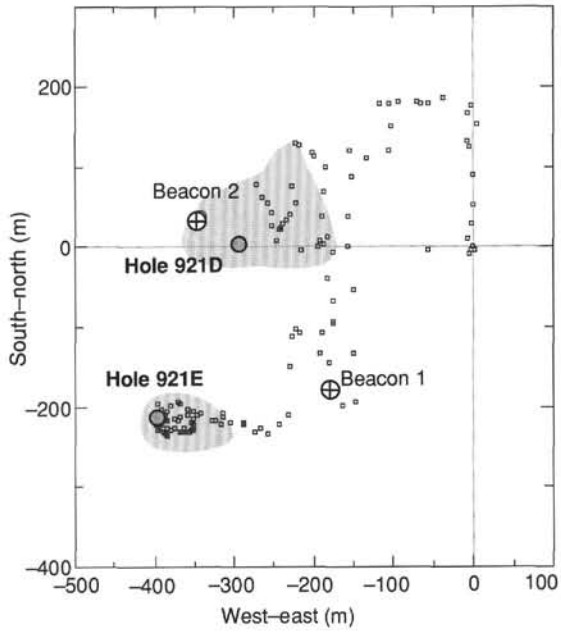

Figure 2. Map of survey area for Hole 921E (23°32.328′N, 45°1.878′W), 27 December. Shaded areas mark outcrop. Open boxes are positioning locations along survey track.

of Hole 921C. The purpose of this new survey was to search for potential locations for HRGB deployment at Site 921. This second survey was conducted predominantly north of the area surveyed 21 December, but in the same general depth interval (Fig. 1). This survey also extended the exploration of the dip-slope outcrops of gabbroic rocks south and east of Hole 921C (Fig. 1). The northern part of the survey area, below 2470 mbsl, was found to be heavily sedimented. By contrast, extensive (gabbroic?) outcrops were explored in the interval between 2470 and 2430 mbsl. These outcrops form a 20- to 30 m-wide north–south strip running almost continuously across the survey area. They are overlain to the west by pelagic ooze and rubble. Drill-string depth estimates along this relatively narrow strip of outcrop suggested that local slopes are somewhat steeper than in the southern survey area. Therefore, these northern outcrops were considered unsuitable for HRGB deployment, and the decision was made to drill another pilot hole (Hole 921D) on the same terrace as Holes 921A, 921B, and 921C (Fig. 1).

The third Site 921 VIT and sonar survey was conducted on 27 December, after Hole 921D had been abandoned. This survey lasted 20 hr and explored a substantially larger area and depth range than the first two surveys. It started at 2680 mbsl, about 300 m east of Hole 921D (Fig. 2) and initially proceeded parallel to contours to the north, then upslope to the west. In this part of the survey, only heavily sedimented slopes and talus deposits were observed. Outcrops of tabular gabbroic(?) rocks, protruding through the thin sediment blanket, were found only above 2560 mbsl. These outcrops were followed upslope to the west, then along slope to the south, over distances of 50 to 100 m in each direction. These outcrops are very similar in appearance to those drilled at Holes 921A, 921B, 921C, and 921D, suggesting that they belong to the same terrane. Slopes were estimated from drill-string lengths to be less than 25°. This area was not selected as a potential drill site because, based on proximity and similar outcrop appearances, much the same problematic drilling conditions as in Holes 921A, 921B, 921C, and 921D were anticipated. The survey continued south toward the first Site 921 beacon, then upslope toward the west (Fig. 2). The southward track was along slope at about 2550 mbsl, on a heavily sedimented area. Going upslope to the west, lightly sedimented talus was encountered, with blocks commonly a few meters to more than 10 m in size. The first outcrops were encountered above 2500 mbsl and form steep, chaotic cliffs commonly over 10 m high, facing east, south, or north. The exposed rocks have a relatively gently east-dipping schistosity, or joint set, similar to that of gabbroic outcrops explored in this same area during *Nautile* dive KN 2 (Auzende et al., 1993). A bench in these chaotic outcrops was encountered at 2460 mbsl. It is 20 to 30 m across, and bounded by straight cliff edges a few meters high, facing north and east. Locally, dip-slope slabs of schistose gabbroic rocks are exposed. Multiple depth estimates from total drill-string length on this small bench suggested that the local slope was within operational limits for the HRGB, and another pilot hole (Hole 921E; Fig. 2) was spudded.

LITHOLOGIC UNITS

Gabbroic rocks and variably deformed and metamorphosed rocks derived from them have been collected from the western median valley wall of the MAR in the 23°30′N region for decades (Table 1, "Introduction," this volume). Many of the samples were collected by dredging, which provides no constraints on the geologic setting of individual samples and is likely to preferentially sample talus accumulations. Samples collected from manned submersibles are typically taken directly from outcrops where the setting with respect to outcrop morphology is documented. In these studies, samples are commonly collected at intervals of tens to hundreds of meters along reconnaissance traverses. The maximum dimensions of samples is seldom greater than about 30 cm.

The range of compositions and textures of these rocks hints at major processes related to the accretion of plutonic material beneath the MAR axis and its modification by deformation and alteration. For example, cumulate textures preserved in igneous rocks suggest that magma bodies of substantial size have existed in this environment. Deformation along gently dipping shear zones and faults has produced material including gneissic metagabbros, mafic schists, mylonites, cataclasites, and fault breccias. Metamorphic recrystallization ranges from transitional granulite facies to sub-greenschist facies. These deformed and altered rocks are believed to reflect the progres-

sive unroofing and hydration of magmatic plutonic rocks attending mechanical extension of the axial lithosphere.

The rationale for drilling into the gabbroic rocks exposed in this environment is to sample relatively long, continuous sections of rock that can further constrain their origin by providing detailed information regarding the rock materials on the scale of centimeters to meters. Such samples provide the potential to investigate the details of magmatic evolution, to document the dimensions of magmatic bodies, and to reveal the nature of contacts between different igneous rock types. Substantial volumes of various rock types also permit a range of geochemical and petrological investigations. Likewise, structural and metamorphic studies involving textural and mineralogical changes that take place over centimeters to meters can be made.

This chapter reports on the first series of holes drilled into the gabbroic terrane of the western median valley wall of the MARK area during Leg 153. During drilling at Site 921, five holes were drilled to depths ranging from 17.1 to 82.6 m, average recovery ranging from 11% to 23% (Table 1; Fig. 3).

The drill holes intersected a heterogeneous package of gabbroic rocks plus minor diabase. A brief summary including the main lithologic variations and any contact relationships observed in each drill hole is presented below. The names of lithologic units presented in this discussion are highly generalized, and the range of compositions and textures found in each unit is discussed more fully in later sections of this chapter (see "Igneous Petrology," "Metamorphic Petrology," and "Structural Geology," this chapter). Lithologic units defined in Holes 921A, 921B, 921C, 921D, and 921E are composed entirely of one rock type, in general. Intervals of sediment and rubble at the top of Holes 921A, 921B, and 921C were not given unit status as they were considered to have been recovered from pelagic sediment and/or talus deposited on top of the gabbroic massif.

Hole 921A

Hole 921A drilled through a cover layer of sediment and altered gabbroic rubble into medium- to coarse-grained olivine gabbro and gabbro characterized by the presence of predominantly brown clinopyroxene, and igneous grain-size layering. The sediment layer was not designated as a unit because it is largely of biogenic rather than igneous origin, and the gabbroic rocks were designated as Unit 1.

Hole 921B

Hole 921B spudded into metagabbro (>50% altered) in which igneous textures are preserved, but within which most of the primary igneous mineralogy is altered (Unit 1). The gabbro is cut by numerous subhorizontal, anastomosing veins of relatively low-temperature minerals and thin cataclastic zones (millimeter to centimeter scale; Fig. 4).

The metagabbro is underlain by an interval of moderately altered, aphyric to sparsely-phyric, olivine-plagioclase diabase (Unit 2). The upper contact between the metagabbro and the diabase was recovered in two pieces. The grain size in the diabase decreases upwards toward the upper contact, but is truncated by one of the subhorizontal shear zones noted above. Below the next five pieces, which are all diabase, a second, irregular, 1-cm-thick chilled upper contact between diabase and gabbro occurs (Fig. 5). The attitude of this contact is unknown because the piece is not oriented, but more pieces of diabase continue below. These relationships suggest an irregular, intrusive contact between metagabbro and diabase that has been locally faulted.

The contact of diabase with the underlying gabbro and olivine gabbro (Unit 3) was not recovered. The principal lithology in this unit is lineated gabbro (Fig. 6), but it contains intervals of olivine gabbro that are probably primary magmatic layers, and irregular layers of highly deformed, oxide-mineral-rich gabbro. Grain-size layering of 1 to 10 cm is common. Clinopyroxene is medium- to coarse-grained and weakly to moderately recrystallized, with elongated grains defining a mineral lineation in more deformed intervals. Plagioclase and olivine are moderately to intensely dynamically recrystallized in these deformed zones.

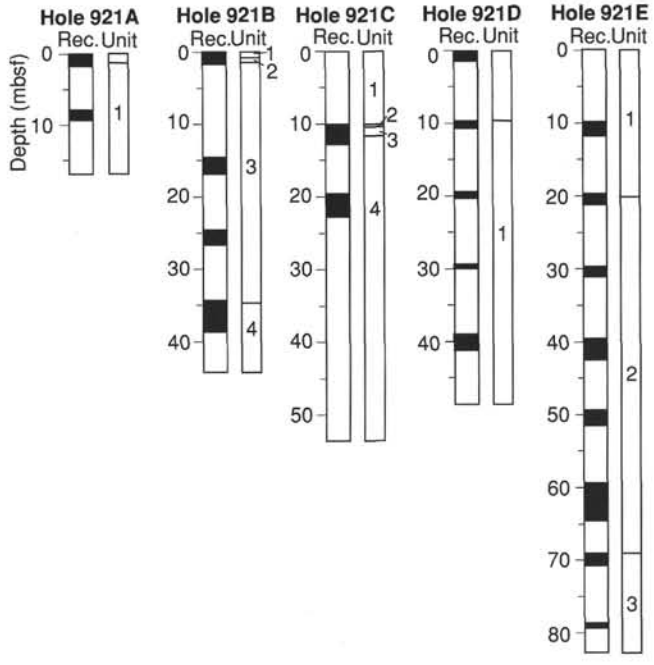

Figure 3. Core recovery columns and lithologic units for Site 921 holes. Black indicates core intervals recovered.

The lineated gabbro unit is underlain by poikilitic olivine gabbro (Unit 4) which is characterized by the presence of large oikocrysts of green clinopyroxene (Fig. 7). It continues to the end of the core (Table 2). The contact between Units 3 and 4 is preserved but sheared, and the original nature of the contact is uncertain.

Hole 921C

Hole 921C intersects four units in a similar sequence to that in Hole 921B, except that the interval of metagabbro/diabase/gabbro (Units 1–3 in both Holes 921B and 921C) is shorter in the latter (~11 m vs. 35 m; Table 2). In Hole 921C the base of this sequence, defined as the contact between lineated gabbro (Unit 3) and underlying poikilitic olivine gabbro (Unit 4), was intersected 10–20 m higher than in Hole 921B. The contact between these units was not preserved in Hole 921C, but was placed between a piece of lineated gabbro and undeformed oxide gabbro in Core 153-921C-2R.

The piece above the contact (Section 153-921C-2R-2) is moderately altered, but exhibits the weak lineation defined by elongated clinopyroxene grains that is typical of Unit 3. The piece below the contact (top of Unit 4) is medium- to coarse-grained, subophitic textured gabbro with a 1-cm-wide coarse-grained oxide gabbro along its upper surface. Pieces below the designated contact in this part of the core are essentially undeformed and contain increasing proportions of coarse green clinopyroxene as granular and oikocryst phases downsection.

Hole 921D

Hole 921D was drilled through a layer of biogenic sediment and gabbroic rubble before intersecting a heterogeneous package of gabbro and olivine gabbro that was all grouped as Unit 1. Gabbro recovered from the top of this hole is commonly, but not consistently, lineated. Rocks recovered from deeper in this hole exhibit less evidence of deformation and contain green poikilitic clinopyroxene.

Several factors contributed to the inability to accurately place any unit boundaries within this hole, despite the recognition that the upper

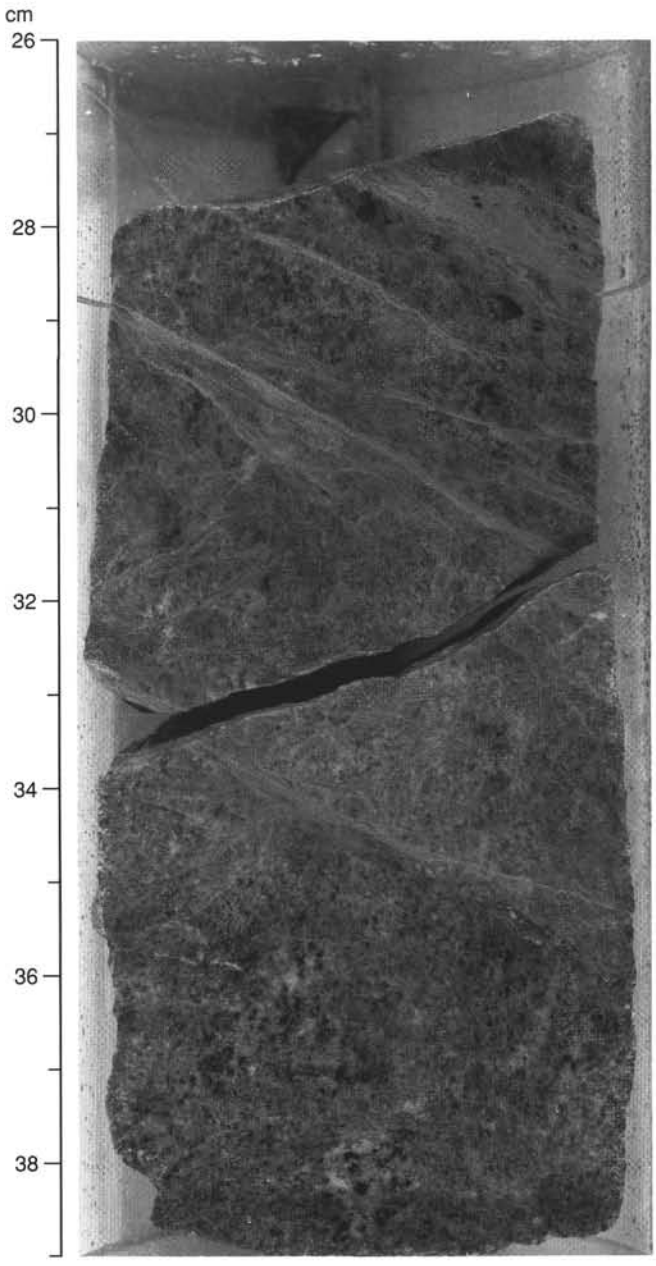

Figure 4. Close-up photograph of cataclastic metagabbro of Hole 921B (Unit 1). Sample 153-921B-1W-1, 26–39 cm. The brittle shear zones are pale green and dip moderately (10° to 25°).

part is dominantly gabbro and the lower part dominantly poikilitic olivine gabbro. Most significantly, the intensity of alteration is relatively high when compared with other holes. Recovery was also low (<15%).

Hole 921E

Hole 921E was spudded at a water depth 40–50 m shallower than Holes 921A, 921B, 921C, and 921D (Table 1). The hole intersected 20–30 m of very coarse-grained to pegmatitic gabbro (Unit 1; Fig. 8) characterized by a high proportion of clinopyroxene relative to plagioclase and weak to extensive recrystallization of the plagioclase.

The contact between the pegmatitic gabbro and the underlying heterogeneous poikilitic olivine gabbro (Unit 2) was defined as a ~2-cm-wide zone of sheared oxide gabbro that separates sheared

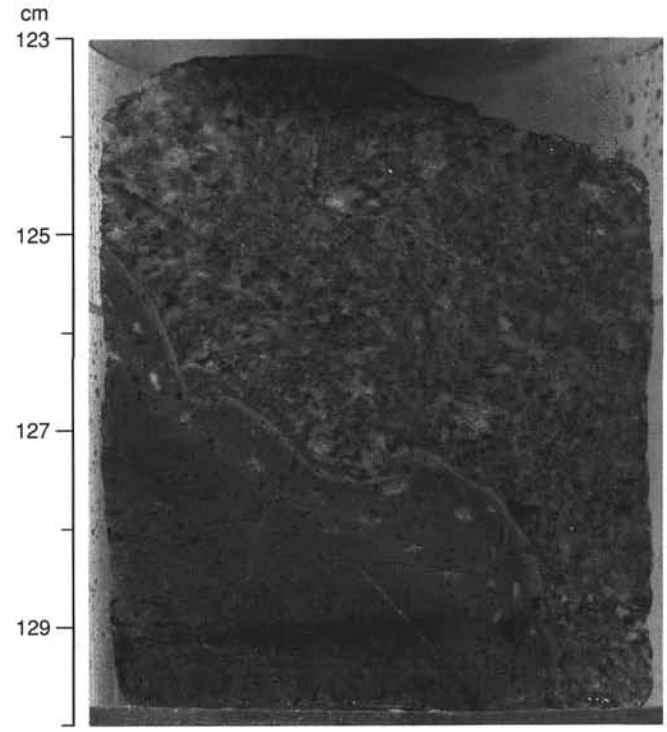

Figure 5. Close-up photograph of chilled margin against host gabbroic rocks in diabase of Hole 921B (Unit 2). Sample 153-921B-1W-1, 123–130 cm.

pegmatitic gabbro above from medium- to coarse-grained gabbro and olivine gabbro below.

The top of Unit 2 is predominantly equigranular and varies from piece to piece from gabbro to olivine gabbro, but it appears to grade into poikilitic olivine gabbro with increasing depth. The heterogeneous poikilitic olivine gabbro, in addition to having green poikilitic clinopyroxene, is conspicuous for its wide range in grain size, modal mineralogy, and texture.

The last two cores within this hole are defined as a separate unit (Unit 3) even though they contain an even wider range of rock types than Unit 2, including diorite, lineated gabbro, poikilitic gabbro, and a gabbroic breccia composed of angular blocks of very coarse-grained gabbro in a matrix of recrystallized plagioclase (Fig. 9). The rock types in these cores vary in composition on the scale of a few centimeters to decimeters, and it was not possible to further subdivide the unit or to establish any trend in composition within it.

Paleomagnetic data (see "Paleomagnetism," this chapter) demonstrate that Unit 2 and Unit 3 have different magnetic polarities. This distinction supports the definition of the last two cores as a separate unit. The polarity changes from reversed in Cores 153-921E-7R and above, to positive in Core 153-921E-9R. The boundary between these two magnetic domains could not be placed more accurately than within the top of Core 8R because of overprinting of polarity signals that could not be resolved aboard ship and the generally small piece size within this section.

IGNEOUS PETROLOGY

Igneous Rock Description

The holes drilled at Site 921 intersected a package of gabbroic rocks that are highly variable in their texture, modal composition, and mineralogy (Table 2). Gabbro or olivine gabbro dominate, but minor oxide gabbro, troctolite, trondhjemite, and diabase are also present. Igneous textures within the gabbroic rocks are dominantly cumulate and range from equigranular to highly inequigranular, the latter particularly developed in rock types that are poikilitic. Primary igneous

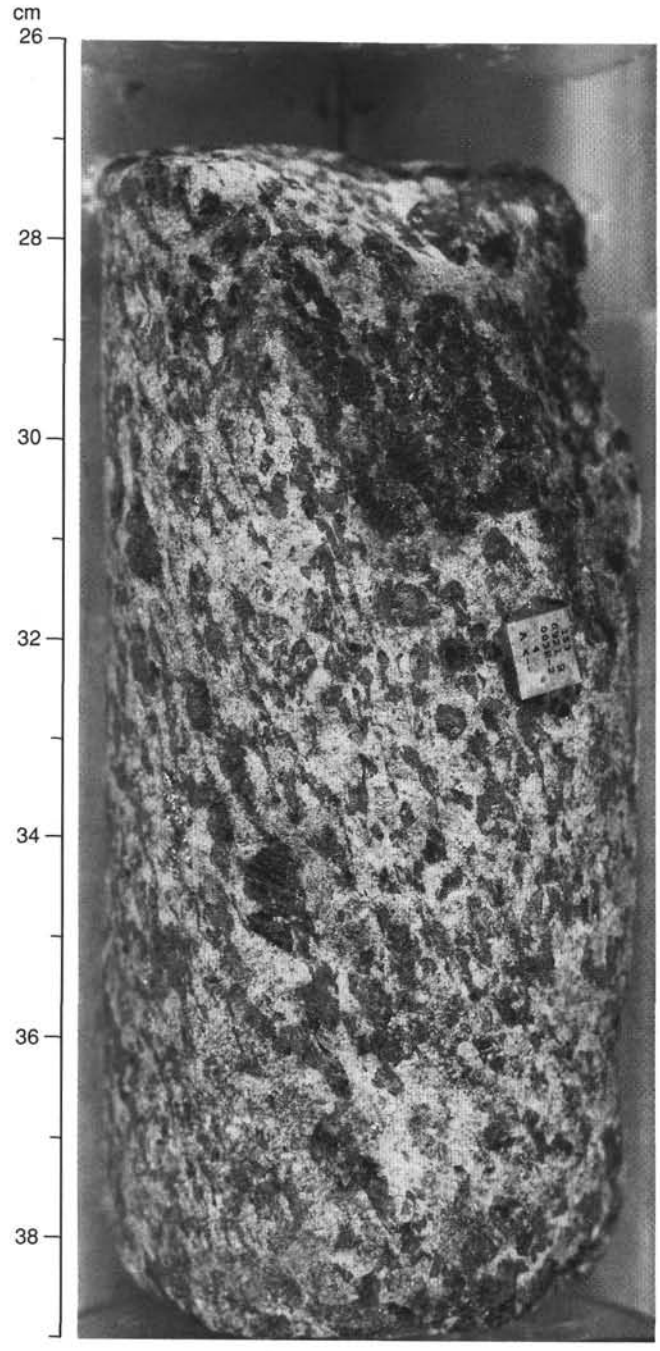

Figure 6. Close-up photograph of lineated gabbro of Hole 921B (Unit 3). Sample 153-921B-3R-2, 26–39 cm.

layering is commonly preserved as variations in the grain size and/or modal mineralogy of the gabbroic rocks. Heterogeneous crystal-plastic to cataclastic deformation has modified and obscured the magmatic textures in some places.

Lithologic Units

Lineated Gabbro

The lineated gabbroic rocks are variable in texture and modal mineralogy and consist of dominantly gabbro with lesser amounts of olivine gabbro and gabbronorite. They are characterized principally by their olivine-poor mineralogy, containing 0% to 10% olivine, and by common mesoscopic grain-size layering on the scale of one to

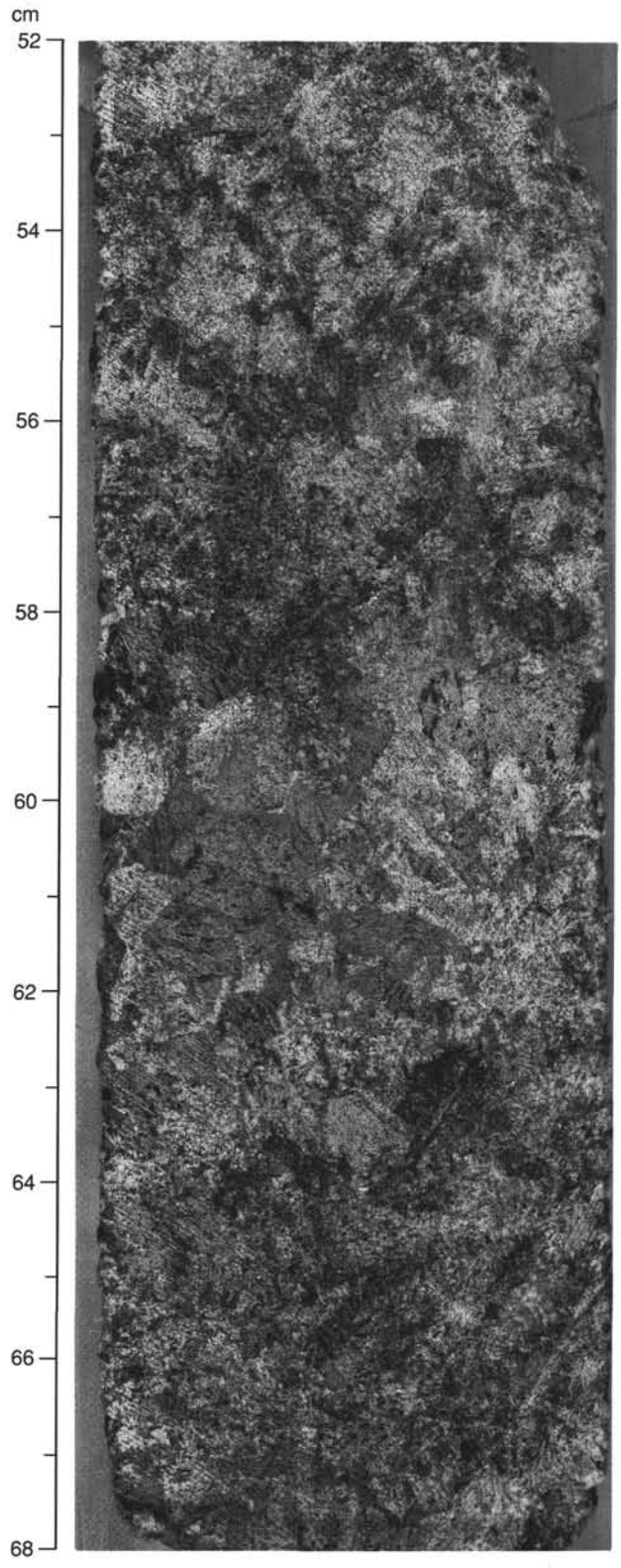

Figure 7. Close-up photograph of poikilitic olivine gabbro of Hole 921B (Unit 4). Sample 153-921B-4R-3, 52–68 cm. Lighter band between 58 and 62 cm contains large poikilitic clinopyroxene grains.

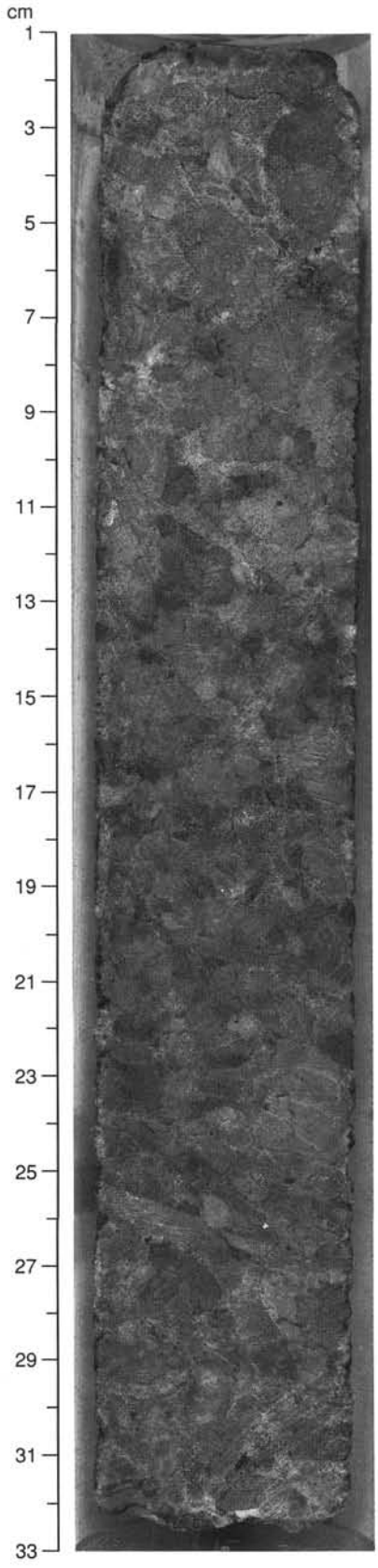

Figure 8. Close-up photograph of coarse-grained gabbro of Hole 921E (Unit 1). Sample 153-921E-2R-2, 1–33 cm.

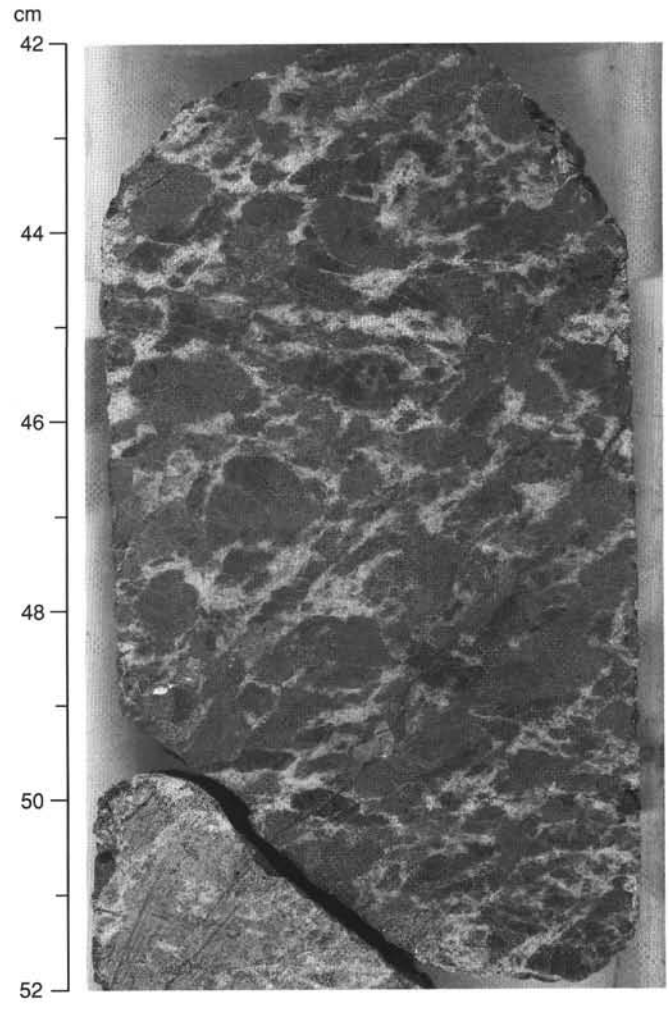

Figure 9. Close-up photograph of gabbroic rock with plagioclase-rich veins cutting angular clasts of coarse-grained clinopyroxene of Hole 921E (Unit 3). Sample 153-921E-8R-1, 42–52 cm. Note two intersecting shear zones. Outside the shear zones, the clinopyroxene grains have no obvious shape preferred orientation; however, thin sections show that the plagioclase-rich matrix consists of small, polygonal, twinned neoblasts, indicative of extensive recrystallization.

20 cm. They typically contain a variably developed lineation defined by the alignment of clinopyroxene mineral grains or aggregates.

Lineated gabbro is present to some degree within all of the gabbroic rock recovered from holes at Site 921, although the greatest proportion occurs in core from Holes 921A, 921B, and 921C, where units have been defined based on this rock type (Table 2). The mineralogy of the lineated gabbroic rocks is dominated by plagioclase (50% to 70%) and clinopyroxene (20% to 50%). Olivine is only rarely present in abundances greater than 8% to 10%. Clinopyroxene is brown or pinkish gray and characteristically is medium- to coarse-grained, but ranges from 1 to 20 mm. Orthopyroxene occurs as rims on clinopyroxene and olivine, typically associated with microscopic shear zones or fractures, or in gabbronorite as subhedral cumulus grains (up to 8%). The plagioclase grain size is rarely representative of the primary igneous grain size due to extensive dynamic recrystallization, but is medium-grained in samples where deformation is minimal. Undeformed examples of this rock type display an allotriomorphic to hypidiomorphic granular texture consisting of anhedral to subhedral clinopyroxene and plagioclase grains, plus anhedral interstitial olivine where present. Iron-titanium oxide and sulfide minerals are disseminated throughout the rocks as accessory phases.

Table 2. Summary of lithologic units Holes 921A–E.

Hole	Unit	Name	Cored interval From	Cored interval To	Curatorial depth to top of unit (mbsf)	Recovered (m)	Recovery (%)
921A		Sediment and rubble	1R-1 (1)	1R-1 (1)	0.00	1.28	20.00*
	1	Olivine gabbro	1R-1 (2)	2R-2 (3)	1.28	1.72	16.00
921B	1	Cataclastic metagabbro	1W-1 (1)	1W-1 (12)	0.00	0.84	11.00
	2	Aphyric to sparsely-phyric diabase	1W-1 (12)	1W-2 (2)	0.98	0.52	11.00*
	3	Lineated gabbro	1W-2 (3)	4R-1 (6)	1.56	4.97	23.00
	4	Poikilitic olivine gabbro	4R-1 (6)	4R-4 (3)	35.54	3.88	43.00
921C	1	Cataclastic metagabbro	1R-1 (1)	1R-1 (3)	0.00	0.31	3.10
	2	Aphyric to sparsely-phyric diabase	2R-1 (1)	2R-1 (4)	10.00	0.30	14.00*
	3	Lineated gabbro	2R-1 (5)	2R-2 (4)	10.34	1.10	14.00
	4	Poikilitic olivine gabbro	2R-2 (5)	3R-3 (5)	11.64	4.38	10.00
921D		Sediment and rubble	1R-1 (1)	1R-2 (1)	0.00	1.64	16.70
	1	Mixed gabbro/olivine gabbro	2R-1 (1)	5R-2 (7)	9.80	4.54	11.70
921E	1	Very coarse-grained to pegmatitic gabbro	1R-1 (1)	3R-1 (4)	0.00	2.60	12.00
	2	Heterogeneous poikilitic olivine gabbro	3R-1 (4)	7R-4 (7)	20.08	15.02	25.00
	3	Varitextured gabbro/olivine gabbro	8R-1 (1)	9R-1 (6)	69.00	2.45	18.00

Notes: Total depth (mbsf): Hole 921A = 17.1, Hole 921B = 44.1, Hole 921C = 53.4, Hole 921D = 48.6, Hole 921E = 82.6. Samples marked with an asterisk (*) indicate average for a core where a unit is a minor component of that core.

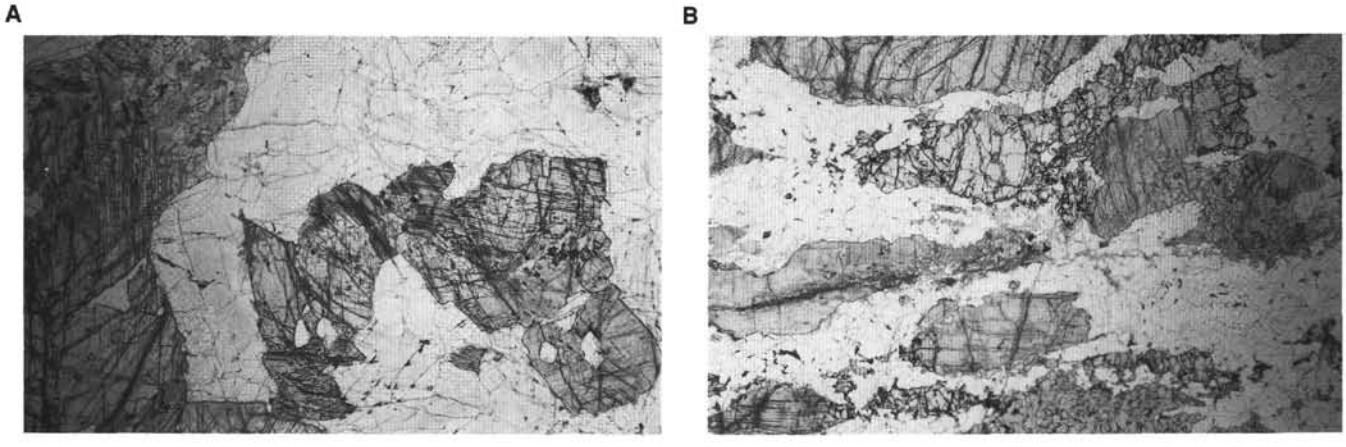

Figure 10. Photomicrographs showing igneous and deformed textures in gabbroic rocks from Holes 921B and 921D. **A.** Sample 153-921B-3R-1, 134–137 cm. Coarse-grained, inequigranular anhedral to subhedral clinopyroxene and subhedral plagioclase laths. Field length is 8 mm. **B.** Sample 153-921D-3R-2, 33–37 cm. Deformed olivine gabbro showing neoblasts of olivine and plagioclase and orientation of neoblasts and elongated porphyroclasts of olivine and clinopyroxene defining the crystal-plastic fabric. Clinopyroxene shows only minimal neoblasts.

In thin section, samples in which the primary magmatic textures are preserved contain euhedral to subhedral clinopyroxene that in some cases exhibits magmatic twins, and randomly oriented, anhedral to subhedral, interlocking plagioclase grains including minor neoblasts along grain boundaries (Fig. 10). Plagioclase compositions, estimated from optical determinations, are highly variable, ranging from An_{45} to An_{80}. Pericline, albite, and carlsbad twinning of plagioclase is preserved in many grains, although most samples show signs of at least mild deformation such as mechanical twins and undulose extinction in plagioclase. Brown amphibole is common as fine rims and blebs around clinopyroxene grains. Iron-titanium oxide mineral grains are very small (<0.1 mm) and are typically concentrated at triple-junction boundaries.

Clinopyroxene typically displays two types of orthopyroxene exsolution. The first type is abundant fine (<0.01 mm) exsolution lamellae resulting in a finely striped appearance in thin section. The second type occurs as blebs. Smaller clinopyroxene patches enclosed or intergrown at grain boundaries also tend to crystallize along zones parallel to the cleavage of larger clinopyroxene grains at the interface between the grains. But they are not in optical continuity with the host grain. These intergrowths typically contain 0.05–0.1 mm blebs of secondary phases, commonly hornblende.

Despite the intensity of the deformation fabric (see "Structural Geology," this chapter), primary grain-size layering is commonly preserved. Modal layering, where present, is subtle and tends to be masked by the intensity of the grain-size layering. Layering is principally defined by the variation in size of clinopyroxene grains as these typically have undergone the least dynamic recrystallization. Layer boundaries are generally diffuse and commonly gradational over 1 to 10 cm (Fig. 11). The grain size varies from fine- to coarse-grained (Fig. 12).

Pegmatitic Gabbro

A distinctive, very coarse-grained to pegmatitic gabbro was recovered in Hole 921E. The gabbro is pink-gray and is composed predominantly of cumulus plagioclase and clinopyroxene with interstitial olivine, and iron oxide and sulfide minerals (Fig. 8). The pegmatitic gabbro is characteristically homogeneous, averaging 50% plagioclase, 46% clinopyroxene, 3% olivine, and <1% iron oxide and

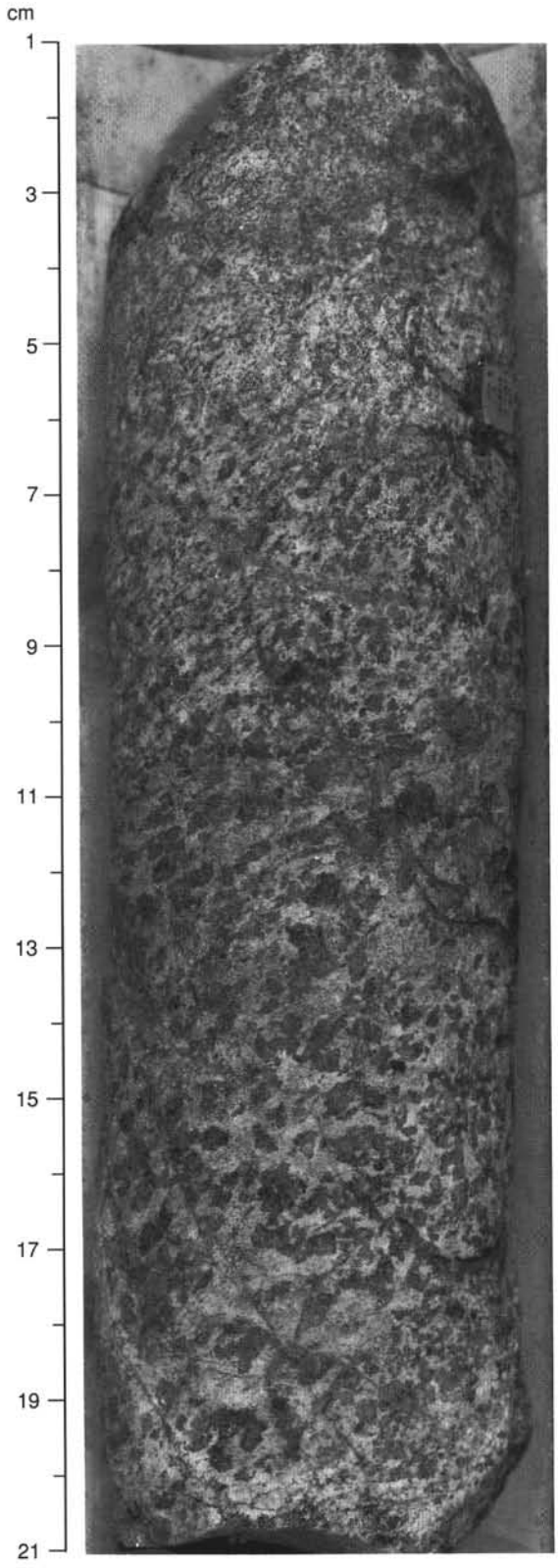

Figure 11. Lineated gabbro (Unit 3), Sample 153-921B-2R-2, 1–21 cm. The specimen is grain-size layered from medium-grained at the top to coarse-grained at the bottom of the piece. The layering dips approximately 45°. The crystal-plastic lineation is moderately developed, particularly in the finer grained layers, and slightly oblique to the layering (steeper in the core). The piece is cut by numerous chlorite-lined fractures.

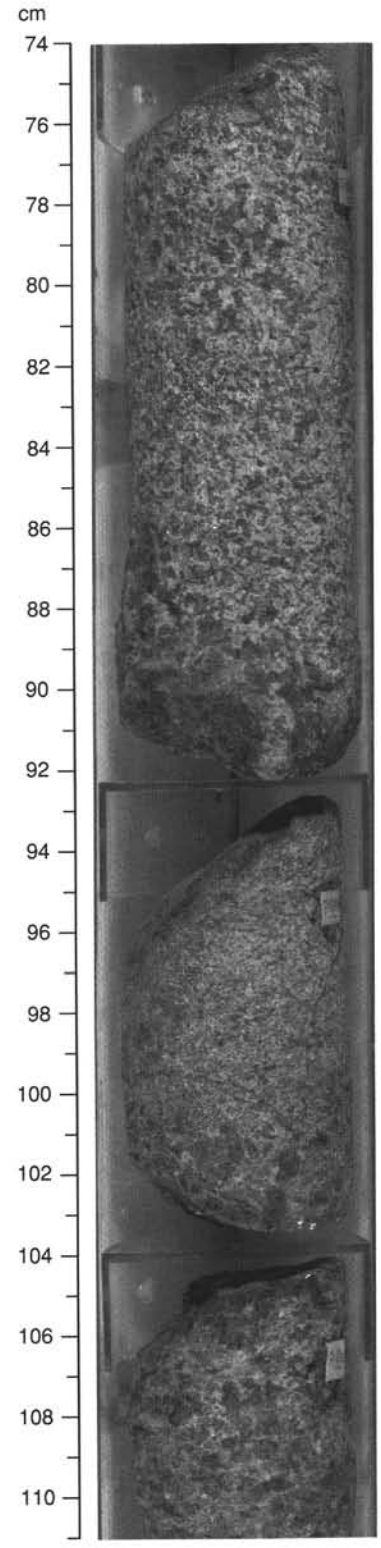

Figure 12. Subhorizontal grain-size layering in lineated gabbro, Sample 153-921B-2R-1, 74–111 cm. The grain size varies within the upper piece from coarse- to medium- and back to coarse-grained (from top to bottom). The center piece is medium-grained with a coarse-grained base, and the piece at the bottom is coarse-grained. The crystal-plastic lineation is poorly developed in this interval.

sulfide minerals, despite a broad range of modal proportions estimated from both hand-sample and thin-section descriptions (14% to 65% plagioclase, 32% to 85% clinopyroxene, and 1% to 10% olivine). This discrepancy is believed to be due to difficulties in estimating proportions because of the large grain size (to 55 mm for clinopyroxene) relative to the size of core pieces and thin sections.

Plagioclase occurs as equant grains to subhedral or euhedral laths up to 28 mm, with an average grain size of 15 mm. Optical determinations of compositions from thin section range from An_{55} to An_{70}. Clinopyroxene is typically irregular in shape, often appearing angular, with a weak, subophitic texture enclosing smaller (1 to 2 mm) euhedral plagioclase laths. Despite this, clinopyroxene typically retains its large, blocky habit indicating its primocryst origin. Cores of large clinopyroxene grains are paler brown than the rims, suggesting that the mineral is compositionally zoned.

Olivine is anhedral and ranges in shape from irregular to elongate, lobate interstitial grains. Orthopyroxene is observed in minor amounts in thin section, but invariably it occurs as smaller grains marginal to olivine or clinopyroxene grains. Iron oxide and sulfide minerals occur disseminated in minor amounts (<1%) throughout the pegmatitic gabbro. Brown hornblende is a common accessory phase occurring as blebs and rims on mafic phases (<2%), usually clinopyroxene.

The igneous texture is weakly overprinted by a crystal-plastic deformation expressed as a shape fabric defined by the alignment of large elongated clinopyroxene crystals. In thin section, plagioclase is intensely recrystallized and displays undulose extinction and deformation twins. Olivine is recrystallized and kink banded, and clinopyroxene crystals are locally bent and exhibit undulose extinction. Where plagioclase is partially recrystallized, porphyroclastic textures are typically developed in which thin, white bands of recrystallized plagioclase separate larger dark-brown angular clinopyroxene grains.

Poikilitic Olivine Gabbro

The poikilitic olivine gabbro is grayish white to dark gray and exhibits a range of textural patterns from spotted to layered that correspond with variations in modal mineralogy. Olivine typically occurs as dark, anhedral, interstitial patches between plagioclase grains, and more rarely as dark oikocrysts up to 15 mm in size.

Plagioclase in the poikilitic olivine gabbro is clear to white and varies in texture from equigranular to subhedral laths that are subophitically, and rarely ophitically, enclosed by either olivine or clinopyroxene, the latter being more common. In most examples, it also retains a magmatic crystal habit. Plagioclase shape preferred orientations range from random to well defined preferred alignment. The magmatic alignment is seen only in localized parts of the core. These zones of plagioclase alignment are relatively small, and the alignment is poorly expressed at the hand-sample scale (Fig. 13). Optical determinations of plagioclase compositions from thin section show the poikilitic olivine gabbro to contain a wide range in plagioclase composition from An_{40} to An_{80}. The poikilitic olivine gabbro rocks are the only rocks apart from veins that are observed to display zoning in plagioclase, although it is only very weakly developed.

Clinopyroxene occurs both as a cumulus and an intercumulus phase, commonly within the same sample. The most prominent habit is as coarse-grained, bright green oikocrysts that are often rimmed by thin, brown clinopyroxene. Less commonly, clinopyroxene forms anhedral, pale brown, interstitial grains within the matrix of olivine gabbro. In thin section, cumulus clinopyroxene is observed to share crystal faces with plagioclase, but invariably the grains become interstitial in their texture and weakly poikilitic at their extremities (Fig. 14). Green clinopyroxene is an interstitial phase in more even-textured parts of the core and, in these rocks, oikocrysts are absent or poorly developed.

Olivine is generally an intercumulus phase, forming dark patches or finely disseminated grains throughout the rocks. Nonetheless, it occurs both as poikilitic grains and as dendritic crystals that in thin

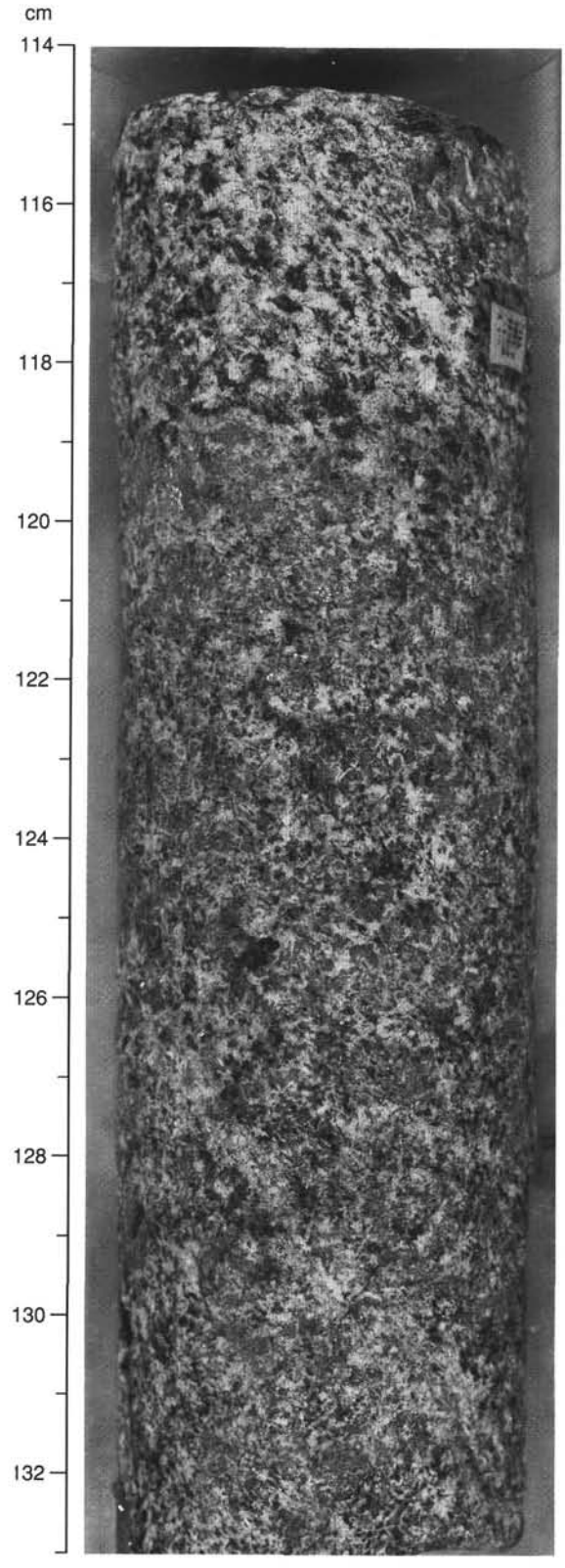

Figure 13. Sample 153-921E-7R-2, 114–133 cm, showing heterogeneous poikilitic olivine gabbro with elongate patches of brown clinopyroxene (gray) parallel to the faint magmatic alignment of plagioclase (30° to 40° dip). Olivine in the troctolite layer is poikilitic (117–120). Equant grains of green clinopyroxene also occur in this sample (122–126).

Figure 14. Sample 153-921E-7R-3, 99–104 cm. Magmatic alignment of plagioclase grains in poikilitic olivine gabbro. Field length is 8 mm.

section are optically continuous on the scale of 2 to 3 cm and represent possible crescumulate crystal growth.

The wide range in textures is reflected in the modal and grain-size heterogeneity of these rocks. Plagioclase is typically the most abundant phase, ranging from 45% to 70%, but most commonly between 55% and 65%. Clinopyroxene and olivine abundance tends to vary inversely, with clinopyroxene ranging from 0% to 45% and olivine from 2% to 35%. Opaque iron oxide minerals are typically present as rare, anhedral, interstitial grains. Modal estimates at the scale of the piece thus classify these rocks as gabbro and olivine gabbro. Variations in the grain size of the primary phases is equally extreme, with plagioclase ranging from 6 to 20 mm, clinopyroxene from 2 to 10 mm for matrix grains and up to 40 mm for oikocrysts, and olivine from 1 to 10 mm with oikocrysts rarely up to 25 mm in size.

Primary magmatic layering is defined by changes in grain size and modal mineralogy on the scale of 1 to 20 cm (Figs. 15, 16, and 17). The variations occur as layers and patches that have margins ranging from relatively sharp to diffuse, and it is in some of these layers that the best examples of plagioclase alignment are observed. Some patches provide evidence for rapid nucleation and crystallization having occurred in the form of elongate, radiating plagioclase crystals with pointed terminations and, sometimes, thin cores of clinopyroxene (harrisitic texture?).

Poikilitic textures are best developed within the layered zones where they are often associated with elongate patches up to 1-cm-thick of cumulus to interstitial brown clinopyroxene (Fig. 13). This produces a fine compositional layering expressed as interlayered troctolite to olivine gabbro and olivine gabbro on the scale of 1 to 5 cm that is overgrown by equant to lath-like oikocrysts of bright green clinopyroxene reaching maximum sizes of 45 mm. The oikocrysts are typically rimmed by thin (~1 mm) dark brown, pyroxene overgrowths.

A pegmatitic, clinopyroxene-rich gabbro layer ~40 mm thick is present in Hole 921C (Fig. 16). The layer consists of brown clinopyroxene with dimensions up to 35 mm in length. Commonly pyroxenes have greenish cores, are ~10 mm wide, with brown rims that can reach ~25 mm in width. Plagioclase is interstitial to subophitically enclosed by clinopyroxene that is similar in color to that in the enclosing olivine gabbro. The layer differs from the host rock, however, in not containing olivine.

Oxide Gabbro

Iron-titanium oxide-rich gabbro, as distinct from the gabbroic rocks containing trace amounts of disseminated iron oxide minerals, is present in Holes 921A, 921B, 921D, and 921E (Table 3). The occurrences are conspicuous for their restricted size and relative volume, rarely exceeding a few centimeters in thickness. Two main types of occurrences are present, the first as above average proportions of

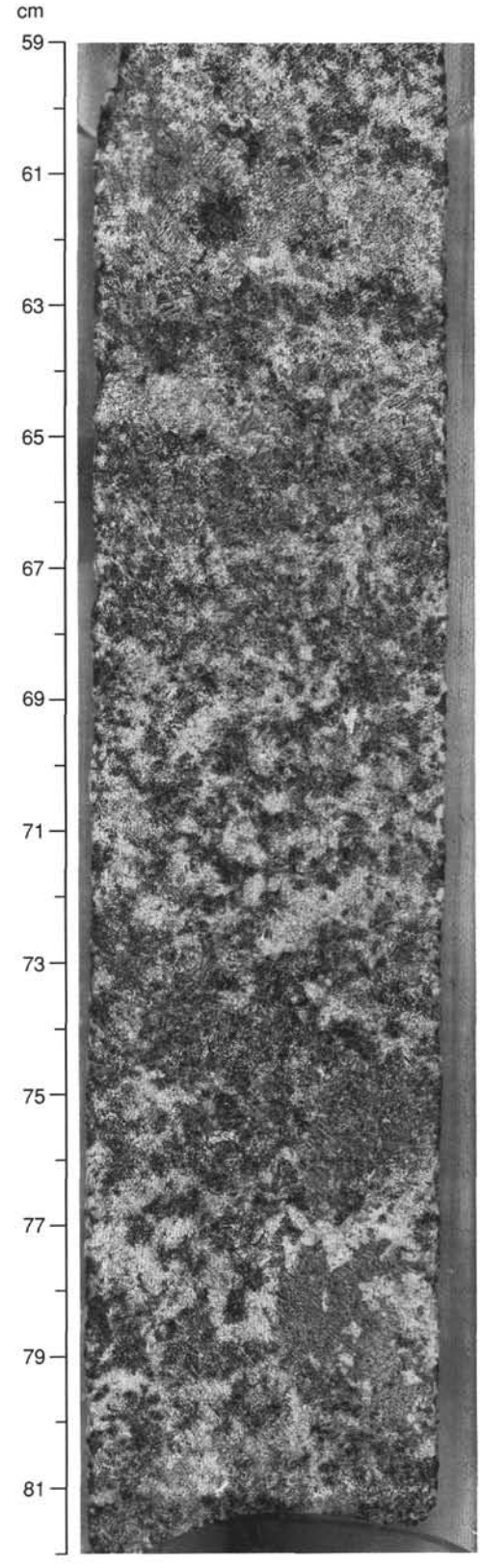

Figure 15. Sample 153-921B-4R-2, 59–82 cm, showing subhorizontal grain-size and modal layering within poikilitic olivine gabbro. The large gray patches are oikocrysts of green clinopyroxene; olivine is anhedral and dark gray, and plagioclase is white and forms subhedral laths. The modal abundance of cumulus clinopyroxene (gray) increases toward the top of the piece.

Table 3. Distribution of veins, oxide gabbro, and pyroxene-rich gabbro layers.

Hole	Unit	Felsic magmatic veins (core-section)	Felsic veins (core-section)	Oxide-rich layers and shear zones (core-section)	Pyroxene-rich layers and pods (core-section)
921A	1	2R-1	—	2R-1	—
921B	1	1W-1	—	—	—
	2	—	—	—	—
	3	2R-1	4R-1	2R-1	—
		2R-2		2R-2	
				3R-1	
				4R-1	
	4	4R-1	4R-1		—
921C	1	1R-1	—	—	—
	2	—	—	—	—
	3	—	2R-2	—	—
	4	2R-2	2R-2	—	3R-1
			2R-3		
			3R-2		
921D	1	3R-1	3R-1	3R-1	—
				4R-1	
921E	1	2R-1	2R-1/2R-2	2R-2	—
	2	3R-1	4R-1	3R-1	—
		5R-1	5R-1 to 5R-3	5R-1	
		6R-2	7R-1	6R-1	
		7R-1 to 7R-4	7R-3	7R-2	
				7R-3	
	3	8R-1	9R-1	8R-1	—
		8R-2			

disseminated grains, sometimes defining layers, within unaltered gabbroic rocks, and a second that may be either primary layers or veins associated with shear zones. These latter occurrences are generally thin (<5 cm) and the intensity of deformation obscures the original textures by which their origin could be recognized with greater certainty. Sheared oxide- and orthopyroxene-rich gabbro is present on the boundary between Units 2 and 3 in Hole 921E (see "Lithologic Units," this chapter).

Disseminated oxide minerals occur sporadically throughout the cores, but generally at relatively shallow depths within the holes. They range from fine- to coarse-grained (up to 12 mm) and form undulating layers to up 1 cm thick that contain 10%–20% oxide minerals. Iron oxide in these layers forms disseminations or trains of grains that are interstitial to plagioclase and clinopyroxene.

Occurrences associated with shear zones are more common, but still volumetrically minor. They form a spectrum of occurrences in both scale and intensity from trains of oxide minerals along millimeter-wide shear zones to concentrations of up to 40% within 2- to 5-cm-wide shear zones that range up to mylonitic in intensity (Figs. 18, 19, 20, and 21). Except for one sample, occurrences of sheared oxide gabbro are all within the lineated and pegmatitic gabbroic rocks and are absent from the poikilitic olivine gabbro. The exception is a small piece that occurs at the top of a new core and just below a designated contact (Units 2 and 3, Hole 921E) containing oxide gabbro; it may have fallen into the hole during core retrieval.

Iron titanium oxide minerals occur as trains and aggregates of fine (0.1 mm) grains ranging up to coarse (3 to 5 mm) grains within shear zones, and as interstitial grains in the adjacent rocks. Brown amphibole replaces clinopyroxene and surrounds iron oxide minerals. Orthopyroxene and apatite are commonly present in these oxide-rich zones.

Typically, the shear zones exhibit a porphyroclastic texture consisting of porphyroclasts of orthopyroxene, clinopyroxene and plagioclase plus relict grains and aggregates of oxide minerals in a fine grained recrystallized matrix of plagioclase and oxide minerals (Fig. 22). These oxide-mineral-rich layers range from planar to irregular or undulating in form, and from subvertical to subhorizontal in orientation. Iron oxide minerals form elongate stringers in the plane of the foliation and sometimes enclose plagioclase neoblasts. Relict grains of oxide minerals are rarely preserved, suggesting that they occurred originally as large, anhedral, interstitial crystals between plagioclase and pyroxene crystals but are thoroughly recrystallized. Magmatic twinning in clinopyroxene is observed in many of the sheared exam-

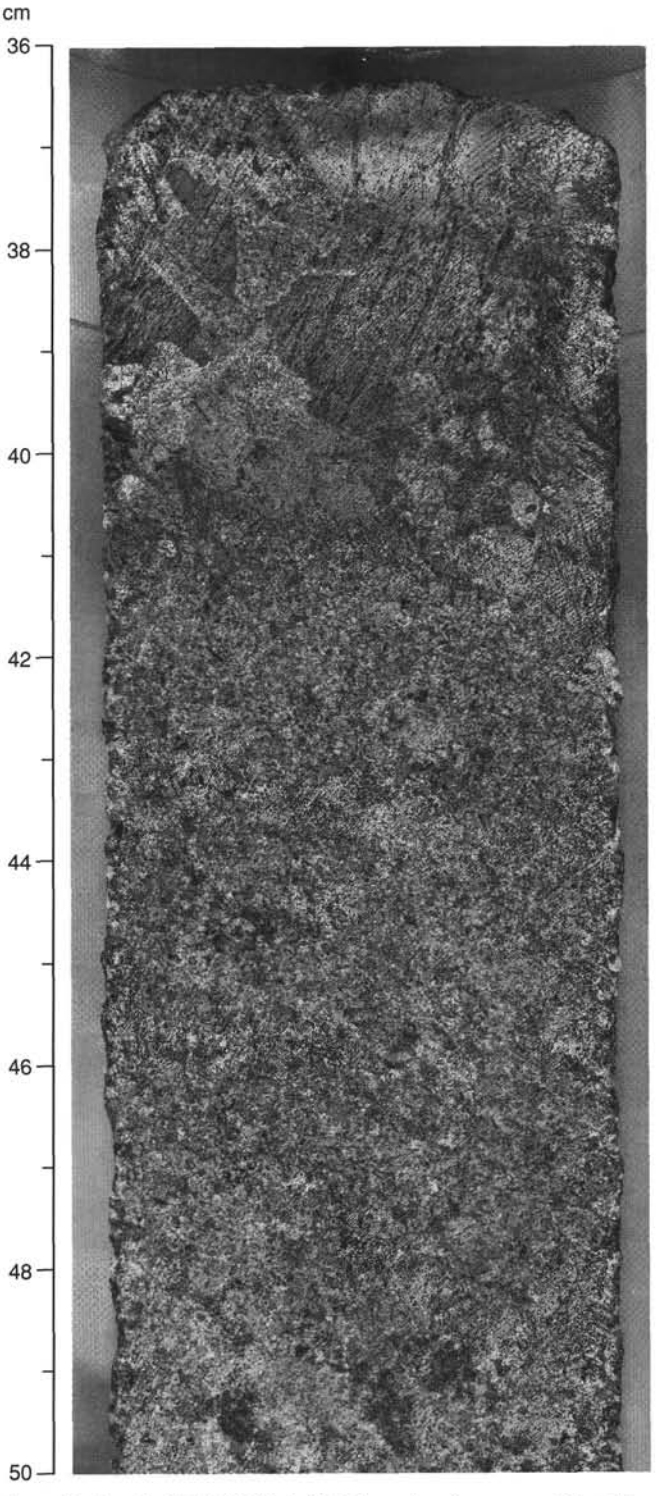

Figure 16. Sample 153-921C-3R-1, 36–50 cm, showing a pegmatitic gabbro layer at the top of the piece. Large pyroxene grain diameters exceed 30 mm. The contact may be either of cumulus origin or intrusive. The finer-grained layer is gabbro, becoming more olivine-rich (dark patches) in the lower medium-grained layer.

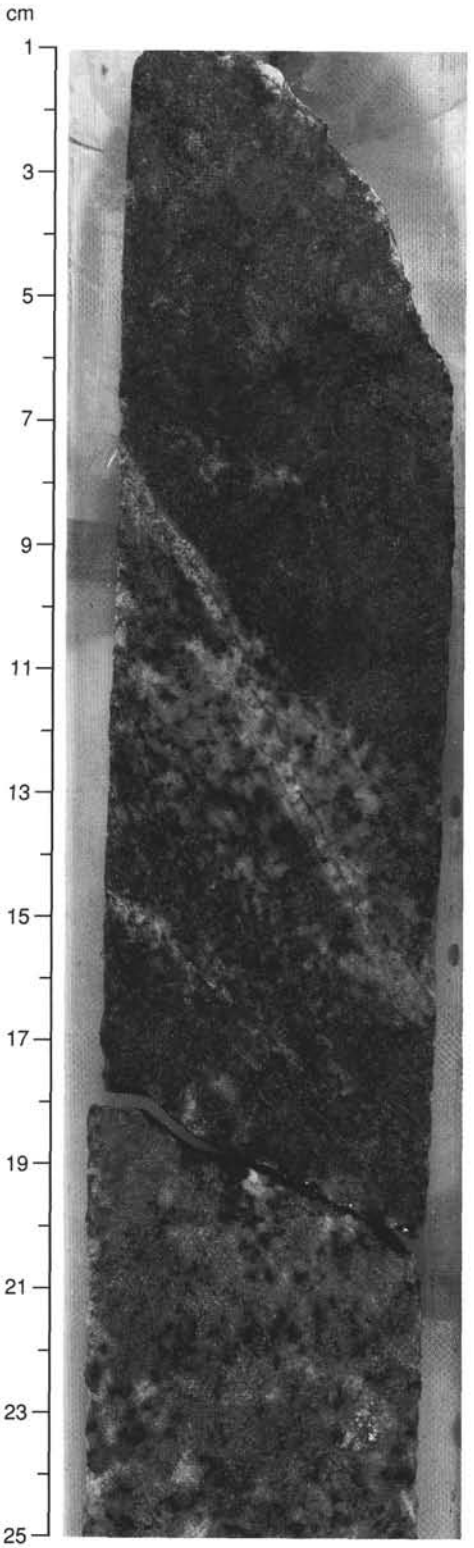

Figure 17. Sample 153-921E-5R-2, 1–25 cm, showing compositional banding between troctolite (7–21 cm) and coarse-grained olivine gabbro at the top and bottom of the core. Layer boundaries are evident between gabbro (1–7 cm) and troctolite, between several diffuse plagioclase-rich and olivine-rich troctolite layers in the center of the piece (particularly 10–16 cm), and across the break between the pieces (19–21 cm). An actinolite ± chlorite vein with a bleached margin cuts the troctolite at ~35° to the long axis of the core.

ples indicating a magmatic origin. Iron oxide minerals are also sometimes disseminated along incipiently recrystallized grain boundaries of phases directly adjacent to these veins.

In only one example are high concentrations of oxide minerals associated with a distinct, undeformed gabbroic layer (Fig. 23). Iron-titanium oxide minerals occur dominantly on the lower contact of this layer but are deformed within a shear zone that runs along the contact. The oxide minerals are intensely recrystallized (<0.2 mm) and form trains in the shear zone. One relatively coarse (5 mm) grain of the oxide mineral, however, displays an equilibrium grain boundary with an orthopyroxene crystal, but is strung out into the adjacent shear zone, suggesting that iron oxide was a primary phase within this zone (Fig. 22C).

Felsic Magmatic Veins

Veins of magmatic or probable magmatic origin occur within all of the Site 921 drill holes (Table 3). The felsic magmatic veins are distinguished here from veins of essentially hydrothermal origin in which only actinolite and chlorite are present. While some of these may have originally been magmatic in origin, they are described elsewhere in this report (see "Metamorphic Petrology," this chapter).

All of the felsic veins contain plagioclase as the major constituent and lesser abundance of clinopyroxene (or pseudomorphs thereafter), brown-green hornblende, quartz, iron oxide minerals, apatite, and zircon. Their compositions are thus broadly trondhjemitic to dioritic.

The felsic veins have a range of macroscopic characteristics from 1- to 2-mm-wide veins observed in thin section to centimeter-scale veins and irregular patches. Wider veins in some cases are branching or have subsidiary veins at high angles to the main vein (Figs. 24 and 25). Felsic patches and veins that are wider than a few millimeters tend to have diffuse, irregular, and non-parallel boundaries, while those less than 2–3 mm wide tend to have sharp, straight, parallel sides (Figs. 25 and 26).

Plagioclase in the felsic veins is strongly zoned and is typically highly altered. Quartz is present in almost all of the magmatic veins and displays slightly undulose extinction in thin section. In fine-grained veins, quartz poikilitically encloses and rims plagioclase. In the coarse-grained veins, quartz occurs as interstitial grains or as fine to corona-like intergrowths with plagioclase on the rims of plagioclase laths. Relict clinopyroxene, green amphibole pseudomorphs after clinopyroxene, iron oxide minerals, apatite, and zircon occur as interstitial grains in the veins.

Similar features are observed in microscopic veins in which thin overgrowths of amphibole or secondary pyroxene develop where the vein wall cuts mafic grains and plagioclase in the adjacent wall rock is albitized and overgrown in optical continuity.

Diabase

Moderately phyric to aphyric diabase was recovered from Holes 921A, 921B, 921C, and 921D. In Hole 921A, diabase occurs as clasts ranging from 5 to 25 mm from talus that was not designated as an igneous unit. Aphyric to sparsely phyric diabase was encountered at shallow depths in Holes 921B and 921C, and two isolated pieces of aphyric diabase were recovered in Hole 921D.

Igneous contacts of diabase with country rock were recovered only from the top contact of diabase in Hole 921B (Fig. 5), although it is truncated by a cataclastic zone (see "Structural Geology," this chapter). The grain size in the diabase decreases toward the contact with the adjacent lineated gabbroic rocks. This decrease in grain size is reflected in a color change from pale pink directly adjacent to the contact grading over 1 to 2 cm into the typical gray of the diabase.

The groundmass of the diabase across this chilled margin consists of a felted mat of plagioclase laths (2 μm in size) and interstitial chlorite. The chilled zone contains plagioclase (to 3.5 mm) laths, rarely containing spinel inclusions, and chlorite pseudomorphs (0.1 to 2 mm) after olivine. Plagioclase crystals adjacent to the cataclastic contact are broken and show undulose extinction.

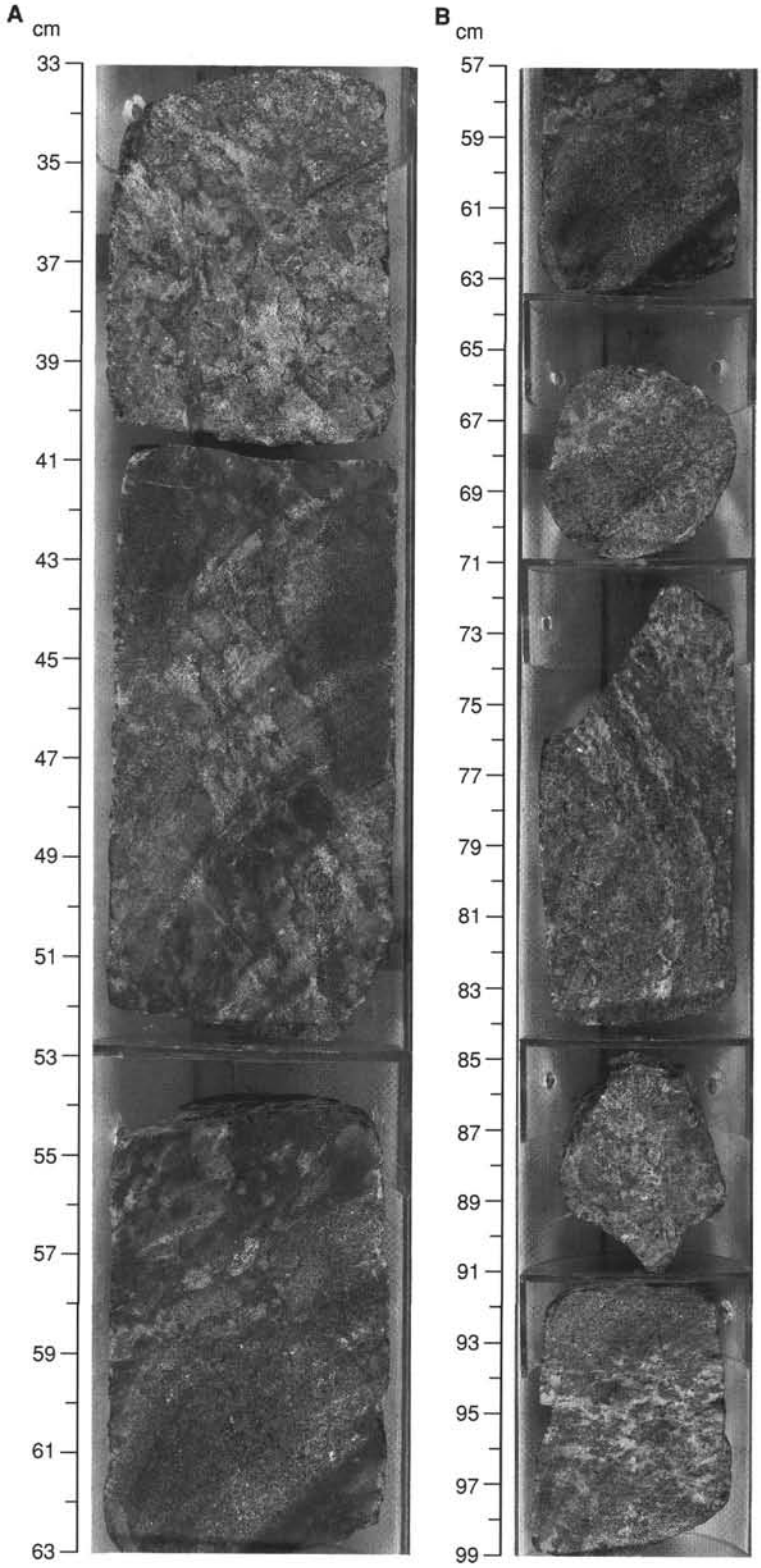

Figure 18. Sinuous zones of oxide gabbro within gabbro and olivine gabbro. **A.** Sample 153-921B-3R-1, 33–63 cm. **B.** Sample 153-921B-3R-1, 57–99 cm. Subvertical, locally arcuate (72–84 cm) compositional banding is defined by plagioclase and pyroxene modal variation and by oxide-rich arcuate bands. A weak foliation parallels the banding.

Diabase contains scattered (<1%) phenocrysts of plagioclase and olivine. Olivine is typically altered to a chloritic mass with very fine-grained sulfide minerals along grain boundaries and within intracrystalline fractures. The groundmass is intergranular to subophitic in texture and consists of a fine-grained aggregate of plagioclase laths (~48%), clinopyroxene (~45%), iron-titanium oxide minerals (2%), and olivine (5%). Clinopyroxene is interstitial to poikilitic within the groundmass, and olivine is interstitial but completely altered to chlorite.

Unit Definition

Units defined within Holes 921A, 921B, 921C, 921D, and 921E (Table 2) generally consist entirely of one of the principal rock types

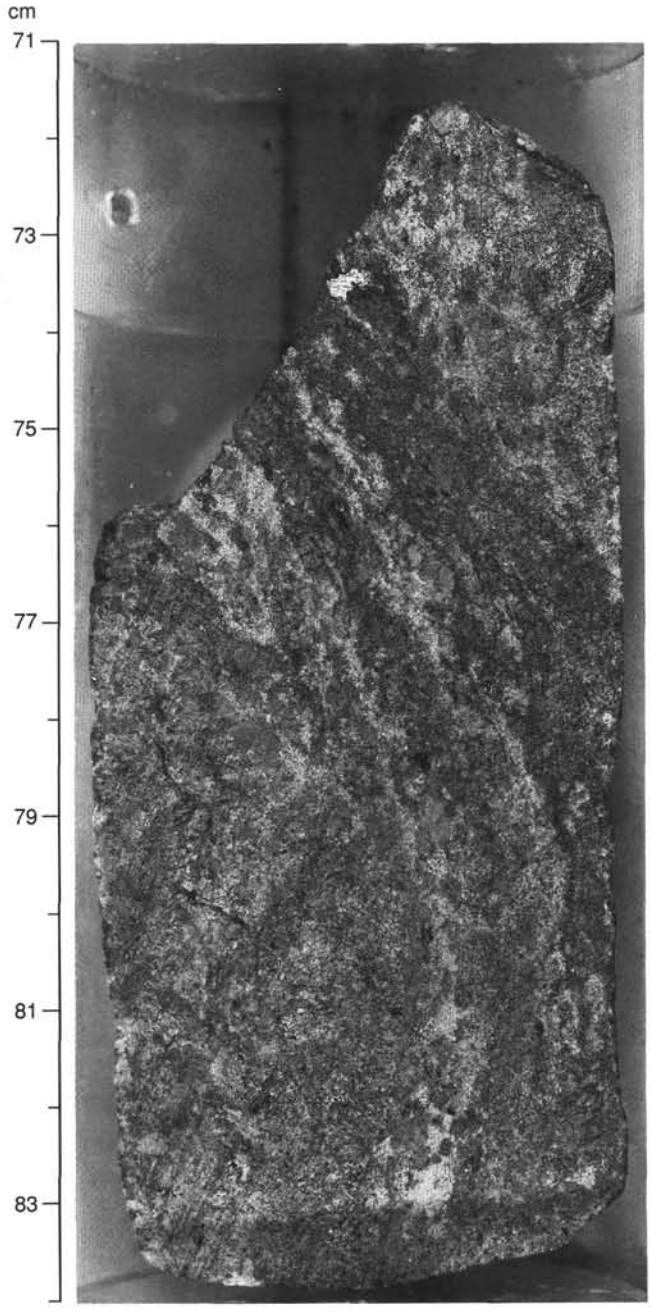

Figure 19. Sample 153-921B-3R-1, 71–84 cm. Close-up of a piece from Figure 18B showing the arcuate trace of compositional banding and a weak foliation parallel to it. The axis of curvature is subhorizontal and banding is near vertical.

described in the previous section. Units are defined either on the basis of major lithologic contrasts or on the basis of changes in the predominant rock type within heterogeneous packages. In the former case, the definition of units and unit boundaries, such as between diabase and gabbroic rocks, is relatively straight forward, irrespective of whether the contacts are preserved.

The definition of units and unit boundaries between heterogeneous packages of gabbroic rocks is more subjective, especially where the contact was not recovered during drilling. As far as was possible, the boundaries were chosen to correspond to changes in modal mineralogy, or in the inferred composition of phases that form the rocks. An example of the latter is the definition of the boundary between Units 3 and 4 in Hole 921C, which was placed at the first appearance of green, rather than brown, clinopyroxene within the gabbro.

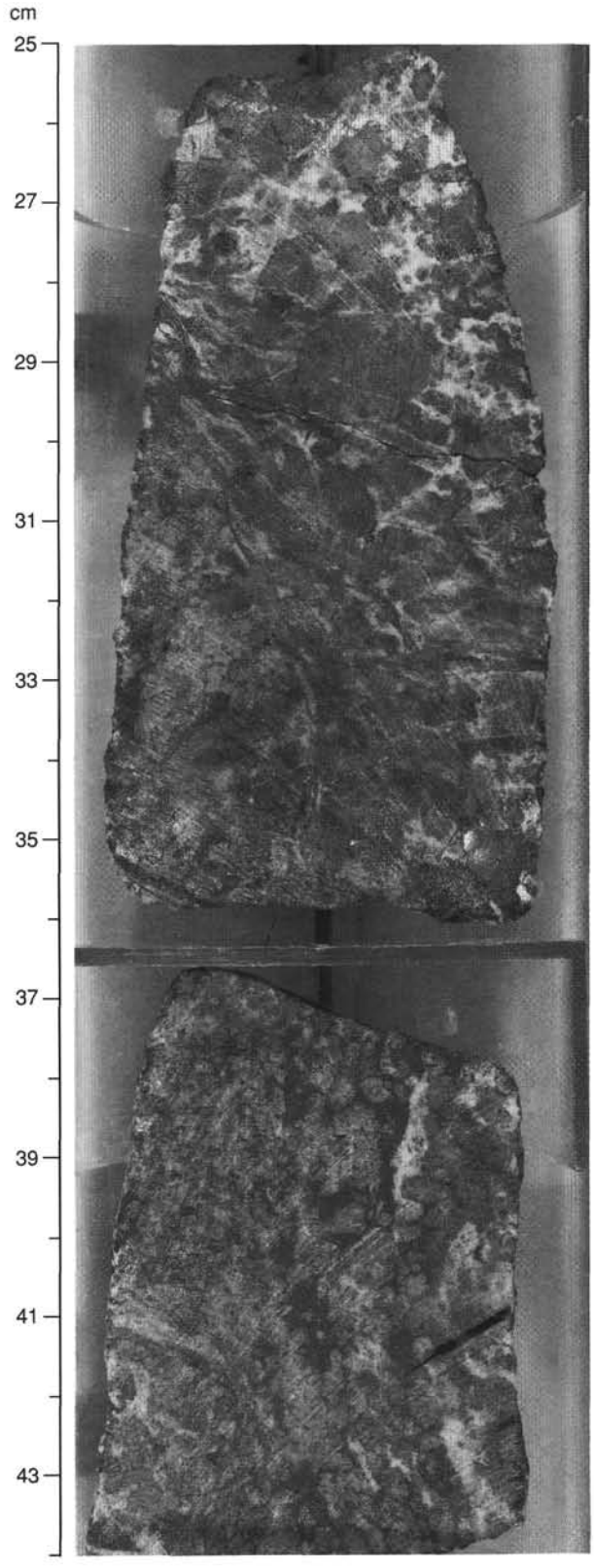

Figure 20. Contact of the pegmatitic gabbro, Unit 1, Sample 153-921E-3R-1, 25–44 cm, with poikilitic olivine gabbro, Unit 2. The contact (28–36 cm) is veined by sheared oxide gabbro and can be traced into at least the next piece in the section.

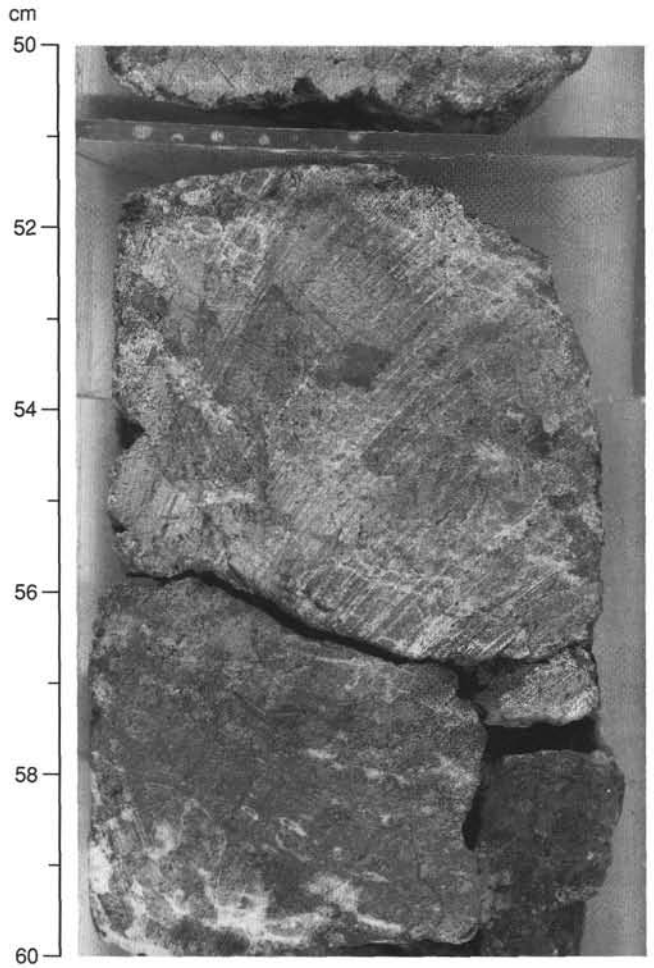

Figure 21. Pegmatitic gabbro, Sample 153-921E-2R-2, 50–60 cm, with moderate development of plagioclase neoblasts and microfractured clinopyroxene grains. The pegmatitic gabbro is cut by a sheared zone of mylonitic oxide gabbro (58–60 cm) oriented subhorizontally.

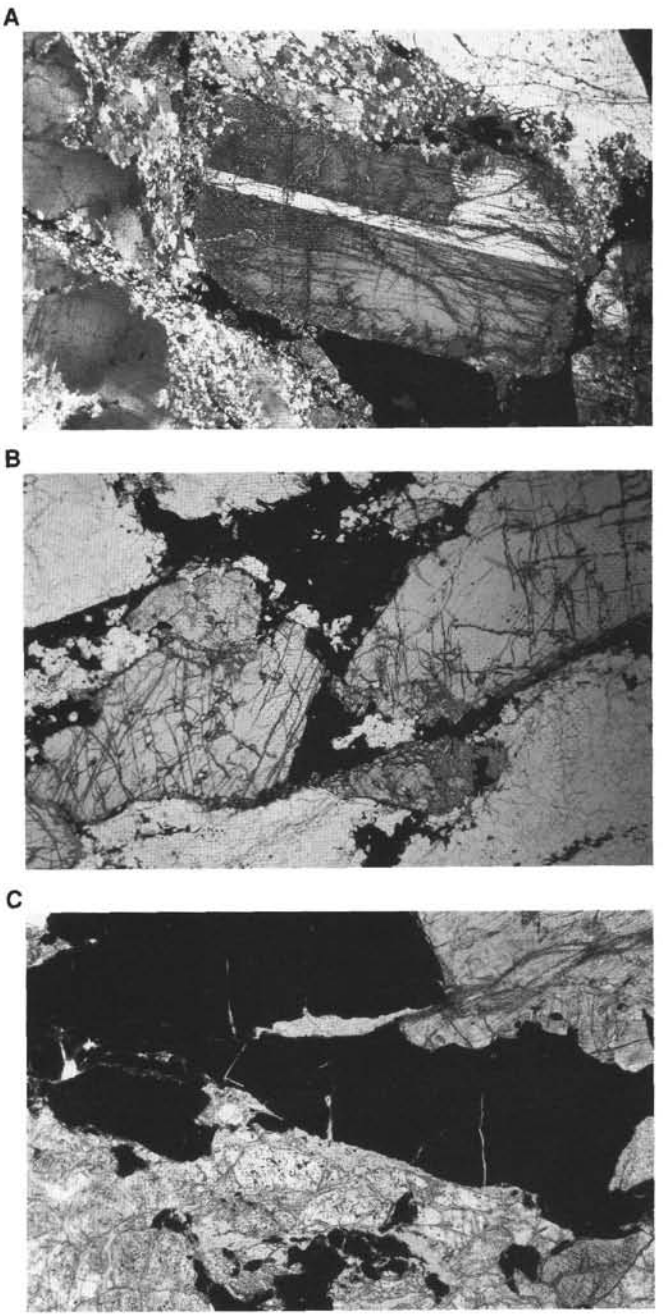

Figure 22. Oxide gabbro occurrences within Site 921 gabbroic rocks. **A.** Sample 153-921E-3R-1, 37–41 cm. Euhedral clinopyroxene displaying magmatic twins is enclosed within an aggregate of plagioclase and iron oxide mineral neoblasts. Field length is 8 mm. **B.** Sample 153-921B-3R-1, 33–36 cm. Porphyroclastic oxide gabbronorite containing orthopyroxene porphyroclasts within an aggregate of iron oxide minerals and plagioclase neoblasts. Field length is 8 mm. **C.** Sample 153-921D-4R-1, 59–62 cm. Large anhedral grain of primary iron oxide mineral is in contact with orthopyroxene. Field length is 2 mm.

Cores 8R and 9R in Hole 921E pose some problem in that they contain a heterogeneous sequence of gabbroic rocks in which the composition, in part, overlaps that of the overlying heterogeneous poikilitic olivine gabbro. The boundary between these units is placed at the top of a core where the rock type changed from heterogeneous olivine gabbro (Unit 2) to a package of rock types that range from olivine gabbro to gabbro and diorite (Unit 3). Within this lower unit, the compositional and textural variability from piece to piece is such that the designation of additional units was impractical. Although both units are heterogeneous in texture and composition, the ranges of compositions only partly overlap and the boundary is thus significant at the unit scale.

The characteristics of each unit (see "Lithologic Units," this chapter) and its contacts, on a hole to hole basis, is presented below. Bracketed names refer to the rock types described in the preceding section.

Hole 921A

All of the core from Hole 921A was assigned to a single unit consisting of olivine gabbro (lineated gabbro) that is olivine-poor (average 8% olivine). The gabbro is undeformed to weakly deformed, and it varies from medium- to coarse-grained from piece to piece. Gabbroic rocks in this interval are characterized by the presence of dark brown, anhedral, cumulus clinopyroxene. Deformation is evident as weak recrystallization of plagioclase and, in Section 153-921A-2W-2, a moderate alignment of clinopyroxene grains. This rock type is characteristic of weakly deformed examples of the lineated gabbro.

Hole 921B

Four units were defined in Hole 921B:

Unit 1 is metagabbro and meta-olivine gabbro (lineated gabbro) that originally comprised ~45% clinopyroxene and ~55% plagio-

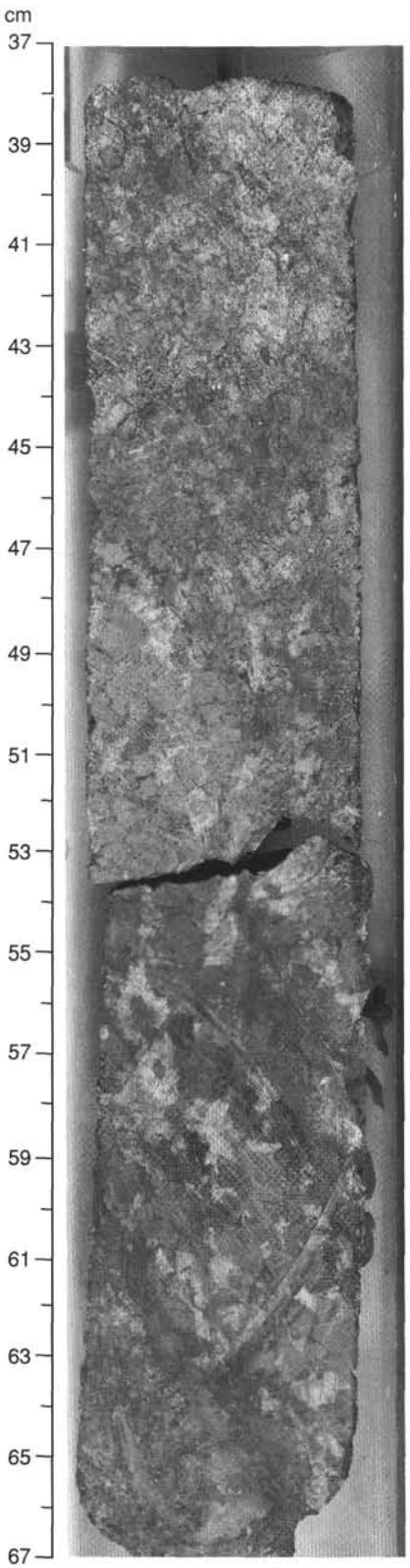

Figure 23. Lineated gabbro cut by 7-cm-thick layer of coarser grained oxide gabbro. The layer has sharp contacts with the lineated gabbro and contains euhedral clinopyroxene and interstitial plagioclase. Iron oxide minerals are concentrated along the lower margin of the layer which is sheared. Sample 153-921D-4R-1, 37–67 cm.

Figure 24. Diorite to trondhjemite vein cutting pegmatitic olivine gabbro. Sample 153-921E-2R-1, 9–13 cm. The vein consists of laths of zoned plagioclase with interstitial clinopyroxene altered to actinolite and chlorite. Note the thin veinlets of diorite extending into the adjacent gabbro from the margins of the vein.

clase, but which is now strongly altered and, as a consequence, is named metagabbro in Table 2. The rocks have been cataclastically deformed after the lineation-producing crystal-plastic deformation, but samples in which alteration and cataclastic textures are less pervasive exhibit a mineral lineation of clinopyroxene grains.

Unit 2 is aphyric to sparsely porphyritic diabase containing olivine and plagioclase phenocrysts. The upper contact of diabase with lineated gabbro (Fig. 5) was recovered in two separate pieces. The upper of these (Section 153-921B-1W-1, Piece 12) contains two chilled contacts, one that faces upward and has shallow dip, and a second that faces downward on the bottom corner of the piece. The upward-facing contact is truncated by a subhorizontal cataclastic shear zone that separates the diabase from lineated gabbro. A third contact was recovered from Piece 17. The diabase cuts cataclastic gabbro. The contact is irregular in shape and chilled, but the facing direction is not known because the piece is not oriented. More diabase occurs downsection within the hole, but its lower contact with lineated gabbro was not recovered.

Unit 3 is grain-size-layered gabbro, olivine gabbro, and minor oxide gabbro (lineated gabbro). The unit is variably deformed, resulting in weak to intense recrystallization of plagioclase and clinopyroxene and localized development of a lineation defined by a shape preferred dimensional fabric defined by clinopyroxene. Layering is evident as grain-size layering between medium- and coarse-grained rocks. Layer thicknesses vary from 2 cm to ~10 to 15 cm (the scale of pieces). In all cases, clinopyroxene is brown, a primocryst phase, and anhedral.

Oxide gabbro/gabbronorite occurs in the interval 153-921B-4R-1, Pieces 4, 5, 7 and 8, 33–90 cm (Figs. 18 and 19) which consists of coarse-grained, equigranular olivine gabbro transected by a 5-cm-wide layer of strongly deformed, oxide gabbronorite. The layer is undulating and subvertical, and appears to form a single, continuous layer. In thin section, the oxide gabbronorite consists of 53% plagioclase, 32% clinopyroxene, 6% orthopyroxene, 8% iron oxide minerals, and <1% olivine. Iron oxide minerals form elongate stringers in the plane of the foliation and enclose plagioclase neoblasts. In places, undeformed relict grains of oxide minerals suggest that they occurred originally as large, anhedral, interstitial grains between plagioclase and pyroxene crystals. Magmatic twinning in clinopyroxene is observed in thin section.

The lower contact of Unit 3 with the underlying Unit 4 was recovered in Core 4R (Sample 153-921B-4R-1, Piece 6A, 40–47 cm; Fig. 27). The lineation in the overlying gabbro is oblique to the contact 2–3 cm from the contact, but it appears to curve into and become

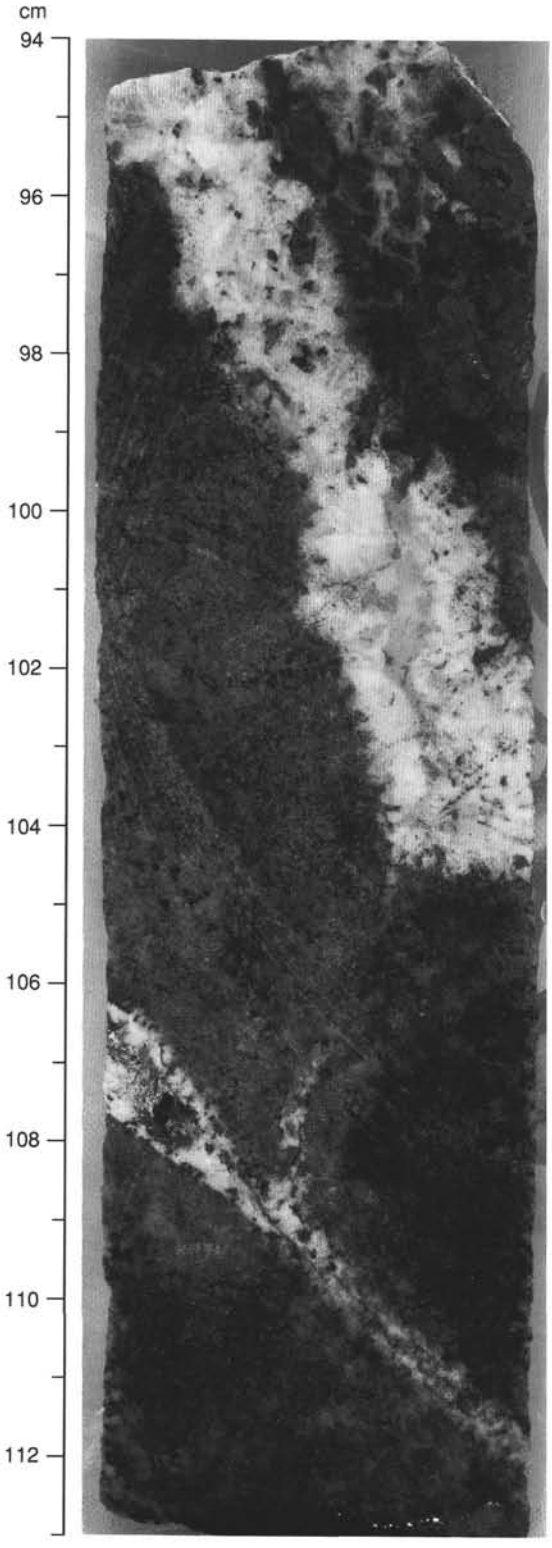

Figure 25. Sample 153-921E-7R-2, 94–113 cm. Plagioclase-rich (trondhjemitic) vein (94–105 cm) and dioritic (106–112 cm) vein in poikilitic olivine gabbro. The dioritic vein contains magmatic green-brown hornblende and has a subsidiary vein that projects toward the trondhjemitic vein. The trondhjemitic vein is cored by a chlorite-actinolite vein. Gabbro between the trondhjemitic vein and the end of the piece is oxide-mineral-rich. Note the sharper contacts on the thinner vein.

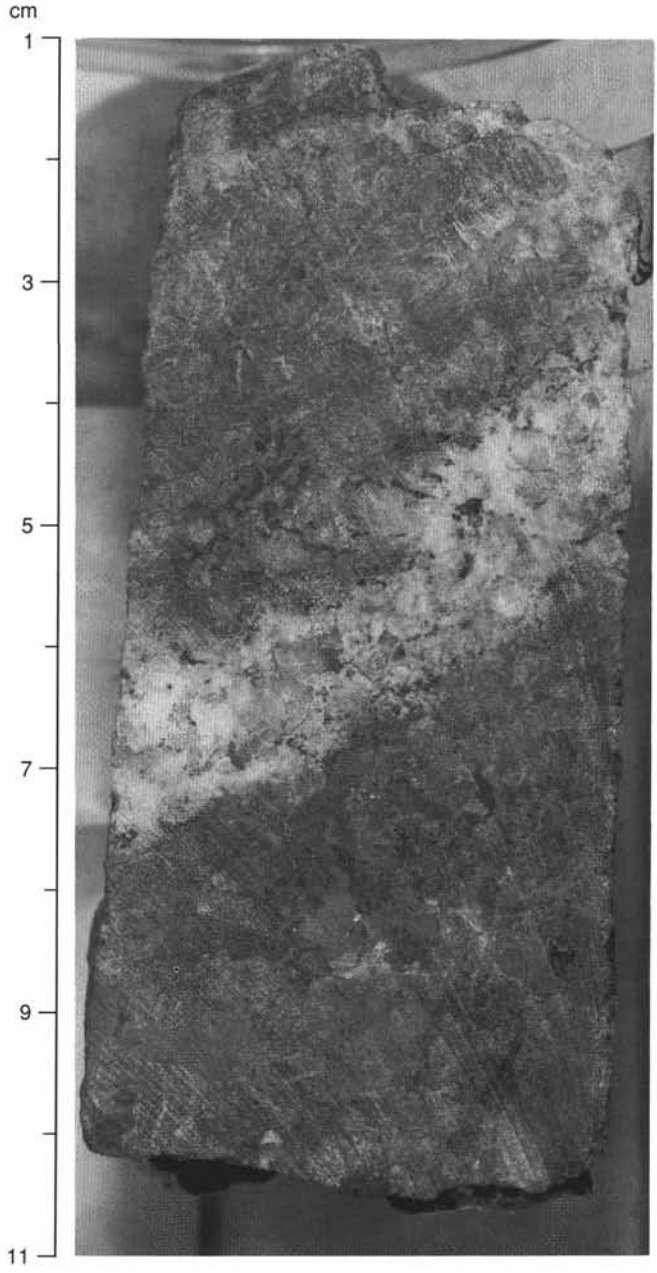

Figure 26. Vein of plagioclase-rich material (trondhjemite?) showing diffuse margins with host gabbro. Sample 153-921E-8R-2, 1–11 cm.

parallel with the contact. In thin section, the contact is marked by a thin (<1 cm) shear zone in which orthopyroxene and iron-titanium oxide minerals are relatively abundant. The texture of the underlying olivine gabbro becomes finer grained and more homogeneous toward the contact which, together with the obliquity of the gabbro lineation above the contact, could be interpreted as evidence for tectonic juxtaposition of Units 3 and 4. The presence of shearing within the contact zone, however, means that any interpretation of timing relationships across the contact is ambiguous.

Unit 4, poikilitic olivine gabbro, consists of olivine gabbro, gabbro, and rare troctolite (Fig. 15) that is magmatically layered on a scale that ranges from 2 to 20 cm. This fine-scale layering is defined by changes in modal mineralogy and grain size with boundaries varying from sharp to diffuse and gradational (Fig. 13 and 15). The unit is characterized by the presence of large, green clinopyroxene

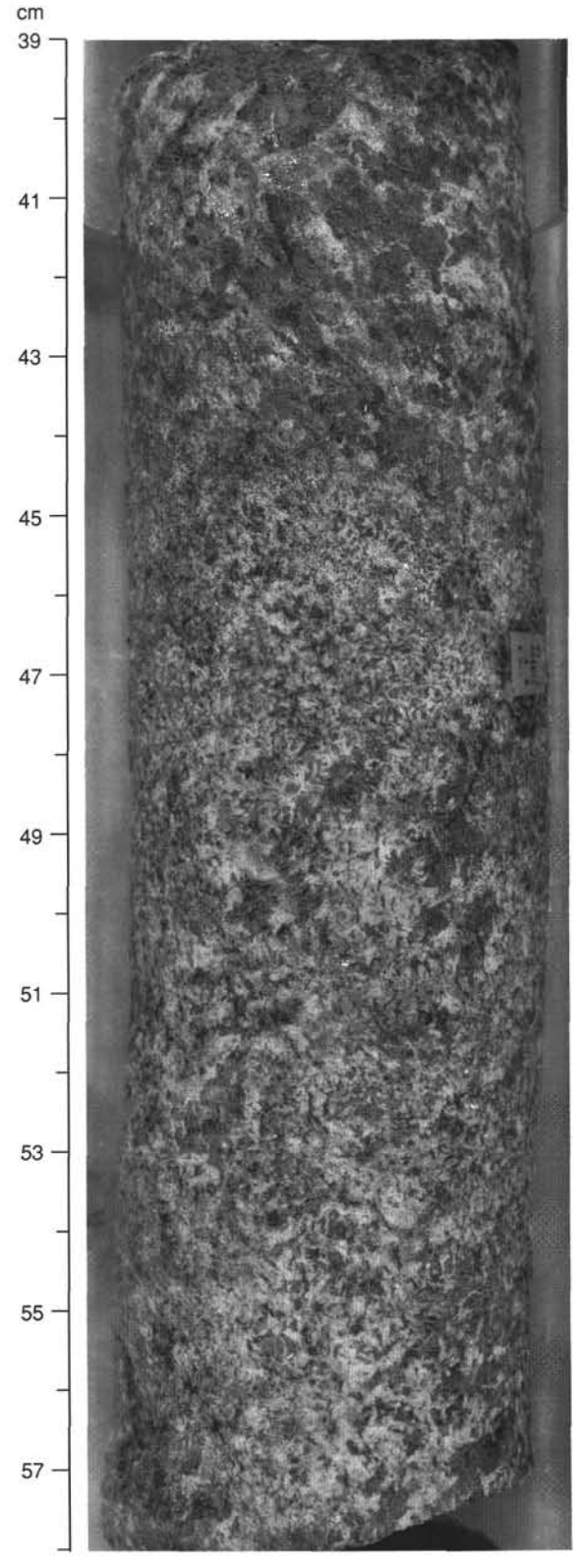

Figure 27. Contact of lineated gabbro (39–44 cm) and poikilitic olivine gabbro (44–58 cm), Units 3 and 4, respectively. The lineation in the gabbro curves into the contact. Note the reduction in grain size in the poikilitic olivine gabbro near the contact. Sample 153-921B-4R-1, 39–58 cm.

oikocrysts that form 5% to 10% of the rock. Evidence for magmatic lamination is restricted to small intervals (<5 cm) where moderate alignment of plagioclase grains occurs within Cores 5R, 6R, and 7R.

Hole 921C

Four units were defined in Hole 921C. Unit 1 of this hole is gabbro (lineated gabbro) that is strongly altered to metagabbro with a subsequent overprint by subhorizontal cataclastic shear zones. Nonetheless, relict brown clinopyroxene preserved as euhedral grains in less deformed rocks, or porphyroclasts in lineated sections, are consistent with the primary lithology being lineated gabbro. Unit 2 is diabase similar to that in Unit 2 of Hole 921B. The unit occurs only within the top of Core 2R, and no contacts were recovered. Unit 3 is gabbro and minor olivine gabbro (lineated gabbro) characterized by the presence of brown clinopyroxene and a moderate to strong mineral lineation. The variations in the mineralogy, degree of development of primary magmatic layering and the crystal-plastic fabric are typical for the lineated gabbro rock type. Oxide gabbro was not recorded in this unit. Unit 4 is poikilitic olivine gabbro and gabbro (poikilitic olivine gabbro) that displays typical characteristics for the poikilitic olivine gabbro lithology, including the presence of poorly defined grain-size and modal layering and coarse green clinopyroxene oikocrysts. The unit contains very coarse gabbro layers (Fig. 16).

The contact of this unit with the overlying lineated gabbro unit was placed between Pieces 4 and 5 in Section 153-921C-2R-2. Piece 4 is moderately altered and shows a weak lineation of clinopyroxene grains, while Piece 5 is a subophitic-textured medium- to coarse-grained olivine gabbro with a 1-cm-wide coarse-grained oxide gabbro along the top of the piece. Olivine gabbro is the predominant rock type below the designated unit boundary. Rocks in the rest of the section are similar in texture to Piece 5 but show a gradual increase in grain size and in the presence of green clinopyroxene as an interstitial and poikilitic phase. The trend continues into the next section, where green clinopyroxene is developed as oikocrysts and gabbro becomes increasingly olivine-rich.

Hole 921D

Hole 921D was not subdivided into separate units because the variability in texture and mineral composition from piece to piece was greater than could easily be accounted for on the unit scale. The upper sections of the hole (Sections 1R-2 to 5R-1) consist predominantly of gabbro and gabbronorite containing brown anhedral clinopyroxene and displaying variable intensities of shape fabrics due to ductile deformation. Oxide gabbro occurs in this unit as a thin, sheared, oxide gabbro adjacent to a 6- to 7-cm-thick coarse-grained gabbro vein.

The first two pieces of Core 153-921D-4R are a coarse grained, subophitic olivine gabbro. This rock type may be related to poikilitic olivine gabbro. The top of Core 5R is strongly altered and contains a single piece of diabase. Samples below the altered zone are interlayered gabbro, olivine gabbro, and minor troctolite, in which the pyroxene is brown to slightly greenish.

Hole 921E

Three units were defined in Hole 921E. Unit 1 in this hole is very coarse-grained to pegmatitic gabbro and olivine gabbro that was not recovered from any of the other holes at Site 921. Clinopyroxene in these rocks is brown, anhedral becoming subhedral in coarser examples, and rarely shows a preferred shape fabric. Plagioclase is preserved as very coarse, twinned laths in weakly deformed samples, but becomes recrystallized into a fine- to medium-grained granuloblastic aggregate where the intensity of deformation increases.

Oxide gabbro occurs in two intervals in this unit, both of which are deformed: a thin, apatite-bearing, mylonitic oxide gabbro (Fig. 21), and a sheared oxide gabbro that has been designated as the unit boundary between pegmatitic gabbro and the underlying poikilitic olivine

gabbro (Fig. 20). Oxide gabbro at this boundary is sheared and cuts subvertically across three pieces. The designated boundary separates the upper pegmatitic gabbro in which olivine gabbro is minor, from coarse-grained gabbroic rocks below the boundary where olivine gabbro dominates and olivine abundance is typically greater than 10%.

Unit 2 has a heterogeneous texture and composition. It consists of olivine gabbro and poikilitic olivine gabbro. Although brown, cumulus clinopyroxene is characteristic of the olivine gabbro just below the contact in Section 153-921E-3R-1, the rock grades into poikilitic olivine gabbro with depth. Clinopyroxene appears as green oikocrysts by the top of the next section downhole (Section 153-921E-4R-1). The intensity of alteration decreases with depth through this unit until the end of Core 7R. Grain-size layering on the scale of 5 to 10 cm increases in intensity and is well developed by Section 153-921E-4R-2.

The rocks are medium- to coarse-grained, but highly variable in their texture and modal mineralogy (Figs. 13, 17, 28, and 29). Modal layering is relatively important when compared to the lineated gabbro and other poikilitic olivine gabbro intersected in other Site 921 holes, and is evident at scales of less than 1 cm. There is an increase in the abundance of cumulus clinopyroxene in the finely laminated cores, and it is in these intervals that thin troctolite units are present.

Very coarse-grained, magmatic-textured layers 10 to 30 cm thick punctuate the medium- to coarse-grained layered intervals (Fig. 28 and 29). These rocks have diffuse boundaries and are extremely heterogeneous in their internal distribution of phases. The heterogeneity is enhanced by their coarse grain size and by the presence of highly elongate, radiating aggregates of plagioclase laths and lobate, probable crescumulate-textured olivine grains. These variations impart an extremely heterogeneous texture to the unit defined by grain size and modal variations, hence the unit name heterogeneous poikilitic olivine gabbro.

Unit 3 is varitextured gabbroic interval that contains rock types ranging from poikilitic olivine gabbro through lineated gabbro, very coarse-grained gabbro breccia, and diorite. The poikilitic olivine gabbro and lineated gabbro samples are similar to rocks described from other units. The pegmatitic gabbro breccia (Fig. 30, interval 153-921E-8R-1, Pieces 3–13) consists of angular, commonly fractured grains of brown clinopyroxene within a matrix of plagioclase porphyroclasts and intensely recrystallized, granuloblastic plagioclase (see "Structural Geology" this chapter). Quartz diorite occurs as the first piece in this unit (Fig. 31) and is medium-grained, consisting of 45% plagioclase, 25% quartz, 20% hornblende(?), 2% biotite, 8% iron oxide minerals and accessory apatite.

Geochemistry

A total of 28 whole-rock samples from Site 921 were analyzed using X-ray fluorescence (XRF) for major-oxide compositions and abundances of the trace elements Nb, Zr, Y, Sr, Rb, Zn, Cu, Ni, Cr, V, Ce, and Ba (Table 4). Trace element abundances were determined from pressed powder pellets prepared from dried (unignited) material. The measured contents of Rb, Nb, Ce, and Ba are, in most cases, near or below detection limits (Table 1, "Explanatory Notes," this volume). These values should be interpreted with care because they have relatively large analytical errors. Vanadium was also analyzed, but because of calibration problems not all results are considered reliable; therefore, only those samples analyzed during runs when standard results were acceptable for this element are reported. Sample preparation techniques and analytical procedures are outlined in the "Explanatory Notes" (this volume).

The objective of the sampling strategy was to establish a chemical characterization of the recovered gabbro section within the restrictions of limited core recovery. Samples were taken of pieces deemed to be representative when sufficient recovery allowed. Unique materials were preserved for more detailed and/or precise shore-based analyses. As a rule, the freshest possible material was selected to reduce the effects of alteration on the chemical data. In a few cases,

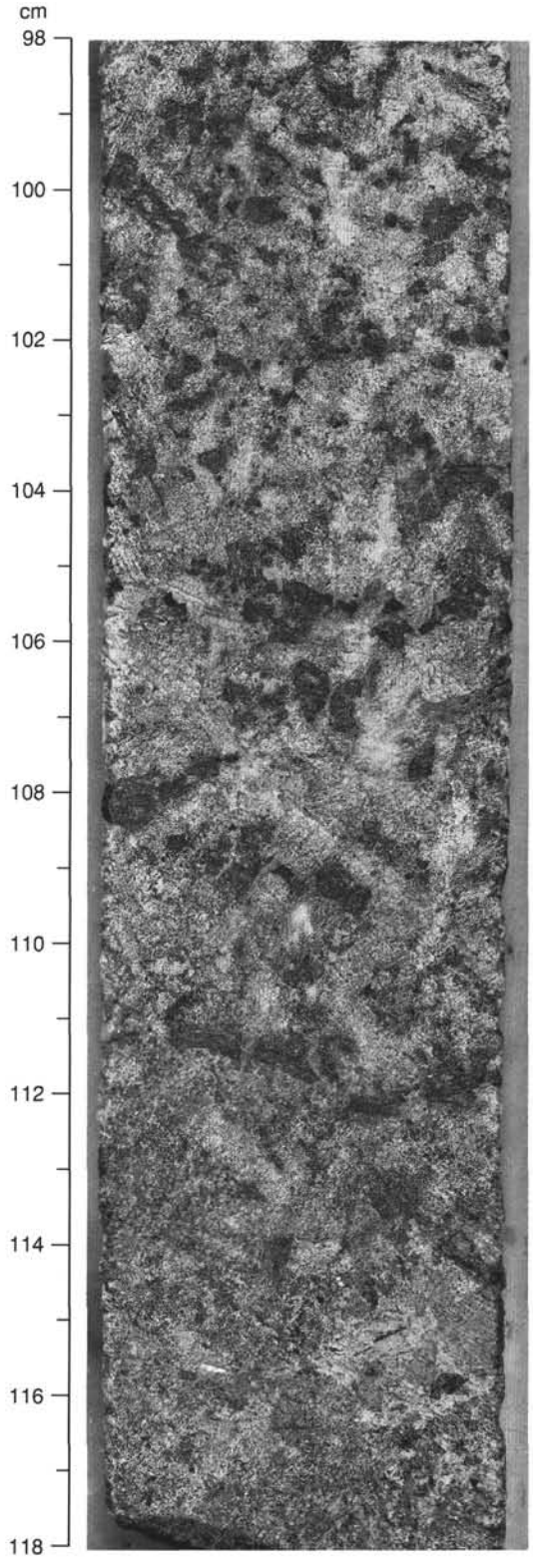

Figure 28. Sample 153-921E-6R-1, 98–118 cm, showing coarse-grained troctolite (98–114 cm) grading downward into finer grained troctolite. Plagioclase forms radiating clumps of subhedral, elongate grains with pointed terminations and sparse, thin, dark cores of clinopyroxene. These textures suggest rapid growth and may indicate melt emplacement with a high thermal gradient between melt and wall rock.

Table 4. Major oxide and trace element analyses for Holes 921A–E.

Hole:	921A	921B	921B	921B	921B	921B	921B	921C	921C	921C	921D	921D	921D
Core, section:	2R-1	1W-1	2R-1	3R-1	3R-1	4R-1	4R-3	2R-1	2R-2	3R-1	2R-1	4R-1	5R-1
Interval (cm):	34–40	64–70	85–88	13–20	133–137	59–65	77–83	110–116	114–120	83–89	55–60	54–59	118–124
Piece:	5	9	11	2	13	6b	8	14	10	5b	6	6b	12c
Depth (mbsf):	8.04	0.64	15.45	24.63	25.83	34.69	37.73	11.1	12.54	20.43	10.35	29.84	40.08
Unit:	1	1	3	3	3	4	4	3	4	4	1	1	1
Rock:	OLGAB	MGAB	GAB	OLGAB	GAB	OLGAB	TROC	OLGAB	OLGAB	OLGAB	GNOR	OXGAB	OLGAB
Type:	1	1	1	1	1	2	2	1	2	2	3	3	2
Major elements (wt%)													
SiO_2	51.21	51.25	49.84	50.69	52.7	49.63	47.36	50.39	50.01	49.7	53.77	48.56	51.17
TiO_2	0.36	0.47	0.38	0.37	0.45	0.27	0.15	0.39	0.44	0.39	0.5	3.41	0.33
Al_2O_3	16.71	17.19	15.15	16.48	15.41	16.71	23.17	17.6	16.7	17.18	17.41	11.85	17.15
Fe_2O_3	6.42	6.17	9.39	5.81	5.78	5.35	4.96	6.62	4.91	4.6	7.2	13.21	5.43
MnO	0.13	0.14	0.16	0.12	0.13	0.1	0.08	0.12	0.1	0.09	0.15	0.25	0.11
MgO	9.67	9.09	12.82	10.23	9.07	12.19	9.93	9.6	11.27	10.68	7.42	8	9.7
CaO	13.64	11.96	10.93	13.92	14.28	14.17	11.62	12.56	15.22	15.14	10.34	12.17	13.37
Na_2O	2.38	2.9	2.25	2.12	2.41	1.58	2.04	2.27	1.61	1.57	3.23	2.32	2.25
K_2O	0.01	0.03	0.02	0.01	0.02	0.01	0.03	0.01	0	0	0.03	0.02	0
P_2O_5	0	0.04	0.01	0	0	0	0	0.01	0	0	0	0.04	0
Total	100.54	99.24	100.96	99.75	100.25	100.01	99.35	99.59	100.26	99.35	100.05	99.83	99.52
LOI	0.18	1.17	0.17	0.2	0.15	0.57	1.25	0.73	0.58	0.43	0.3	0.79	0.85
H_2O	1.23	1.91	0.88	0.68	0.61	0.95	1.93	1.34	0.99	0	0	2.87	1.21
CO_2	0.06	0.06	0.04	0.06	0	0.02	0.05	0	0	0	0	0	0.02
Trace elements (ppm)													
Nb	0	2	0	0	0.5	1	0	0	0	1	1	4	0
Zr	14.5	58	25	17.5	12	10	7	17	20	18	16	75	10
Y	9	21	10	10	11	6	3	8	9	8	11	28	8
Sr	136	147	137	135	131.5	105	172	141	121	126	170	116	154
Rb	1	1	1	1	1	2	1	1	2	2	0	0	1
Zn	29	45	50	26.5	24	23	21	36	20	18	43	76	24
Cu	102	26	95	109.5	92	96	98	88	81	81	33	125	86
Ni	106.5	95	128	134.5	81	268	326	127	203	201	44	87	116
Cr	315.5	108	86	544.5	98.5	1723	30	736	1880	1896	47	57	248
TiO_2	0.36	0.42	0.36	0.385	0.435	0.27	0.15	0.37	0.42	0.38	0.46	3.12	0.32
V	191	NA	NA	NA	204	NA	NA	NA	NA	NA	NA	NA	NA
Ce	1	3	1	1.5	1	0	0	0	0	0	0	14	0
Ba	0	0	0	0	0	0	0	0	0	0	0	29	0
Mg#	0.78	0.77	0.76	0.8	0.79	0.84	0.82	0.77	0.84	0.84	0.71	0.59	0.81
Zr/Y	1.6	2.8	2.5	1.8	1.1	1.7	2.3	2.1	2.2	2.3	1.5	2.7	1.3
Cr/Ni	3	1.1	0.7	4	1.2	6.4	0.1	5.8	9.3	9.4	1.1	0.7	2.1

Notes: Mg# calculated as the molar ratio of $Mg/(Mg + Fe^{tot} * 0.85)$. Rock: OLGAB = olivine gabbro, MGAB = metagabbro, GAB = gabbro, TROC = troctolite, GNOR = gabbronorite, OXGAB = oxide gabbro. Unit = lithologic unit defined on the basis of mineralogical characteristics. LOI = loss on ignition. Type = lithologic type defined on the basis of mineralogical and geochemical characteristics (see text for discussion). Type designation for Sample 153-921B-1W-1, 64–70 cm, is based on mineralogy of inferred protolith. NA = not analyzed.

Table 4 (continued).

Hole:	921D	921E	921E	921E	921E	921E	921E	921E	921E	921E	921E	921E	921E	Type 1	Type 2
Core, section:	5R-2	2R-2	3R-1	4R-1	5R-2	6R-1	6R-2	7R-1	7R-2	7R-3	7R-3	8R-1	9R-1	average	average
Interval (cm):	56–63	24–30	138–144	44–50	125–131	97–101	45–48	92–99	77–83	83–86	89–93	56–62	52–58		
Piece:	5	1	15	5	7	11b	4	9a	3	2	2	8	4		
Depth (mbsf):	40.91	11.39	21.18	30.14	41.89	50.47	51.45	60.32	61.58	62.98	63.04	69.56	79.12		
Unit:	1	1	2	2	2	2	2	2	2	2	2	3	3		
Rock:	OLGAB	OLGAB	OLGAB	OLGAB	OLGAB	OLGAB	OLGAB	OLGAB	OLGAB	OLGAB	OLGAB	GNOR	GAB		
Type:	2	1	2	2	2	2	2	2	2	2	2	3	1		
Major elements (wt%)															
SiO_2	47.01	50.69	51	50.94	49.28	47.11	51.39	50.36	50.08	49.04	50.15	53.39	51.6	50.97	49.7
TiO_2	0.2	0.61	0.41	0.28	0.21	0.32	0.29	0.33	0.27	0.33	0.34	0.67	0.49	0.39	0.31
Al_2O_3	20.03	15.37	17.42	20.63	21.72	17.26	17.91	15.62	16.91	18.81	17.74	14.68	16.35	16.27	18.29
Fe_2O_3	6.76	7.56	5.82	4.54	5.31	6.88	4.75	5.77	5.26	6.51	5.55	8.74	6.38	6.8	5.4
MnO	0.11	0.14	0.12	0.09	0.09	0.11	0.1	0.12	0.1	0.11	0.11	0.19	0.13	0.13	0.1
MgO	13.3	9.65	9.52	7.72	9.22	15.93	9.82	11.85	11.1	11.47	10.87	9.3	9.01	10.28	10.89
CaO	10.11	13.18	13.43	12.88	11.34	10.52	14.17	14.3	13.87	11.79	13.76	10.63	13.17	13.07	13.25
Na_2O	1.95	2.25	2.44	2.63	2.63	1.67	2.09	1.7	1.73	2.04	1.86	2.75	2.33	2.29	1.97
K_2O	0.02	0.02	0.03	0.02	0.01	0.02	0.01	0	0.02	0	0	0.02	0.02	0.01	0.02
P_2O_5	0	0.01	0	0	0	0.01	0	0	0	0	0	0	0	0.01	0.01
Total	99.51	99.48	100.17	99.73	99.8	99.83	100.53	100.05	99.36	100.1	100.37	100.37	99.47	100.22	99.92
LOI	0.97	0.29	0.55	0.55	0.53	1.81	0.27	0.59	1.42	0.42	0.36	_0.16	0.25	0.29	0.72
H_2O	1.43	0.47	0	0	1.18	2.96	0.57	0.89	1.54	1.11	1.04	0.23	0	0	0
CO_2	0.02	0	0.03	0.03	0.04	0.02	0	0.01	0	0	0.01	0	0	0	0
Trace elements (ppm)															
Nb	0	0	0	1	0	1	1	0	1	0	0	0	0	0.5	1
Zr	11	36	26	21	9	18.5	10	16	14	15	14	21	17	17.2	15.27
Y	4	14	11	9	4	5.5	6.5	9	8	7	8	14	12	9.6	7.23
Sr	154	130	147	165	184	123	153.5	129	130	166	152	138	139	136.1	144.12
Rb	1	1	1	1	1	1	1	1	2	1	1	2	1	1	1.31
Zn	35	41	29	20	22	33	17	27	23	30	23	50	31	33.1	23.54
Cu	85	106	52	62	49	65	80.5	77	52	79	78	29	91	97.3	73.12
Ni	327	124	124	115	161	358	151.5	195	235	234	201	44	115	115.4	213.27
Cr	29	207	383	244	94	300.5	322.5	1210	1520	239	623	43	183	356.1	805
TiO_2	0.19	0.56	0.39	0.26	0.19	0.295	0.285	0.32	0.28	0.32	0.35	0.62	0.43	0.38	0.3
V	NA	NA	NA	NA	NA	166	180	NA	NA	NA	NA	NA	NA	197.5	173
Ce	0	0	1	0	0	1	3	0	0	0	0	0	0	1.13	1.67
Ba	0	0	0	0	0	0	0	0	0	0	0	0	0	0	
Mg#	0.82	0.75	0.79	0.8	0.8	0.84	0.83	0.83	0.83	0.8	0.82	0.71	0.77	0.78	0.82
Zr/Y	2.8	2.6	2.4	2.3	2.3	3.4	1.5	1.8	1.8	2.1	1.8	1.5	1.4	1.82	2.13
Cr/Ni	0.1	1.7	3.1	2.1	0.6	0.8	2.1	6.2	6.5	1	3.1	1	1.6	2.9	3.9

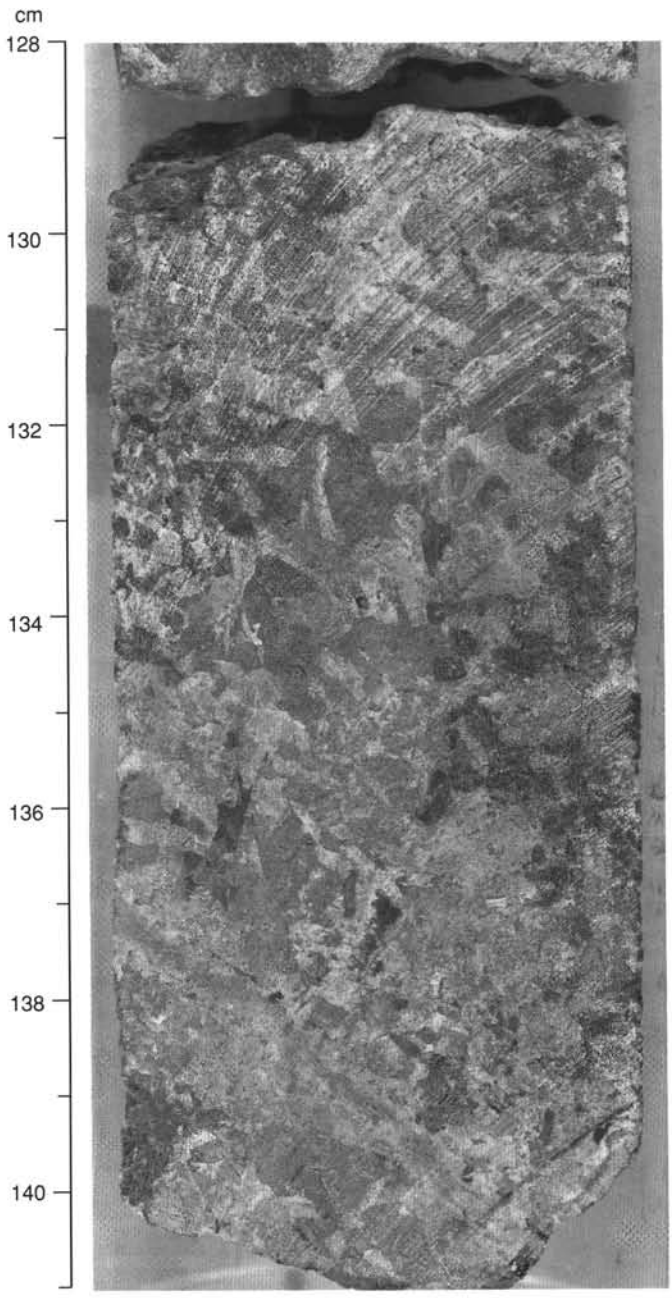

Figure 29. Sample 153-921E-7R-1, 128–141 cm. Poikilitic olivine gabbro displaying a heterogeneous texture and grain-size distribution. Olivine (dark gray) and clinopyroxene (light gray) are irregularly distributed through the rock and are both poikilitic. The grain size varies from medium-grained in the bottom left and upper right, to coarse and very coarse-grained in a diagonal band across the center of the specimen. A chlorite vein cuts the bottom right of the specimen.

strongly altered samples were taken in order to characterize the extent of alteration in intervals where fresh material was unavailable. Samples weighing 35–55 g were prepared from quarter-cores or from minicores used for measuring paleomagnetic and physical properties.

In addition to the standard sample designation (hole, core, section, and interval in centimeters), Table 4 includes information on the nominal depth in meters below seafloor (mbsf), the unit number within the respective hole and a rock name code for each sample. The range of rock types analyzed includes 17 olivine gabbros, 3 gabbros, 2 diabases, 2 gabbronorites, 1 metagabbro, 1 troctolite, 1 olivine microgabbro, and 1 oxide gabbro.

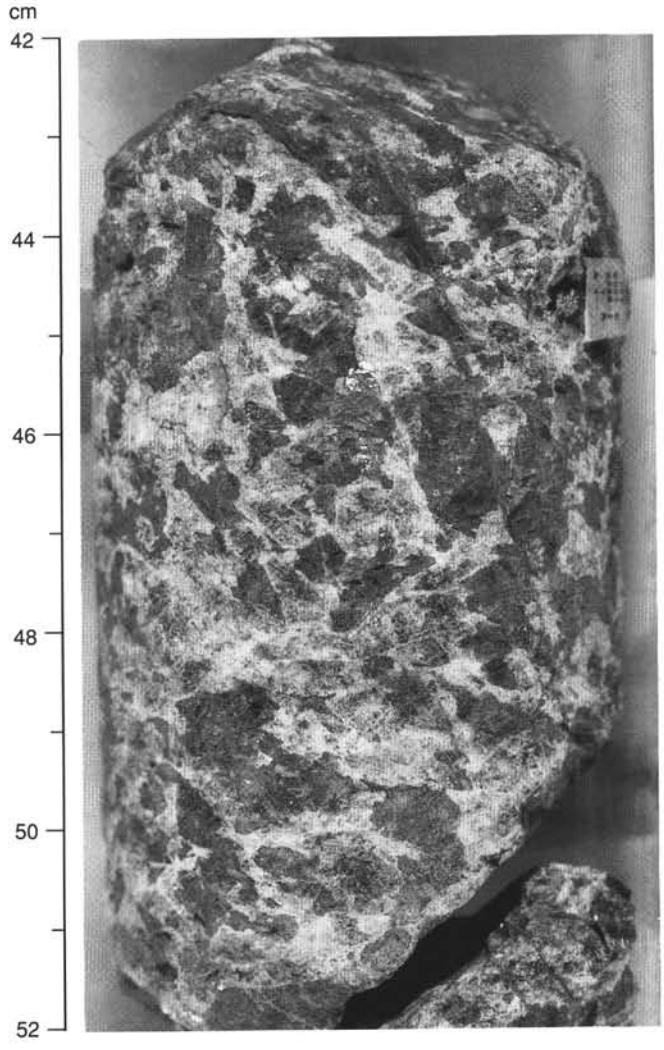

Figure 30. Pegmatitic gabbro, Sample 153-921E-8R-1, 42–52 cm. Plagioclase is fine grained and clinopyroxene shows fragmentation of grains. See front face of this same core piece in Figure 9.

A brief summary of the petrographic features of the samples analyzed is given in Table 5. In general, the rocks are composed of plagioclase (44%–78%), clinopyroxene (4%–42%), and olivine (0%–14%) with trace amounts of iron oxide and sulfide minerals; a more detailed description of the petrographic and mineralogical characteristics of the gabbroic rocks from Site 921 is given in the preceding parts of this section.

Gabbro and Olivine Gabbro

Most of the analyzed samples from Site 921 are olivine gabbros, although even within this single rock type, modal proportions of mineral phases vary significantly (55%–69% plagioclase, 0%–20% olivine, and 11%–38% clinopyroxene). Nevertheless, this variation can be reduced to two major gabbroic lithologies. Type 1 consists of gabbro and olivine gabbro in which brown clinopyroxene occurs as a cumulus phase. These rocks are mostly from the lineated gabbro and pegmatitic gabbro rock types described above. Type 2 consists of olivine gabbro and troctolite in which the clinopyroxene is poikilitic and generally emerald green, and which principally comes from sections of poikilitic olivine gabbro. Type 1 samples are principally gabbro and olivine gabbro in Unit 1 in Hole 921A, Unit 3 in Holes 921B and 921C, and Units 1 and 3 in Hole 921E. Portions of Unit 1 in Hole 921D may also be a part of this group, but their relationships

Table 5. Petrographic summary for samples analysed by XRF.

Core, section, interval (cm)	Piece	Depth (mbsf)	Unit	Rock	Type	Alteration (%)	Grain size	Olivine		Cpx		Opx		Plagioclase		Accessory minerals			
								Original	Relict	Original	Relict	Original	Relict	Original	Relict	Sulfides	Magnetite	Apatite	Zircon
153-921A-																			
2R-1, 34–38	5	8.04	1	Olivine gabbro	1	1	f-c	14	13	27	27			59	59		1		
153-921B-																			
1W-1, 64–67	9	0.64	1	Metagabbro	1*	67	m			18	5			78	29		5	tr	tr
1W-2, 5–8	2	1.47	2	Diabase		30	f	0.5	0					1	1		2		
2R-1, 85–88	11	15.45	3	Gabbro	1		c	1	0.7	38	31	1	1	60	45	tr			
3R-1, 16–20	2	24.66	3	Olivine microgabbro	1	2	f	10	9	35	34			55	55		tr		
3R-1, 134–137	13	25.84	3	Gabbro	1	1	m-c	1.6	1	42	42			56	56	tr	tr		
4R-1, 59–65	6B	34.69	4	Olivine gabbro	2	2	m-c	15	14	20	19			65	65	tr	tr		
4R-3, 77–83	8	37.73	4	Troctolite	2	4	c	15	12	4	3			81	81		tr		
153-921C-																			
2R-1, 7–10	1	10.07	2	Diabase		30	f	0.5	0					1	1				
2R-1, 113–116	14	11.13	3	Olivine gabbro	1	5	f-m	16	12	21	20			62	62		1		
2R-2, 114–117	10	12.54	4	Olivine gabbro	2	2	m-c	8	6	36	36			56	56	tr	tr		
3R-1, 83–89	5B	20.43	4	Olivine gabbro	2	3	m-c	6.5	4.5	38	37			56	56	tr	tr		
153-921D-																			
2R-1, 55–60	6	10.35	1	Gabbronorite	3	5	c			23	22	5	3.3	73	73	tr	1		
4R-1, 54–59	6b	29.84	1	Oxide gabbro	3	9	c			40	31			44	40	3	16		
5R-1, 118–121	12C	40.08	1	Olivine gabbro	2	1	c	6	5.5	28	27			66	66		tr		
5R-2, 56–63	5	40.91	1	Olivine gabbro	2	3	c	22	19	8	8			70	70		1		
153-921E-																			
2R-2, 24–30	1	11.39	1	Olivine gabbro	1	2	c	6	5	37	36			56	56		1		
3R-1, 138–144	15	21.18	2	Olivine gabbro	2	9	c	15	12	20	15			65	64		1		
4R-1, 44–50	5	30.14	2	Olivine gabbro	2	8	m	7	5	26	23			66	63				
5R-2, 125–131	7	41.89	2	Olivine gabbro	2	6	c-m	20	16	11	9			69	69				
6R-1, 97–101	11B	50.47	2	Olivine gabbro	2	4	c	24	21	7	6			68	68		1		
6R-2, 45–48	4	51.45	2	Olivine gabbro	2	2	m	10	9	25	24			65	65	tr	tr		
7R-1, 92–96	9A	60.32	2	Olivine gabbro	2	3	c	15	14	30	29			55	54	tr	tr		
7R-2, 77–83	3	61.58	2	Olivine gabbro	2	21	c	5	4	30	10			65	65	tr	tr		
7R-3, 83–86	2	62.98	2	Olivine gabbro	2	3	c	12	10	30	29			57	57	tr			
7R-3, 93–94	2	63.08	2	Olivine gabbro	2	3	c	20	18	20	19			60	60	tr	tr		
8R-1, 56–62	8	69.56	3	Gabbronorite	3	16	c			20	15	20	19	60	50		tr		
9R-1, 52–58	4	79.12	3	Gabbro	1	1	c	2	1.5	33	33			65	65		tr		

Notes: All modes visually estimated from thin section except Sample 153-921B-2R-1, 85-88 cm, which is visually estimated from macroscopic inspection of the core. Percent minerals listed for diabase refer to phenocryst phase abundances. Type = lithologic type defined on the basis of mineralogical and geochemical characteristics (see text for discussion). Abbreviations: tr = trace, f = fine grained, m = medium grained, c = coarse grained. *Type designation for Sample 153-921B-1W-1, 64–67 cm is based on mineralogy of inferred protolith.

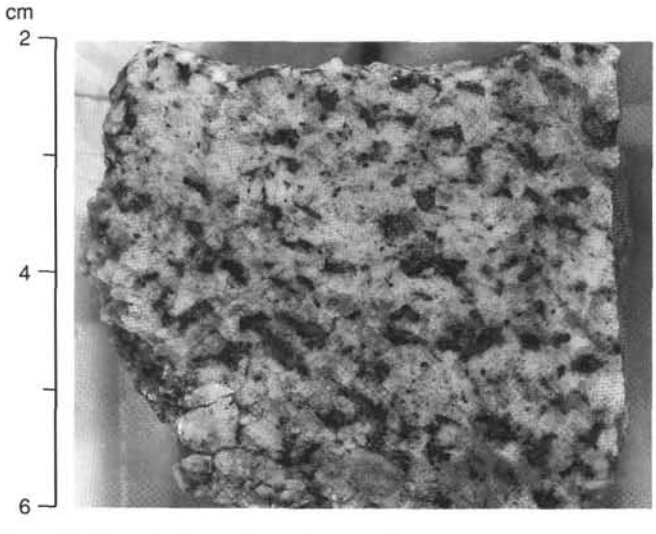

Figure 31. Quartz diorite consisting of zoned plagioclase-quartz and interstitial hornblende(?) altered to actinolite and chlorite. This sample is the first piece below the contact between Units 2 and 3 in Hole 921E. Sample 153-921E-8R-1, 2–6 cm.

are less clear. The Type 2 group corresponds predominantly to olivine gabbro and poikilitic olivine gabbro in Unit 4 in Holes 921B and 921C and Unit 2 in Hole 921E. Metagabbro in Unit 1 in Holes 921B and 921C was also sampled.

The modal proportions of plagioclase, clinopyroxene, and olivine are highly variable within both lithologic groups, and there is no systematic difference in the modal abundance of phases between them (Table 5). In addition to these two major lithologic types, gabbronorite and oxide gabbro occur as volumetrically minor intervals principally in intervals in which Type 1 rocks are found; these rock types are loosely grouped as Type 3.

Average compositions of Type 1 and Type 2 gabbroic rocks are listed in Table 4; because of the small number of analyses available for the gabbronorites and oxide gabbro, Type 3 data have not been averaged. Comparisons of Type 1 and Type 2 averages show that Type 1 gabbros have higher contents of SiO_2, Fe_2O_3, and Na_2O as well as incompatible trace elements (e.g., Zr, Y) and lower abundances of compatible trace elements (e.g., Cr and Ni). Al_2O_3 is also slightly lower in Type 1 gabbroic rocks, whereas MgO and CaO are present in similar abundances in the two groups. Mg#s average slightly less in Type 1 gabbroic rocks.

By comparison with the two predominant lithologic groups, gabbronorite is recognizable geochemically by significantly higher SiO_2, Fe_2O_3, TiO_2, Na_2O, Y, and Zr, and lower Mg#, Cr, Ni, and Cu. Al_2O_3 is quite different between the two gabbronorite samples analyzed from Site 921 (Samples 153-921D-2R-1, 55–60 cm, and 153-921E-8R-1, 56–62 cm), which reflects the different modal proportions of plagioclase and pyroxene in these samples.

Although iron oxide-rich gabbro occurs in several intervals at Site 921, it is, volumetrically, a minor component of the core. Therefore, only one interval of oxide gabbro was sampled for shipboard analysis. Sample 153-921D-4R-1, 54–59 cm, is significantly different from the other gabbroic rocks analyzed, having much higher Fe_2O_3 (13.21 wt%) and TiO_2 (3.41 wt%) contents, but lower Al_2O_3, SiO_2, Cr, and Ni. The relationship of oxide gabbro to other gabbroic rocks at Site 921 is unclear. The oxide gabbros are typically associated with zones of intense deformation, and it is not clear whether they are primary layers or related to injections of evolved magma into the gabbroic cumulates. Geochemically, they are among the most evolved compositions recovered and their association with felsic veins may not be fortuitous. However, limited data precludes determining whether they are derived from either major lithologic type encountered. It may be significant, however, that oxide gabbro occurs most commonly in gabbroic sequences with Type I compositions that appear to be more evolved and enriched in incompatible trace elements.

Metagabbroic rocks are also relatively uncommon at Site 921, occurring most conspicuously in Units 1 of Holes 921B and 921C. Only one sample (Sample 153-921B-1W-1, 64–70 cm) of metagabbro was analyzed. The sample selected is pervasively altered (67% total alteration). It is believed that the high degree of alteration of this section is caused by intense deformation and hydration associated with closely spaced cataclastic shear zones. The protolith of the metagabbroic rocks in both Holes 921B and 921C is mineralogically and texturally similar to gabbro downsection, suggesting these are not distinct gabbroic packages but are portions of the same rocks that differ in their degree and style of alteration and deformation. Compositionally, compared to less altered gabbro, the metagabbro analyzed has higher SiO_2, Na_2O, and P_2O_5, but lower CaO; it also has significantly higher concentrations of all the incompatible trace elements (Nb, Zr, Y, and Zn; Table 5). It also has a high H_2O content (1.91 wt%), consistent with the abundance of secondary hydrous phases (e.g., actinolite, brown amphibole, chlorite, epidote, and clay minerals) observed in thin section.

The geochemical differences between these rock types are shown graphically in Figure 32 where representative major-element oxides and trace elements are plotted against Mg#. Collectively, the trends are consistent with derivation as cumulates of progressively more-evolved basic magmas. With the exception of the oxide gabbro, SiO_2, TiO_2, and Na_2O show a well-defined negative correlation with Mg#, especially in the range 0.6 to 0.9. The distribution of Al_2O_3 against Mg# (not shown) shows no obvious correlation, but CaO shows a broad decrease with decreasing Mg#. However, the distribution is more scattered at high Mg#s, with a few samples trending to low CaO contents. Similarly, Al_2O_3 is poorly correlated relative to indices of magmatic evolution (Mg#), but the CaO/Al_2O_3 ratio shows a well-defined negative correlation relative to percent modal plagioclase (Fig. 33) as well as against Sr abundance (Fig. 33). This indicates that modal plagioclase content is controlling the abundance of these elements in the bulk rock. Although these may reflect a primary compositional difference resulting from cumulus processes, it may also be a function of sample sizes that are too small to homogenize the modal heterogeneity in coarse-grained rocks. Such results may be skewed toward a particular cumulus phase rather than reflect the true bulk composition of the mineral assemblage. Distinguishing between these two possibilities will require detailed shore-based mineral chemistry studies.

Shown for reference in Figure 32 are the data for the Hole 735B gabbro. The two data sets substantially overlap, although the extremes of the compositional range seen in the Hole 735B suite are not present in this preliminary data set from Site 921. It is not necessarily an indication that such compositions are absent from Site 921. In fact, intervals of oxide-rich gabbro and other evolved compositions (including diorite) were recovered at Site 921, but only one oxide gabbro was sampled for shipboard analysis. Nonetheless, a broader range of compositions have been analyzed from gabbroic rocks recovered from dredging nearby on the Mid-Atlantic Ridge (Miyashiro and Shido, 1980; Tiezzi and Scott, 1980)

Incompatible trace elements such as Y and Zn from Site 921 show well-defined negative correlation with Mg# (Fig. 32), consistent with either derivation of the gabbro from progressively evolved melts and/or with increasing percentage of trapped intercumulus melt at lower Mg#. In general, the Type 2 poikilitic olivine gabbro has lower Y and Zn than Type 1 gabbro and Type 3 gabbronorites and oxide gabbro. Sr contents show a negative correlation with the CaO/Al_2O_3 ratio, as do plagioclase modal proportions (Fig. 33).

Highly compatible trace elements (Ni and Cr) show a wide range of concentrations over a very small range in Mg values (Fig. 32G and H). For Mg numbers greater than 0.8, Ni ranges from 155 to 358 ppm, whereas for Mg# values less than 0.8, Ni ranges from 44 to 128 ppm.

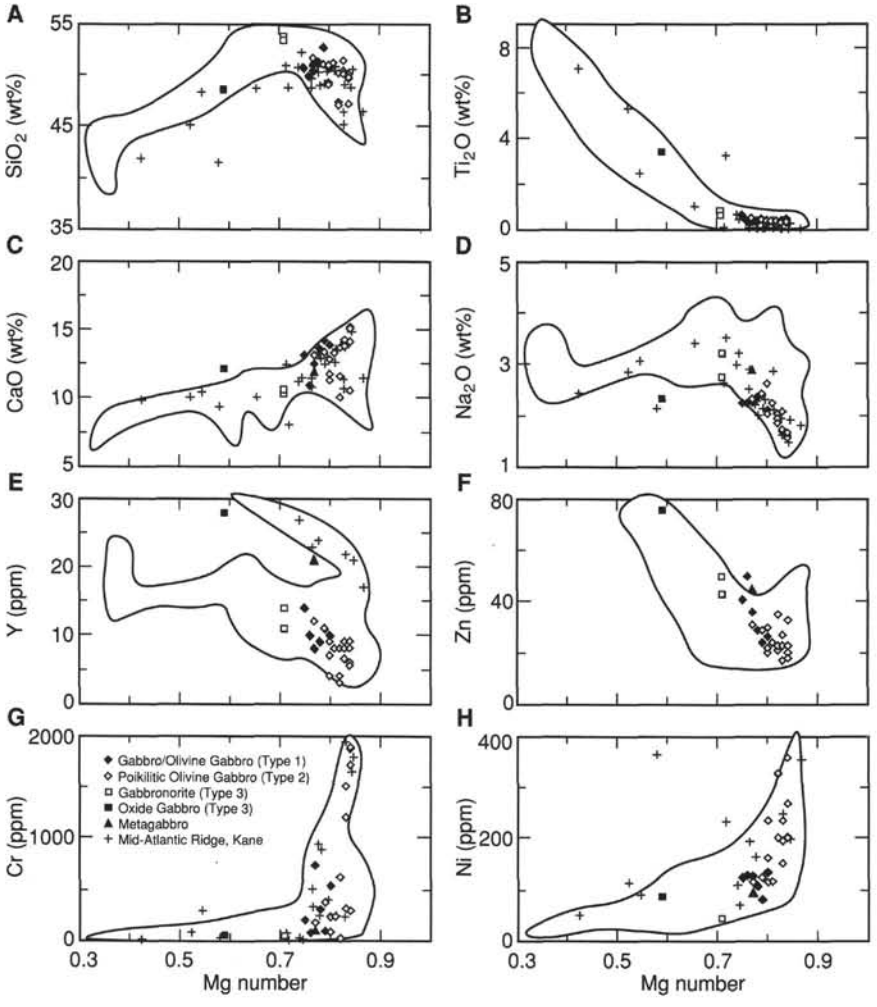

Figure 32. Mg#s vs. SiO_2, TiO_2, CaO, Na_2O, Y, Zn, Cr, and Ni in gabbroic rocks from Site 921. Data for Hole 735B (white field) from Leg 118 *Initial Reports* volume. Data for Mid-Atlantic Ridge gabbroic rocks from Miyashiro and Shido (1980) and Tiezzi and Scott (1980).

These variations reflect not only differences in the modal proportions of olivine and clinopyroxene within any particular sample, but also differences in the chemical compositions of the mafic phases in the samples. Ni contents typically are high in all olivine-rich gabbros from Site 921, but they are particularly high in poikilitic olivine gabbro. Type 2 poikilitic olivine gabbro has Ni contents greater than 100 ppm and values reach as high as 358 ppm.

In addition, although the range of values is large and overlaps that of other gabbro types, the Type 2 gabbros contain the highest Cr contents (up to 1896 ppm) and Cr/Ni ratios (up to 9.4; Fig. 34), particularly in those samples containing green oikocrystic clinopyroxene. In contrast, Type 1 gabbro and olivine gabbro have a more restricted range of Ni and Cr concentrations (81–135 ppm and 86–545 ppm, respectively) and the evolved rocks (gabbronorite and oxide gabbro) exhibit only a very limited range of Ni and Cr values (44–87 ppm and 43–57 ppm, respectively). These differences demonstrate the greater modal heterogeneity within the Type 2 poikilitic olivine gabbro when compared with Type 1 gabbroic rocks recovered at Site 921. They also tend to indicate that the melts in equilibrium with the Type 2, Type 1, and Type 3 rocks were in equilibrium with progressively more evolved magmas, although there is considerable overlap between Type 1 and Type 2 samples based on fractionation indices (e.g., Mg#).

The amount of bound water (and/or CO_2) in the gabbroic rocks can be estimated from determinations of loss on ignition (LOI) and more directly through measured H_2O and CO_2 contents. CO_2 contents are uniformly low (<0.06 wt%), but H_2O contents range from 0.23 to 2.96 wt%. Although LOI and H_2O contents are positively correlated, the H_2O contents are nearly always higher than the LOI, because the

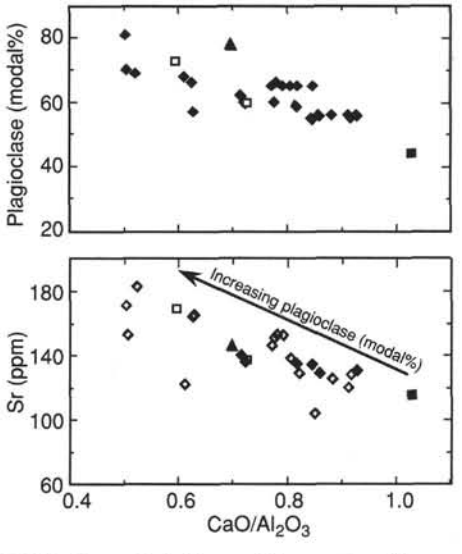

Figure 33. CaO/Al_2O_3 vs. plagioclase modal percent and Sr concentration (in ppm) in gabbroic rocks from Site 921. CaO and Al_2O_3 in weight percent. Symbols as in Figure 32.

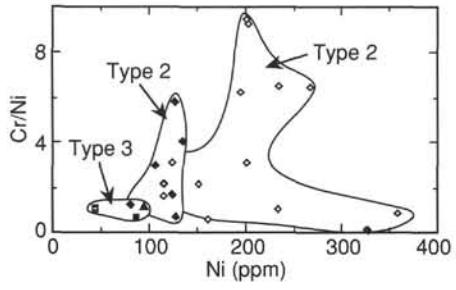

Figure 34. Cr/Ni vs. Ni in gabbroic rocks from Site 921. Symbols as in Figure 32.

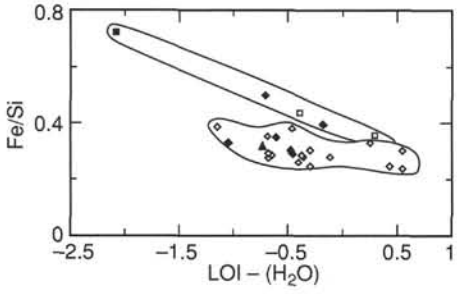

Figure 35. Fe/Si vs. LOI–H_2O in gabbroic rocks from Site 921. Symbols as in Figure 32.

weight loss on ignition is offset by the weight gain due to oxidation of the ferrous iron. Figure 35 shows a negative correlation observed between Fe content (normalized to Si) and the difference between the measured H_2O and the loss on ignition. The data appear to fall into two groups that have slightly different slopes. One group has a fairly shallow negative slope and predominantly consists of the Type 2 poikilitic olivine gabbro, but includes some Type 1 olivine gabbro. The other group has a steeper negative slope and includes the more evolved Type 3 gabbronorites and oxide gabbro as well as some Type 1 gabbro. This diagram demonstrates that for a given Fe/Si ratio, Type 2 poikilitic olivine gabbro tends to show a greater discrepancy between the LOI and the measured H_2O than the Type 1 and Type 3 rocks. Since there is no consistent difference in total alteration between the two groups, these trends must reflect the greater primary Fe^{2+}/Fe^{3+} in Type 2 gabbro. In these data the measured H_2O content is a better indication of the percent total alteration than the loss on ignition.

Although the LOI and H_2O contents generally correlate with degree of alteration estimated visually from hand specimen and/or thin section, this is not always the case. Sample 153-921E-6R-1, 97–101 cm, has the highest H_2O content and LOI recorded in the Site 921 samples, yet the thin-section description of this sample visually estimated only 4% total alteration. Gabbro in this section of the core displays rapid changes in the relative modal proportions of primary phases and in texture on a centimeter scale. Because this sample was taken as a minicore and the thin section was cut from the top surface, the residue of the sample ground and analyzed maybe significantly more altered than that represented in the thin section.

Diabase

Two diabase samples were analyzed: Samples 153-921B-1W-2, 5–8 cm, and 153-921C-2R-1, 3–7 cm. The results are listed in Table 6, with average values for whole-rock basalt and glass from the Kane Fracture Zone area. The two samples are sparsely phyric diabase, containing less than 2% total phenocrysts of olivine and plagioclase. Olivine phenocrysts and portions of the intergranular groundmass are

Table 6. Major oxide and trace element analyses for Site 921 diabase.

Hole:	921B	921C			
Core, section:	1W-2	2R-1			
Interval (cm):	5–8	3–7	Kane	Serocki	
Piece:	2	1	basalts	basalts	
Depth (mbsf):	1.47	10.03	average	average	
Unit:	2	2	$n = 52$	$n = 28$	NMORB
Major elements (wt%)					
SiO_2	49.08	50.19	49.99	50.22	
TiO_2	1.38	1.31	1.50	1.68	
Al_2O_3	16.96	16.89	15.95	16.14	
Fe_2O_3	9.39	9.49	9.62	9.69	
MnO	0.18	0.15	0.17	0.17	
MgO	7.99	7.61	8.12	7.60	
CaO	11.86	11.8	11.46	11.27	
Na_2O	2.58	2.69	2.55	2.94	
K_2O	0.01	0.02	0.14	0.18	
P_2O_5	0.08	0.07	0.16	0.17	
Total	99.51	100.21	99.66	100.06	
LOI	1.93	1.41			
H_2O	2.57	2.19			
CO_2	0.01	0			
Trace elements (ppm)					
Nb	2	2		4	2.33
Zr	84	84	106	128	74
Y	22	21	34	37	28
Sr	133	133	131	140	90
Rb	1	1	2.08	1.7	0.56
Zn	61	58	77	86	
Cu	72	76	68	62	
Ni	134	119	129	106	
Cr	303	283	287	228	
TiO_2	1.31	1.29			1.27
V	240	237	267	262	
Ce	8	11	9.81		7.5
Ba	9	0			6.3
Mg#	0.66	0.65	0.66	0.65	
Zr/Y	3.8	4.0	3.1	3.5	2.6

Notes: Mg# calculated as the molar ratio of $Mg/(Mg + Fe^{tot}*0.85)$. Average basalt from Kane Fracture Zone area from Bryan et al. (1981); average Serocki Volcano from Humphris et al. (1990). NMORB data from Sun and McDonough (1989).

partially altered to chlorite and clay minerals and the total alteration is visually estimated at 30%. This degree of alteration is reflected in the high values for LOI and H_2O, which range from 1.41 to 1.93 wt% and 2.19 to 2.57 wt%, respectively.

The two analyses are chemically very similar in both major and trace element abundances, suggesting that the two samples come from the same dike. The samples have relatively high Mg#s (0.65–0.66) but typical N-MORB compositions, particularly for the incompatible trace elements (see Table 6). In fact, Mg#s and TiO_2 contents are comparable to the parental magma composition (0.66 and 1.5 wt%, respectively) identified by Bryan et al. (1981) for basalt from the Kane Fracture Zone area (Table 6). This observation, combined with the high Ni and Cr contents (119–134 and 283–303, respectively) suggest that these rocks have undergone limited low-pressure fractional crystallization since generation in the mantle.

Diabases from Site 921 differ substantially from the high-MgO diabase samples analyzed from Site 920 (see "Igneous Petrology," "Site 920," this volume), having lower compatible elements (MgO, Ni, and Cr), and higher incompatible elements (TiO_2, P_2O_5, Zr, Y, Zn, and Cu). The lower Mg numbers of the Site 921 diabase samples (0.65–0.66 vs. 0.77–0.79) suggest that they are more evolved than those from Site 920 (see "Igneous Petrology," "Site 920," this volume). Nevertheless, ratios of incompatible trace elements suggest that the diabase samples from Sites 920 and 921 could be generated from similar source regions. Because the partition coefficients between crystals in mafic liquids and melt are low for both Zr and Y, these elements are not easily fractionated relative to one another during crystallization processes. They can, however, be fractionated during small degrees of partial melting. Figure 36 shows that the ratios for Sites 920 and 921 diabase are indistinguishable; both sites are similar

to, although slightly higher than, the average erupted basalt compositions from the Kane Fracture Zone area (Bryan et al., 1981) and from Serocki Volcano (Humphris et al., 1990).

Cross-hole Correlation

A possible correlation of units between the Site 921 holes is presented in a southwest to northeast section (Fig. 37). The relative positions of the holes with regard to their depths in mbsf are also indicated.

Deformed gabbro and olivine gabbro in the tops of Holes 921A, 921B, and 921C are correlated on the basis of their similar textures and composition. Gabbro in these units is generally olivine-poor (<10%), clinopyroxene is nearly always dark brown and cumulus, and grain-size layering on the scale of 1 to 10 cm is common. They typically have Type 1 geochemical characteristics: lower Mg#, Cr, Ni, higher TiO_2, and incompatible trace-element abundance. Included within these intervals are deformed oxide gabbro that have more evolved Type 3 geochemical characteristics. Ductile deformation is evident as widespread recrystallization of plagioclase and olivine, and the localized development of a preferred mineral elongation defined by alignment and/or recrystallization of pyroxene.

A probable correlation of this rock type with at least the upper part of Hole 921D is indicated, but because of limited recovery and a slightly greater degree of alteration, only one unit was defined in this hole. The top of Hole 921D contains gabbronorite, gabbro, and olivine gabbro that have brown clinopyroxene as a cumulus phase, as well as an interval of oxide gabbro, a similar association to that observed in the deformed gabbroic rocks. In addition, the samples analyzed from this interval have Type 3 geochemical characteristics.

Poikilitic olivine gabbro in Holes 921B and 921C, and possibly at the base of Hole 921D, are correlated on the basis of (1) the olivine-rich composition, typically olivine gabbro but ranging up to troctolite in very thin bands, (2) the typical occurrence of a weak fabric in plagioclase that defines a magmatic mineral alignment, (3) the presence of distinct modal layering and laminations, (4) the presence of green clinopyroxene as a cumulus and oikocrystic phase, (5) the similar, very weak to absent development of a deformation fabric, and (6) high MgO and Ni contents typical of the Type 2 geochemical group.

Although Hole 921E is relatively far from the other Site 921 holes, the heterogeneous poikilitic olivine gabbro (Unit 2) in this hole displays similar macroscopic and geochemical characteristics to Unit 4 in Holes 921B and 921C, and therefore these two units are tentatively correlated. Olivine-rich gabbro in the bottom of Hole 921D has high Mg#s, and Cr and Ni contents, combined with low Y, Zr, and Zn concentrations, which suggests that they are similar to the Type 2 poikilitic olivine gabbro, and therefore correlate with these units in Hole 921B and 921C. However, one of the Type 1 samples in Hole 921D (Sample 153-921D-5R-1, 118–124 cm) has higher SiO_2 and Na_2O than other Type 1 gabbro and may be intermediate in composition between Types 1 and 2.

The pegmatitic gabbro in the top of Hole 921E is not directly correlated with any units in Holes 921A, 921B, 921C, and 921D. It is nonetheless similar in modal mineralogy to undeformed gabbro that contains only brown cumulus clinopyroxene in Holes 921A and 921B. The one sample of pegmatitic gabbro analyzed from this unit has Type 1 geochemical characteristics consistent with this correlation.

Diabase in Holes 921B and 921C are correlated on the basis of their proximity, similar apparent thickness and similar chemical compositions. The relationship to a single piece of diabase in Hole 921D (Section 153-921D-5R-1, Piece 2) is unclear. All three intersections of diabase are associated with conspicuous alteration zones in the adjacent gabbro.

Discussion

The proposed cross-hole correlation suggests that there are two, or possibly three, major gabbroic units within the Site 921 holes. These units are (1) gabbroic rocks typified by the presence of brown cumulus clinopyroxene, olivine abundance typically in the range 0%–10%, and the absence of well developed poikilitic textures, and (2) poikilitic olivine gabbroic rocks containing green intercumulus clinopyroxene, 10%–25% olivine, and typified by the presence of oikocrysts of clinopyroxene in excess of 25 mm in size. The pegmatitic gabbro defined as Unit 1 in Hole 921E may be a separate gabbro unit, but it is macroscopically similar to the gabbroic rocks in that it typically contains brown cumulus pyroxene as the predominant mafic phase.

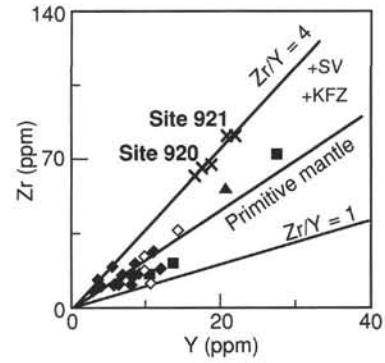

Figure 36. Zr vs. Y for diabase (crosses) from Sites 920 and 921 and gabbroic rocks from Site 921 symbols for gabbroic rocks (Fig. 32). SV = average Serocki Volcano (Humphris et al., 1990); KFZ = average erupted basalt from the Kane Fracture Zone area (Bryan et al., 1981).

Optical determinations of plagioclase compositions suggest that all of these rocks have similar plagioclase compositions within the range An_{45} to An_{80}. The pegmatitic gabbro apparently has a more restricted range of compositions (An_{55} to An_{70}), but the number of determinations is few. The overall variability of plagioclase compositions is caused by the evolution of magmas from which they crystallized. Variability of plagioclase compositions within individual samples could be caused by evolution of intercumulus melts.

Ternary plots of modal mineralogy illustrate the considerable heterogeneity for gabbro sampled from Site 921, particularly for the poikilitic olivine gabbroic rocks that show a greater degree of olivine enrichment (Fig. 38). However, the ranges of poikilitic olivine gabbro and lineated gabbro overlap considerably. The pegmatitic gabbro shows a greater tendency to pyroxene enrichment than either of the other two major gabbro types.

The differences between the poikilitic olivine gabbro and other gabbroic rocks are also apparent when modal and geochemical data are compared as a function of depth. Figure 39 shows data plotted for Hole 921E in which there are a significant increase in the maximum modal abundance of olivine in the poikilitic olivine gabbro compared with the overlying pegmatitic gabbro and underlying varitextured gabbro units. This trend corresponds with an increase in Mg# and a decrease in TiO_2 content in the poikilitic olivine gabbro. The range of modal olivine abundance is high, with minimum values similar to those in pegmatitic and lineated gabbro. The modal olivine and TiO_2 data are gradational across the boundary between pegmatitic and poikilitic gabbros but change rapidly across the lower contact between poikilitic olivine gabbro and underlying varitextured gabbro. The higher Mg#s within poikilitic olivine gabbro indicate that the melts from which these rocks crystallized were significantly more primitive than those in equilibrium with both the pegmatitic (Unit 1) and varitextured (Unit 3) gabbro. In addition, Mg# within the poikilitic olivine gabbro increases with depth, indicating that a range of primitive melt compositions existed during the crystallization of these rocks. A similar correlation between the mineralogy and geochemistry of the upper units in Hole 921E is observed in Holes 921B and 921C.

In contrast to the correspondence observed between mineralogy and elemental abundance trends with depth, ratios of highly incompatible trace elements (Zr/Y) show a gradual decrease in ratio with increasing depth, that is independent of unit boundaries (Fig. 36). Zr and

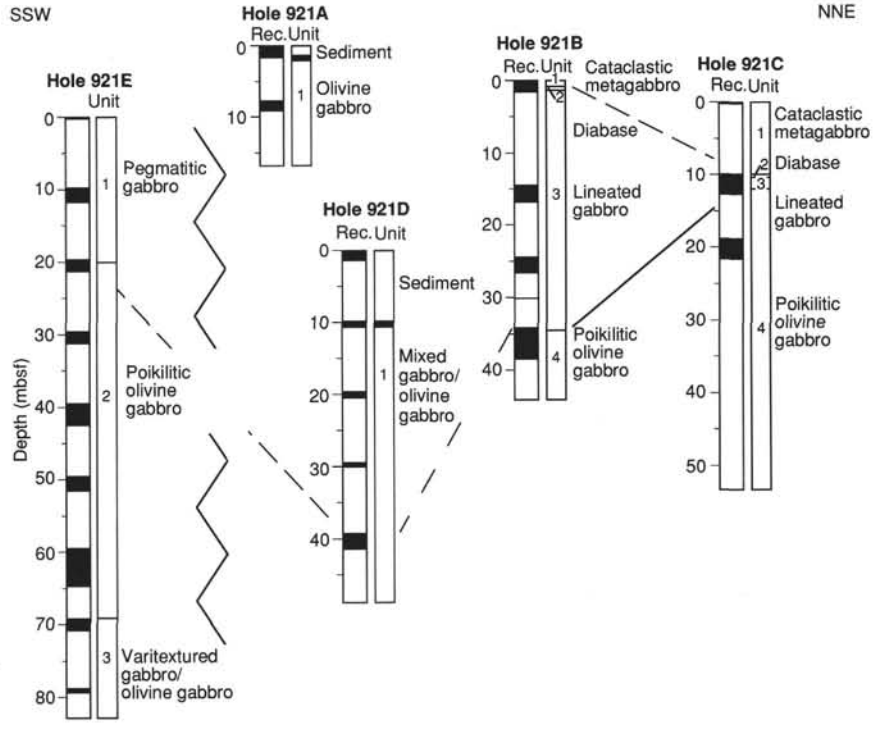

Figure 37. Proposed correlation based on petrological and geochemical characteristics for Site 921 drill holes. Holes reduced to a common datum (depth mbsf). Zig-zag line next to Hole 921E means that it is located over 200 m south of Hole 921A (see Figs. 1 and 2). Solid lines indicate correlations for which the evidence is strong; dashed lines indicate possible correlations.

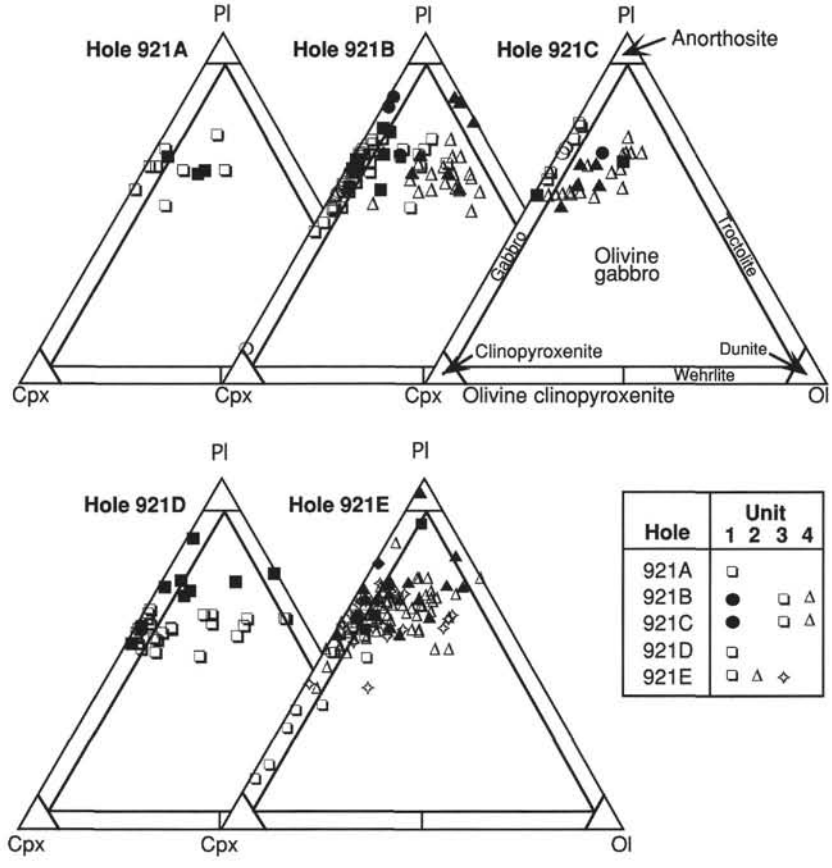

Figure 38. Modal proportions of olivine, plagioclase, and clinopyroxene plotted on the rock classification scheme used for this report (see "Explanatory Notes," this volume). Open symbols are estimates from visual core description, closed symbols are estimates from thin section.

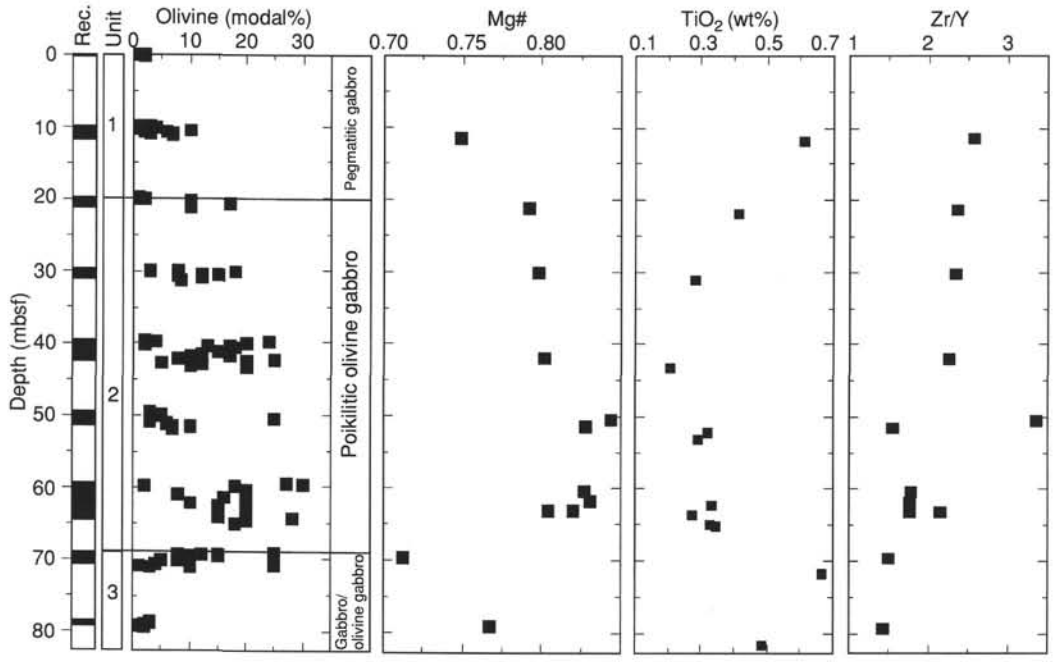

Figure 39. Plot of olivine (modal percent), Mg# (wt%), TiO_2, and Zr/Y against depth for Hole 921E. Modal data based on visual core descriptions.

Y are not easily fractionated relative to one another during crystallization of clinopyroxene, olivine, and plagioclase. This apparent trend may have implications for magma chamber or partial melting processes in the Site 921 gabbroic rocks as well as the postulated correlation between units, but must await shore-based studies to be resolved.

Thus there are both substantial differences and subtle similarities between the pegmatitic and lineated gabbroic rocks and the poikilitic olivine gabbroic rocks at Site 921. The differences are most apparent in the mineralogy, geochemistry, and extent of deformation within each of the units. Oxide gabbro and oxide gabbronorite crystallized from melts with relatively evolved compositions. Oxide-mineral rich layers and veins are most abundant in the pegmatitic and lineated gabbroic rocks, only occurring rarely in the more primitive poikilitic olivine gabbro. Felsic veins occur throughout the sequence, but those of trondhjemitic composition are most abundant in poikilitic olivine gabbro.

Basalt erupted from the vicinity of the Kane Fracture Zone tends to have among the highest Na_2O values for the Mid-Atlantic Ridge (Klein and Langmuir, 1987; Bryan et al., 1994), although values vary from 2.4 to 3.3 wt% (Bryan et al., 1981, 1994). The Site 921 diabase samples fall within the middle of this range, having the same values as the average basalt for this region (Klein and Langmuir, 1987). Using elements like Na_2O and FeO, Klein and Langmuir (1987) identified a correlation between averaged major-element compositions of MORB and regional average axial depth of the ridge. In particular, they noted that deeper ridges (such as the MARK area) tend to produce magmas that are higher in Na_2O, but have lower FeO and CaO/Al_2O_3 ratios at a given MgO content. The Site 921 diabase samples are consistent with Klein and Langmuir's observations.

METAMORPHIC PETROLOGY

Gabbroic rocks recovered at Holes 921A through 921E show varying intensities of metamorphism ranging from pervasive in the lineated gabbros and interlayered cataclastic intervals, to slight (less than 10%) in most undeformed gabbroic rocks. Metamorphism at near magmatic temperatures resulted in dynamic recrystallization of plagioclase and, to a lesser extent, clinopyroxene and olivine. Lower temperature hydrous alteration of the gabbroic rocks, which overprints the high-temperature crystal-plastic fabrics, is dominated by static metamorphism. This background alteration is most intense near magmatic felsic veins filled by secondary plagioclase, quartz, amphibole, epidote, chlorite, rare prehnite, and oxide minerals, adjacent to late hydrothermal veins. Secondary minerals within the veins include actinolite, chlorite, and smectite. The background static metamorphism is associated with fine microfracture networks that facilitated fluid flow throughout the gabbroic sequences. In the following discussion, the principal features of alteration are described in terms of the relationships between metamorphic phases, deformation, and the thermal evolution affecting gabbroic rocks from Site 921.

Gabbroic rocks recovered at Site 921 include variably deformed olivine gabbros, poikilitic olivine gabbros, gabbronorites, oxide gabbros, gabbros, and coarse-grained to pegmatitic gabbros. Average alteration intensities throughout Holes 921A–E are generally slight (9% in Hole 921A) to moderate (15% in Hole 921D); however, alteration is heterogeneous, and replacement may reach values of 80%–90% locally (Figs. 40 and 41). This alteration is typically most intense adjacent to felsic magmatic veins and veinlets, and in cataclastic intervals where it is generally dominated by formation of secondary phases after olivine and clinopyroxene (Table 7).

Alteration of Primary Phases

Olivine

Alteration of olivine is heterogeneous throughout Holes 921A through 921E, and ranges from slight to pervasive. Fine-grained iron oxide minerals along microfractures and rimming grain boundaries typically represent the earliest alteration phase (Figs. 42 and 43). Later phases include talc, chlorite, and smectite, which commonly form complex pseudomorphs after olivine (Figs. 42, 43, 44, and 45; Table 7). In some samples, secondary phases form well-developed coronitic rims with talc and oxide minerals occurring in the cores of olivine grains, followed by actinolite-tremolite-rich bands, and an outer rim of chlorite adjacent to plagioclase grains. In some samples, olivine is also surrounded by a fine-grained mosaic of secondary orthopyroxene (Figs. 43 and 45). In any one sample, coronitic development is heterogeneous, and one or more alteration phases may be absent.

Clinopyroxene

Brown amphibole associated with clinopyroxene is the earliest hydrous mineral in Site 921 gabbroic rocks, where it occurs as blebs

Table 7. Site 921 metamorphic summary.

Lithology	Mineralogy: Primary	Mineralogy: Secondary	Fluid inclusions
Gabbroic rocks	Olivine	Talc, coronitic tremolite-actinolite-chlorite, chlorite-smectite, magnetite	
	Clinopyroxene	Secondary clinopyroxene, brown amphibole, pale green amphibole (cummingtonite?), chlorite, actinolite, smectite, magnetite	Clinopyroxene contains primary vapor-dominated, low-salinity inclusions
	Orthopyroxene	Secondary orthopyroxene, pale green amphibole (cummingtonite?), talc, chlorite, smectite, magnetite	
	Plagioclase	Secondary plagioclase, actinolite, chlorite, epidote, prehnite, clay	Plagioclase contains secondary vapor to liquid-dominated inclusions containing brines, low-salinity, low-temperature fluids, and methane?
	Apatite, zircon, titanite, magnetite		Apatite contains carbon dioxide-rich inclusions, brines, and low-salinity, low-temperature inclusions
Diabase	Olivine	Chlorite, magnetite, smectite	
	Clinopyroxene	Actinolite, chlorite, magnetite	
	Plagioclase	Secondary plagioclase, clay	Plagioclase contains secondary, liquid-dominated, low-temperature, low-salinity inclusions
	Groundmass	Smectite, chlorite	

Lithology	Vein types	Facies intensity
Gabbroic rocks	Magmatic: plagioclase, quartz, amphibole, pyroxene? Hydrothermal: amphibole, chlorite prehnite, actinolite, epidote, chlorite ± smectite, zeolite ± calcite veins	Amphibolite to zeolite, <5%–100% altered
Diabase	Chlorite + actinolite and chlorite + clay (smectite) veins	Greenschist to zeolite, 10%–85% altered

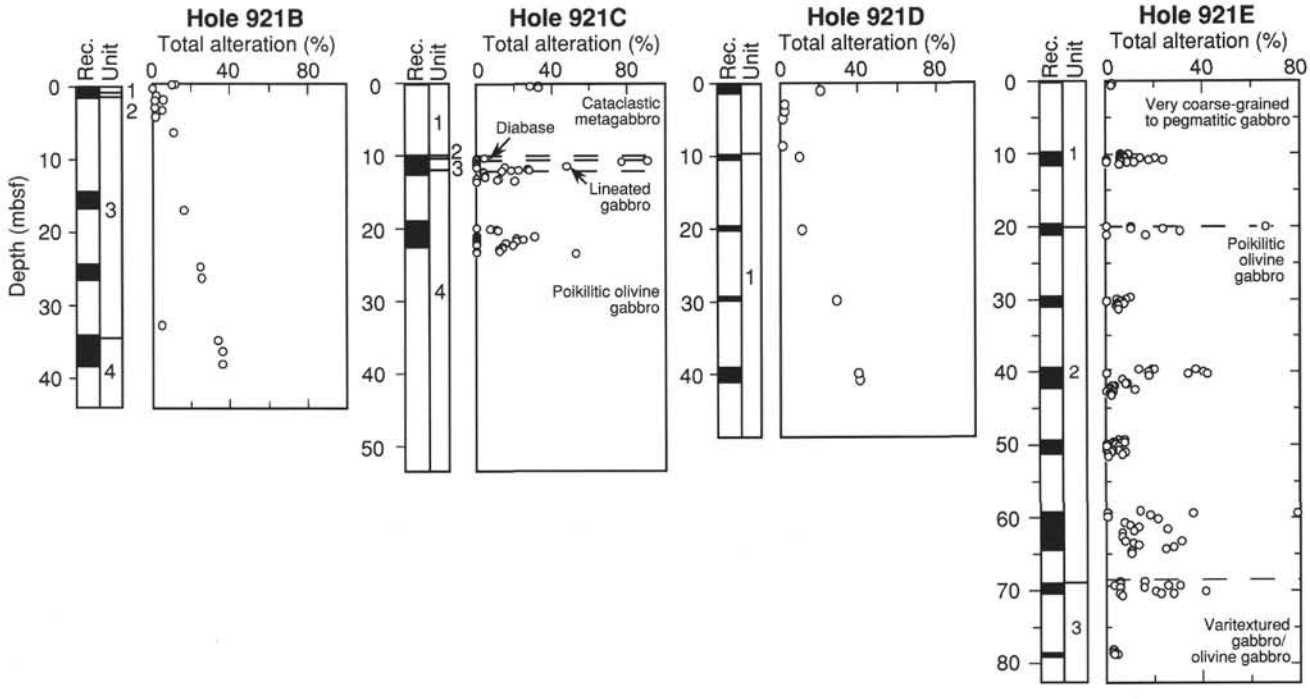

Figure 40. Downhole variation of total percent alteration in gabbroic rocks from Holes 921B, 921C, 921D, and 921E, from visual core descriptions.

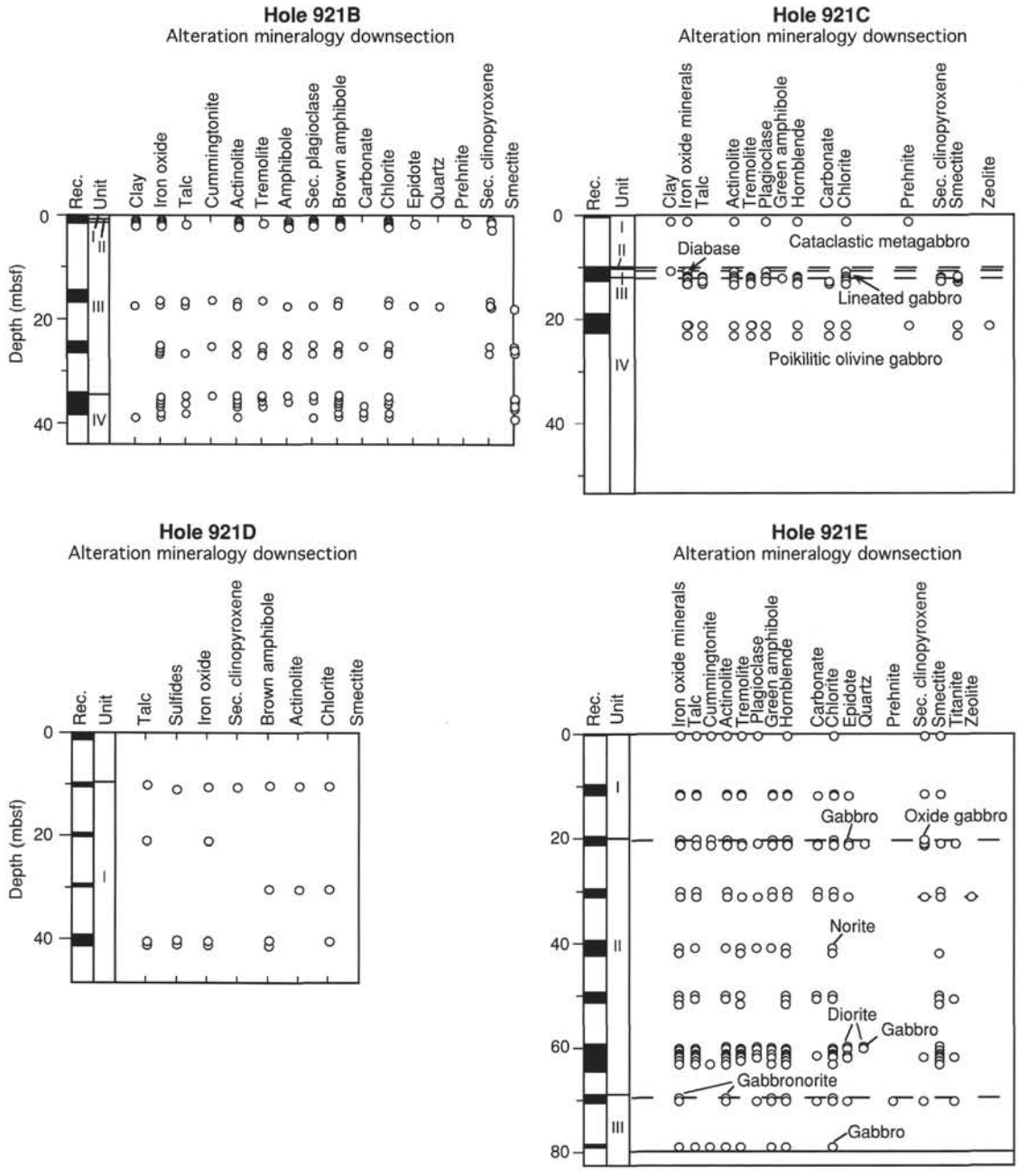

Figure 41. Downhole variability of the alteration mineralogy for Holes 921B, 921C, 921D, and 921E, based on thin-section descriptions.

along the cleavages and exsolution lamellae of clinopyroxene grains and as rims around clinopyroxene or iron-titanium oxide minerals (Figs. 45 and 46). Brown amphibole is ubiquitous throughout all gabbroic lithologies, though its modal abundance never exceeds 3% and is commonly below 1%, and it is generally rimmed or partly replaced by a light green, prismatic and/or fibrous amphibole.

Actinolite and chlorite compose the most common and abundant secondary phases after clinopyroxene in the gabbroic rocks, where they form fine-grained rims on clinopyroxene and adjacent plagioclase grains (clinochlore and pennine; Fig. 47). Secondary hydrothermal clinopyroxene occurs in minor amounts as fluid-inclusion-rich, irregular patches after primary clinopyroxene. It is a common phase in felsic veins that cut the gabbros (e.g., Sample 153-921E-3R-1, Piece 12, 107–113 cm), and in localized pervasively altered zones.

Orthopyroxene

Alteration of orthopyroxene is highly variable (<10%–100%), with finer grains commonly more intensely altered. Cummingtonite is common after orthopyroxene, and typically forms fine-grained fibrous rims along grain boundaries and fills crosscutting microfractures. It is associated with a fine-grained rust-colored mineral that in some samples gives orthopyroxene grains an oxidized appearance (e.g., 153-921D-R-1, Piece 6, 57–60 cm). In intensely altered zones,

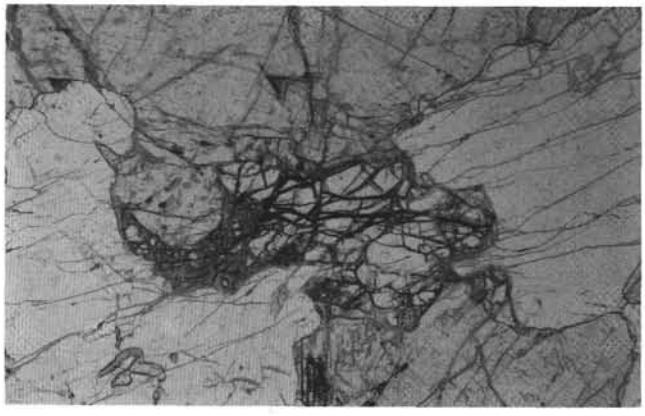

Figure 42. Typical alteration of olivine in relatively fresh gabbro: olivine is partially altered to smectite and cut by microfractures lined by iron oxide minerals (Sample 153-921E-7R-3, Piece 2, 93–94 cm). Field length is 3 mm; polarized light.

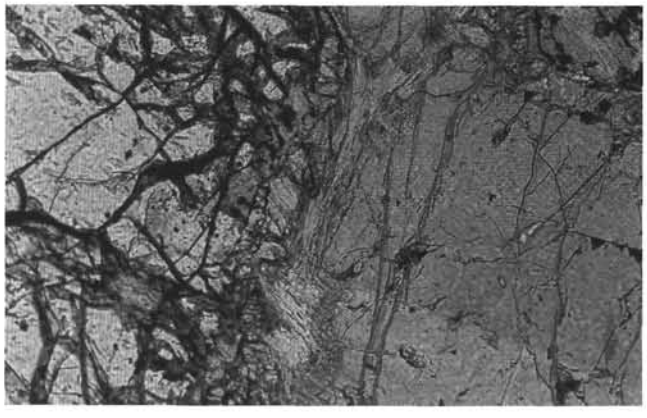

Figure 43. Acicular actinolite at the contact between plagioclase and relatively fresh olivine (Sample 153-921E-7R-2, Piece 1A, 4–7 cm). Field length is 1.5 mm; polarized light.

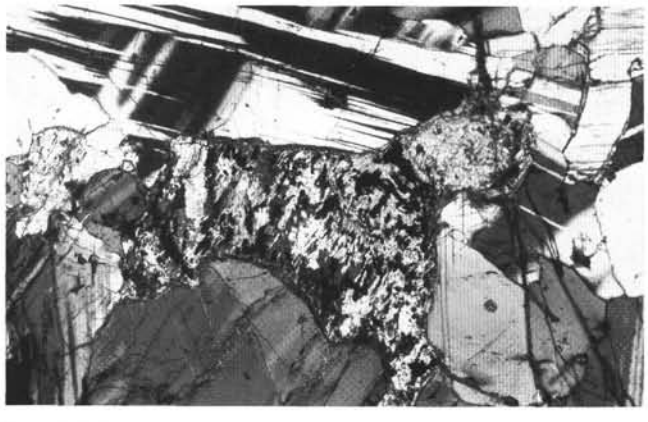

Figure 44. Complete replacement of olivine by fibrous talc, smectite, and iron oxide minerals (Sample 153-921D-5R-1, Piece 12C, 121–124 cm). Field length is 3 mm; polarized light.

amphibole completely replaces orthopyroxene, forming fine-grained fibrous patches.

Plagioclase

Plagioclase is generally slightly to moderately altered; many samples lack apparent alteration phases. Alteration predominantly

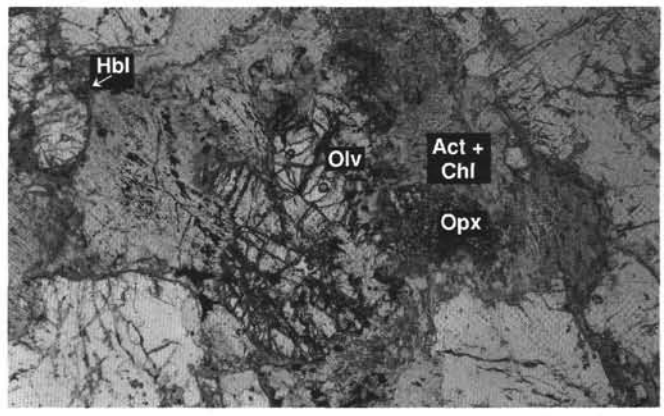

Figure 45. Fine-grained mosaic of secondary orthopyroxene (opx) forms dark patches around olivine (olv) (Sample 153-921E-4R-2, Piece 1B, 26–30 cm). Outer alteration rims of actinolite and chlorite (act + chl) are visible against adjacent plagioclase. Note also the thin rim of brown amphibole (hbl) around a clinopyroxene grain in the upper left corner of photograph. Field length is 3 mm; polarized light.

involves the formation of secondary plagioclase, though actinolite, chlorite, epidote, prehnite, and clay minerals are present locally as well. Alteration is most evident near irregular microcracks where secondary plagioclase occurs as discontinuous veinlets cutting plagioclase, and as irregular fluid-inclusion-rich patches (Figs. 43 and 48). Intensely altered grains are typically associated with cataclastic intervals, felsic veins and adjacent host rocks. In these areas, minor epidote, chlorite, and prehnite are common.

Alteration of Gabbroic Rocks

Olivine Gabbro

Olivine gabbros recovered from Site 921 are generally unaltered, with ≈65% of the rocks exhibiting only slight to negligible alteration intensities. Alteration is dominated by secondary phases after olivine, which commonly form complex intergrowths. Alteration intensities of olivine range from <10% to 100%, with replacement by variable amounts of talc, fine-grained iron oxide minerals, and smectite (Fig. 44). In many samples, olivine grains are only slightly altered, and alteration is limited to formation of minor oxide minerals. With progressive alteration, talc, amphibole, and smectite rim grain boundaries and form irregular patches (Figs. 43 and 45). Talc, amphibole, and oxide minerals form complex intergrowths after olivine in some samples (Fig. 44). Hornblende locally forms discontinuous rims around olivine. In highly deformed and strained zones that are common within the olivine gabbros (see "Structural Geology," this chapter), olivine exhibits deformation bands, heterogeneous grain-size reduction, and local development of fine-grained neoblasts that form elongate aggregates. Olivine in these zones is associated with fine-grained clinopyroxene, and together they compose mafic-rich bands that define a moderately to well-developed foliation in some samples (e.g., Sample 921B-1W-2, Piece 4, 26–29 cm). Clinopyroxene grains within the olivine gabbros are slightly to highly altered. Hornblende forms discontinuous rims and occurs as fine-grained blebs within clinopyroxene grains (Figs. 45 and 46A). Secondary clinopyroxene is rare. Plagioclase is generally only slightly altered, with alteration limited to minor fine microfractures filled with actinolite ± chlorite.

Gabbronorite

Rare gabbronorite intervals that occur in Holes 921D and 921E are moderately to highly altered and contain localized zones of dynamic recrystallization (e.g., Samples 153-921D-2R-1, Piece 6, 57–60 cm, and -921E-8R-1, Piece 8, 62–68 cm; see "Structural Geology," this

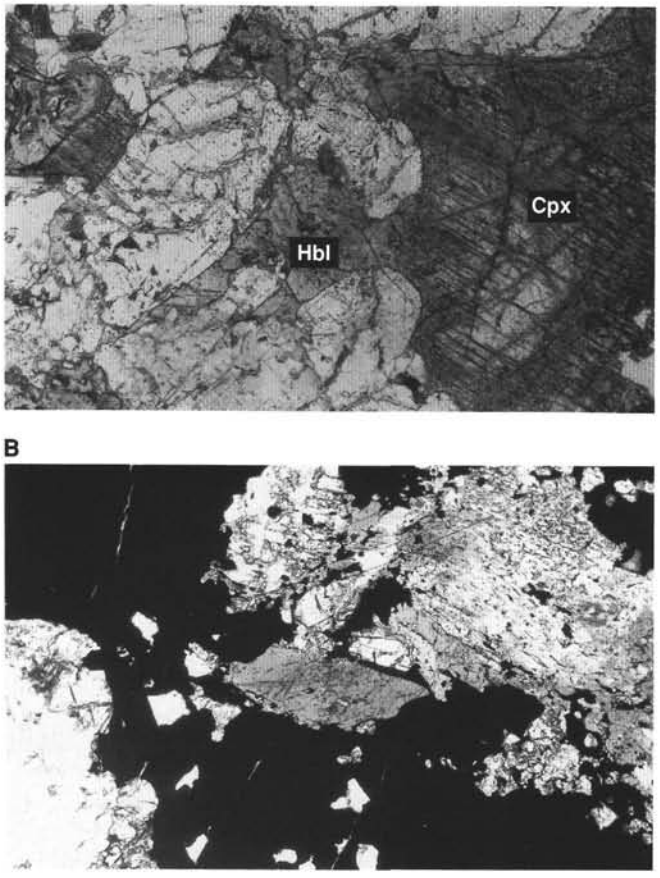

Figure 46. **A.** Brown amphibole (hbl) rimming and partially replacing clinopyroxene (cpx), Sample 153-921E-5R-2, 14–17 cm. Field length is 3 mm; polarized light. **B.** Brown amphibole rimming Fe-Ti oxide mineral, Sample 153-921E-3R-1 (Piece 5, 37–44 cm). Field length is 6 mm; polarized light.

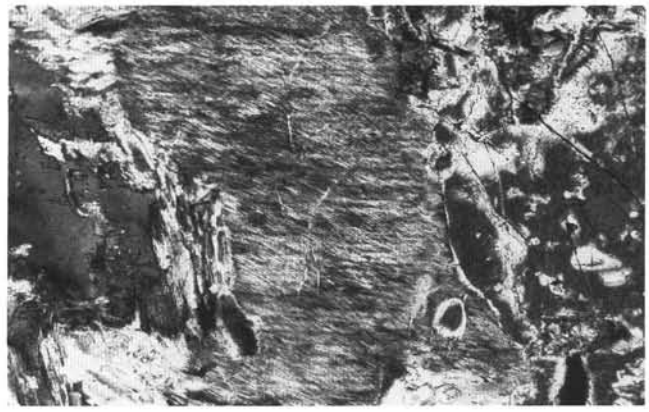

Figure 47. Fibrous actinolite replacing and rimming clinopyroxene (Sample 153-921E-3R-1, Piece 12, 107–113 cm). Field length is 1.5 mm; polarized light.

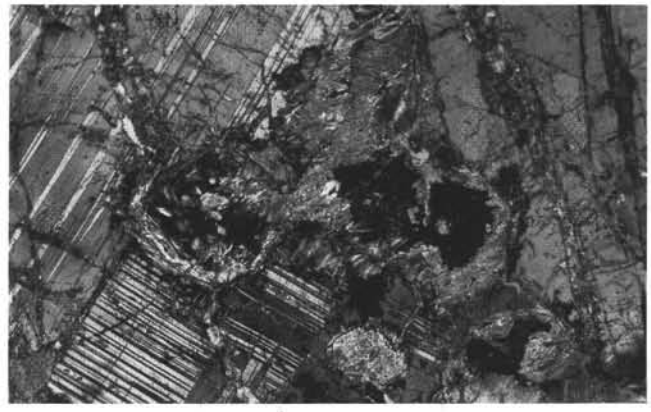

Figure 48. Patches of actinolite and chlorite crystallizing near actinolite-chlorite veins at the expense of plagioclase (Sample 153-921E-5R-2, Piece 1A, 14–17 cm). Field length is 3 mm; polarized light.

chapter). Orthopyroxene grains are moderately to highly altered, with veinlets and rims of fine-grained cummingtonite common. Locally, grains are pervasively altered to fine-grained fibrous amphibole that forms intergrown patches. Associated clinopyroxene grains are moderately altered and contain fine-grained inclusions of hornblende, discontinuous rims of hornblende, and fibrous rims of actinolite. Moderately coarse-grained green amphibole rims clinopyroxene in highly altered zones adjacent to felsic veins. In localized zones of deformation, clinopyroxene grains are recrystallized to fine-grained, clear, anhedral crystals. Plagioclase grains are slight to highly altered, and locally contain glide twins, patchy extinction, and sutured grain boundaries (e.g., Sample 153-921E-8R-1, Piece 8, 62–68 cm). Alteration is generally limited to actinolite and chlorite that occur in crosscutting microfractures and less commonly along grain boundaries. In intensely altered samples, secondary plagioclase is abundant, forming irregular patches and discontinuous veinlets. Fluid inclusions are abundant in these areas. Fine-grained neoblastic grains of plagioclase that exhibit moderately to well-developed mosaic textures form discontinuous bands a few grains in width in the deformed samples.

Oxide Gabbros

Oxide gabbro layers and stringers (see "Igneous Petrology," this chapter) are typically plastically deformed and contain porphyroclasts of clinopyroxene (Sample 153-921E-3R-1, Piece 5, 37–41 cm), orthopyroxene (Samples 153-921E-1W-1, Piece 9, 64–67 cm, and 153-921B-3R-1, Piece 4A, 33–36 cm), and plagioclase that are enclosed in a fine-grained, dynamically recrystallized plagioclase matrix. Relict grains of oxide minerals wrap the porphyroclasts and enclose fine-grained plagioclase. Locally, the oxide minerals are fractured and cut by chlorite veinlets (e.g., Sample 153-921D-4R-1, Piece 6B, 59–62 cm). Clinopyroxene porphyroclasts within the oxide gabbros are slightly to highly altered and host fine-grained blebs of hornblende. Locally, hornblende forms well-developed coarse-grained crystals that are slightly altered to green amphibole along grain boundaries. Secondary clinopyroxene and actinolite pervasively replace clinopyroxene grains in some samples, and shear zones are present locally (e.g., Sample 153-921D-4R-1, Piece 6B, 59–62 cm). Orthopyroxene porphyroclasts are rounded to sigmoidal in shape locally and are typically slightly altered to fine-grained amphibole that rims grain boundaries and fills crosscutting microfractures. Plagioclase porphyroclasts are highly strained as indicated by glide twinning, patchy extinction, and sutured grain boundaries, and alteration is generally slight to moderate. Dynamically recrystallized hydrous minerals are rare; they include minor amounts of brown and green amphibole.

Static hydrous replacement of the igneous and recrystallized phases is commonly more pervasive in the oxide gabbros (20%–40%) than in the surrounding gabbroic rocks. This static alteration is particularly intense along the oxide gabbro contacts where clinopyroxene grains are pervasively replaced by actinolitic hornblende, and plagioclase is pervasively replaced by secondary plagioclase and clay minerals. In these highly altered zones, amphibole and to a lesser extent chlorite define a weakly developed anastomosing foliation (e.g., Sample 153-921D-4R-1, Piece 6B, 59–62 cm).

Figure 49. Fine-grained neoblasts of plagioclase rimming a plagioclase porphyroclast in Sample 153-921E-1R-1 (Piece 3, 34–37 cm). Field length is 12 mm; polarized light.

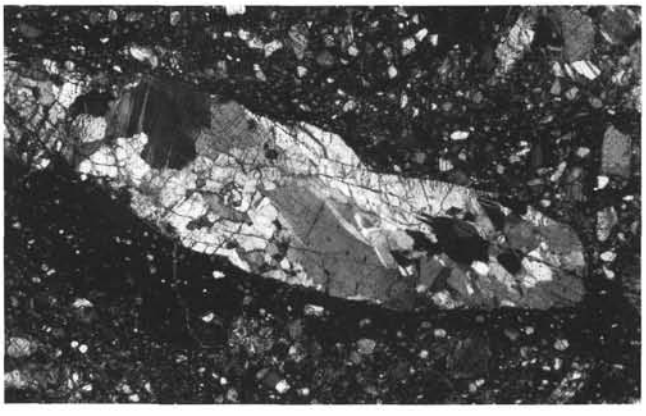

Figure 50. Polycrystalline plagioclase clast in the fine-grained matrix of a cataclastic gabbro (Sample 153-921B-1W-1, Piece 7A, 45–48 cm). Field length is 3 mm; polarized light.

Gabbro and Pegmatitic Gabbro

Gabbros at Site 921 exhibit an average alteration intensity of 15%. Alteration is heterogeneous both downhole and between holes, however, and varies from slight to pervasive, with the highest intensities in Holes 921B and 921C. Alteration intensity of olivine in the gabbros is moderate to pervasive (15%–95%) and includes oxide minerals, talc, tremolite, smectite, and chlorite as secondary phases (Table 7). Alteration of olivine between and within samples is generally heterogeneous, with modal proportions of secondary phases highly variable. Clinopyroxene exhibits variably well-developed fibrous pods and patches of actinolite-tremolite and lesser amounts of chlorite. It is commonly rimmed by fibrous actinolite and hornblende, and secondary clinopyroxene is abundant locally. In gabbroic host rocks cut by felsic veins, brown amphibole and secondary clinopyroxene are especially well developed. In deformation zones, clinopyroxene is recrystallized to fine-grained neoblastic grains that lack alteration phases (e.g., Sample 153-921E-3R-1, Piece 12, 107–113 cm). Plagioclase alteration is slight to pervasive, with the highest intensities associated with cataclastic deformation and crosscutting felsic veins. In these zones, plagioclase is typically turbid in appearance due to replacement by secondary plagioclase, which is fluid-inclusion-rich, and by clay minerals. Grains may be crosscut by abundant microfractures of actinolite ± chlorite. Epidote and prehnite are abundant locally.

Lineated and Gneissic Gabbros

Crystal-plastic deformation of gabbroic rocks at Site 921 resulted in well-developed, shape preferred orientations defined by bands of recrystallized olivine and clinopyroxene that alternate with plagioclase-rich bands (Figs. 6 and 49). The deformed gabbroic rocks include lineated and gneissic gabbros that are abundant in parts of Holes 921B, 921C, and 921D and have been grouped into separate lithologic units in Holes 921B and 921C (see "Introduction," this volume). In these rocks clinopyroxene neoblasts (50 to 100 µm) form elongated tails around clinopyroxene porphyroclasts (see "Structural Geology," this chapter). Plagioclase and olivine neoblasts exhibit moderately to well-developed mosaic textures (Fig. 49). Olivine in these deformed rocks is replaced by talc and oxide minerals, and/or by chlorite/smectite near veins. Clinopyroxene porphyroclasts are slightly to pervasively replaced by chlorite and actinolite, with pervasive replacement occurring adjacent to veins. Plagioclase grains exhibit slight to moderate alteration intensities with alteration dominated by secondary plagioclase and minor actinolite ± chlorite.

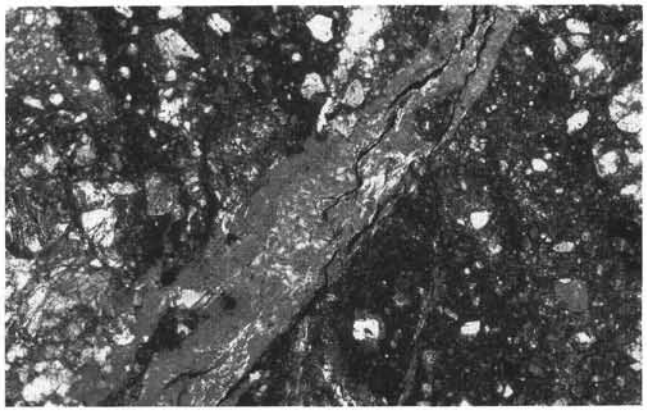

Figure 51. Chlorite and smectite vein cutting the cataclastic matrix in a cataclastic gabbro (Sample 153-921B-1W-1, Piece 7A, 45–48 cm). Field length is 3 mm; polarized light.

Cataclastic Gabbros

Cataclastic fabrics are restricted to decimeter-thick zones (Fig. 4). They are relatively abundant in the upper sections of Holes 921B and 921C, where they affect the lineated gabbro units (see "Structural Geology," this chapter). Zones with cataclastic fabrics are also present in all the other lithologic units of Site 921 and overprint all igneous and crystal-plastic deformation textures. These cataclastic zones are characterized by closely spaced shear zones, which result in a submillimeter-scale banding parallel to the elongation of clasts of the original gabbroic lithology (Fig. 50). These clasts are surrounded by fine-grained cataclastic material with clasts of primary minerals (dominantly clinopyroxene), and of secondary minerals, which include brown amphibole, chlorite, actinolite, prehnite, and minor epidote in a microcrystalline gouge.

Brown to green amphibole occurs in cracks that cut primary clast-forming minerals (Sample 153-921B-1W-1, 45–48 cm). Lamellar aggregates of deformed actinolite and chlorite develop in the fine-grained gouge at the contact of the clasts. In Sample 153-921B-1W-1 (Piece 9, 64–67 cm), undeformed fibrous, radiating actinolite and chlorite have apparently grown into the fine-grained cataclastic matrix from the surfaces of the clasts. In this matrix, fine-grained clinopyroxene clasts are commonly surrounded by thin chlorite rims and actinolite fibers. Undeformed chlorite-smectite veins and carbonate veins also locally cut the cataclastic matrix (Figs. 51 and 52). Clinopyroxene clasts locally are replaced by actinolite and plagioclase is replaced by prehnite and actinolite (Sample 153-921B-1W-1, 64 cm).

Samples of cataclastic gabbros have been affected by subsequent static alteration, ranging from very slight to complete replacement of clinopyroxene and olivine along the margins of actinolite, chlorite, and prehnite veins. In the gabbro, a few centimeters away from the

Figure 52. Carbonate vein cutting the cataclastic matrix in a cataclastic gabbro (Sample 153-921B-1W-1, Piece 7A, 45–48 cm). Field length is 6 mm; polarized light.

Figure 53. Plagioclase clasts in cataclasite to gouge are replaced by prehnite (Sample 153-921C-1R-1, Piece 3, 29–34 cm). Field length is 3 mm; polarized light.

cataclastic shear zones, the primary minerals in large gabbroic clasts show no alteration. Near cataclastic shear zones, plagioclase clasts are dusty gray to brown and display intensely developed microcracks and related veins of clay minerals. Numerous secondary fluid inclusion trails enhance their dusty appearance. Alteration of plagioclase is dominated by irregular patches of secondary plagioclase with undulose extinction, or crystallization of secondary plagioclase in parallel, 10-mm-wide veins restricted to the plagioclase porphyroclasts. Fine aggregates of chlorite and actinolite crystallize at grain boundaries between plagioclase and altered clinopyroxene and along fractures. Rare disseminated grains of green epidote replace the plagioclase. Pervasive alteration of plagioclase clasts surrounded by gouge has resulted in total replacement by prehnite and subordinate chlorite and quartz(?) (Fig. 53). Clinopyroxene exhibits a localized dusty coating, and very fine-grained oxide minerals occur along cleavages. Brown amphibole rimmed by pale green amphibole has crystallized on clinopyroxene grain boundaries and along cleavages.

Felsic Veins

Trondhjemitic and dioritic veins cutting the gabbroic rocks are submillimeter to centimeter in scale, and exhibit sharp to diffuse contacts and moderately to well-developed alteration halos (Fig. 54; e.g., Sample 153-921E-7R-1, Piece 4, 25–29 cm, and 153-921E-7R-1, Piece 6B, 52–53 cm). The felsic veins contain plagioclase, quartz, minor clinopyroxene, and accessory phases, which include oxide minerals, apatite, and zircon (Figs. 54, 55, and 56; see "Igneous Petrology," this chapter). Alteration of the primary mafic phases is commonly pervasive, and felsic minerals are slightly to highly altered. Coarse-grained quartz and unzoned plagioclase exhibit complex intergrowths adjacent to highly zoned plagioclase grains (Figs. 55 and 56). Secondary minerals after plagioclase include granular to well-crystallized epidote, secondary plagioclase as patches and irregular discontinuous veinlets, prehnite, actinolite, chlorite, and clay minerals (Fig. 56). Quartz grains commonly contain abundant fluid inclusions that occur along healed microfractures, and less typically as isolated inclusions: halite daughter minerals are present but not common. Clinopyroxene grains are pervasively altered to actinolite, secondary clinopyroxene, and minor brown amphibole (Fig. 54). Brown to green amphibole rimming clinopyroxene grains form well-developed crystals at vein-gabbro contacts (e.g., Sample 153-921E-3R-1, Piece 12, 107–113 cm). Oxide minerals adjacent to clinopyroxene grains are generally replaced by titanite and locally are enclosed in fibrous intergrowths of actinolite and chlorite.

Aphyric to Sparsely Phyric Diabase

Diabase dikes that crosscut the gabbroic rocks in Holes 921B (Unit 2) and 921C (Unit 2; see "Igneous Petrology," this chapter) are

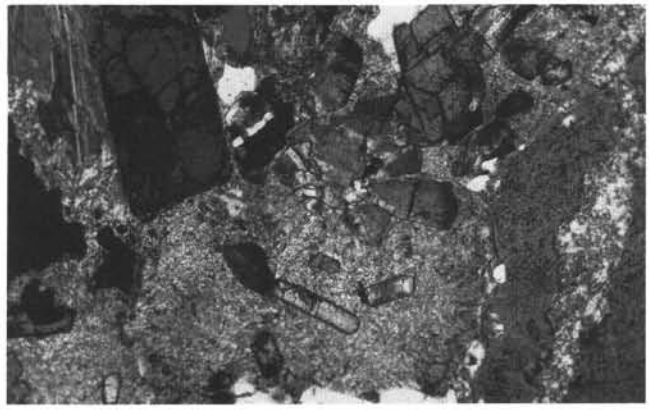

Figure 54. Secondary mineralogy in a felsic vein: epidote and smectite have replaced plagioclase (Sample 153-921B-2R-2, Piece 8, 113–118 cm). Zircon occurs as primary phase. Field length is 6 mm; polarized light.

Figure 55. Quartz and secondary plagioclase exhibiting a micropegmatitic texture around zoned plagioclase (Sample 153-921E-3R-1, Piece 12, 107–113 cm). Field length is 6 mm; polarized light.

moderately phyric. Alteration of the dikes is heterogeneous, with alteration of groundmass phases varying from 15% to 90%. The most intense alteration occurs at a chilled contact between the diabase and an adjacent cataclastically deformed gabbro (Sample 921B-1W-1, Piece 12, 97–100 cm). In this sample, chlorite and clay minerals pervasively replace the groundmass phases. Although fresh olivine is absent, chlorite, fine-grained oxide minerals, and less commonly

Figure 56. Euhedral plagioclase and lobate quartz in felsic vein (Sample 153-921A-2R-1, Piece 12, 119–124 cm). Field length is 1 mm; polarized light.

amphibole, which form subhedral to euhedral aggregates within the diabase, may represent pseudomorphs after olivine phenocrysts. Plagioclase phenocrysts are partly replaced by clay minerals (e.g., Samples 153-921B-1W-1, Piece 12, 97–100 cm, -921B-1W-2, Piece 2, 5–8 cm, and -921C-2R-1, Piece 1, 7–10 cm, and are commonly cut by microveins of chlorite and clay minerals. Irregular patches of secondary plagioclase, which are fluid inclusion-rich, commonly replace phenocryst and mesocryst laths. Plagioclase phenocrysts may be replaced locally by epidote and zeolite minerals. Clinopyroxene phenocrysts are relatively unaltered, with minor rims of chlorite and actinolite. The diabases are cut by fine veinlets of chlorite ± actinolite, prehnite(?), and clay minerals.

Hydrothermal Veins

Most hydrothermal veins at Site 921 are filled by actinolite and/or chlorite and less commonly by variable amounts of smectite, epidote, prehnite, and carbonate minerals. The veins are generally less than a millimeter to several millimeters in width with sharp contacts, and exhibit variable orientations and geometries (see "Structural Geology," this chapter). XRD traces were measured on representative samples of vein-filling minerals to confirm identification. Crosscutting vein relationships observed in the core indicate that the earliest veins are filled by tremolite, actinolite, epidote, and chlorite and that aragonite veins form a late vein set (see "Structural Geology," this chapter).

Actinolite and actinolite + chlorite veins and veinlets (Fig. 57) are the most common types of veins at Site 921 (Table 7). They are densely distributed locally and cut high-temperature crystal-plastic fabrics. They are most abundant in cataclastically deformed intervals, where they govern the pervasive background static metamorphism. Prehnite and carbonate veins are common in cataclastically deformed gabbros (Fig. 52) and generally are discordant to the deformational fabrics. Other veins within the cataclastic gabbros contain chlorite, smectite, and sulfide minerals (Fig. 51).

Down- and Intra-hole Variations

There is no apparent difference in the occurrences of alteration minerals between holes at Site 921 and alteration intensities are broadly similar between the holes (Figs. 40 and 41). The total percentage of alteration is highly variable, though there is a general to well-defined trend of increasing alteration intensities downhole (Fig. 40). The variations observed are generally independent from the primary magmatic mineralogy and textures. Increased alteration intensities typically correlate with an increase in density of microfractures and veins, which are generally higher in gabbro affected by crystal-plastic or cataclastic deformation.

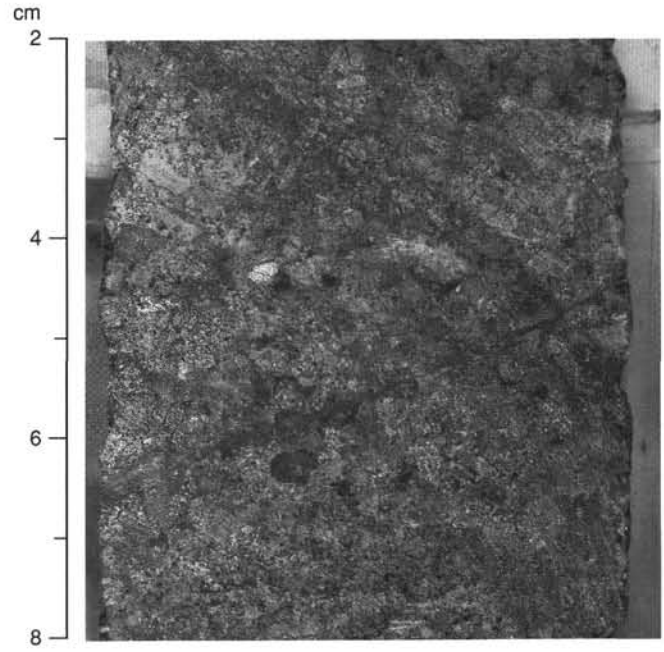

Figure 57. Pervasive alteration of clinopyroxene to actinolite and chlorite at the margin of a chlorite-actinolite vein. Sample 153-921D-5R-2 (Piece 1, 2–8 cm).

Discussion

Deformational and metamorphic relationships in gabbroic rocks recovered from Site 921 exhibit a progressive evolution from magmatic conditions to those dominated by circulation of low-temperature seawater. In intensely metamorphosed shear zones, crystal-plastic fabrics that are associated with dynamic recrystallization of most or all igneous phases exhibit a progressive evolution to fabrics associated with brittle failure. Recrystallization of olivine, plagioclase, and clinopyroxene, coupled with synkinematic growth of hornblende, occurs in discrete crystal-plastic shear zones throughout Site 921. These zones are best developed in the lineated gabbros of Unit 2 in Holes 921B and 921C, and indicate that recrystallization and deformation probably occurred at minimum temperatures of 700°–900°C (Spear, 1981; Liou et al., 1974). Circulation of fluids at lower amphibolite to greenschist facies conditions along microfracture and vein networks, which crosscut the high-temperature crystal-plastic fabrics, resulted in the pervasive overprint of the high-temperature mineral assemblages by green amphibole locally and in the resultant background static metamorphism of the gabbroic sequence.

In cataclastic gabbro, the transition between ductile and brittle deformation likely initiated near amphibolite facies conditions as evidenced by brown amphibole filling fractures in the gabbroic clasts. The presence of both deformed and undeformed fibrous chlorite and actinolite aggregates in the cataclastic shear zones, coupled with the development of prehnite, smectite, and carbonate-bearing veins, indicates that cataclastic deformation and associated fluid flow continued down to greenschist to zeolite facies conditions.

STRUCTURAL GEOLOGY

The five holes drilled at Site 921 yielded 43 m of structurally heterogenous gabbroic rocks. These rocks record a wide variation in structural styles and intensities not only from hole to hole but in some places on a centimeter to centimeter scale. The relatively low percentage of core recovered and general shallowness of the holes precludes a detailed analysis of the geographical and structural relationships; nevertheless, the structural characteristics of many of the rock pieces

recovered provide some natural groupings that are a starting point for more detailed analyses. The major structural divisions observed in the cores from this site include: (1) essentially undeformed gabbro, olivine gabbro and diabase; (2) pervasively deformed gabbro dominated primarily by a lineation defined by elongated clinopyroxene grains; (3) gabbro with localized ductile to semi-brittle shear zones; and (4) gabbro and metagabbro with zones of intense cataclasis. Discrete hydrothermal veins and sparse magmatic veins cut all those lithologies.

Thin-section observations were used to verify and supplement the core description of mesoscopic structures. Textural terms used and microstructural assemblages are discussed in the "Structural Geology" section of the "Explanatory Notes" (this volume) and are summarized in Figure 17 of that chapter. Sampling of the core for thin sections was not continuous, therefore inferences about sections of core that were not sampled are necessarily extrapolations from those pieces where the observations of meso- and microstructures are well-linked.

Magmatic Fabrics

A significant proportion of gabbroic rocks from Site 921 (close to 50%) display a coarse- to medium-grained primary cumulate to poikilitic textures with random orientation of primary igneous minerals (see "Igneous Petrology," this chapter). At some places, primary igneous layering is defined by subtle and diffuse grain-size and/or compositional variations (Fig. 12). Crystal-plastic fabrics overprint the magmatic textures of the gabbroic rocks from Site 921 in many places. In some places this is obvious even in hand specimen, however, elsewhere textural modification by crystal-plastic deformation is more subtle.

Mesoscopic penetrative structures can result from a purely magmatic process (accumulation and/or reorientation by magmatic flow) or from a sub-solidus process (crystal-plastic deformation). Where the preferentially oriented minerals have "primary" igneous shapes such as large clinopyroxene oikocrysts and elongated subhedral plagioclase laths with straight twins, the structure is referred to as a magmatic fabric. Fabrics observed in the cores that are interpreted to have resulted from magmatic flow have a mineral shape-preferred orientation defining a foliation and/or lineation with no sign of internal distortion, stretching, or flattening of minerals and lack of any evidence of grain-size reduction. Pyroxene in these rocks generally occurs as single crystals with continuous cleavages and as oikocrysts. Thin section observations verify that some rocks having a shape-preferred orientation are devoid of recrystallization or deformation microstructures (Fig. 58).

Crystal-plastic Fabrics

Lack of preferred mineral orientation does not necessarily indicate primary igneous texture. Observation of the rocks in thin section shows that extensive development of small, untwinned, polygonal plagioclase neoblasts does not necessarily result in any shape preferred orientation, especially in the case of coarse-grained rocks.

A porphyroclastic fabric defined by a shape-preferred orientation of flattened and/or elongated olivine and pyroxene porphyroclasts is observed in many of the gabbroic rocks. Where the crystals defining the fabric have elongate anhedral shapes, with evidence for stretching and development of asymmetric recrystallized tails, the structure is interpreted as a crystal-plastic fabric. At some places, the shape preferred orientation shows a weak but measurable obliquity to layering (Fig. 11). In hand-sample, it is difficult to decipher the extent of deformation in the lineated specimens due to extensive recrystallization. For example, the strongly lineated rock in Figure 6 shows neoblasts of plagioclase surrounding relict grains, whereas a piece that looks less deformed in hand specimen (Sample 153-921C-2R-1, Piece 15, 125–134 cm) has plagioclase that is composed completely of a mosaic of small anhedral grains with sutured boundaries and rare twins, indicating extensive recrystallization (Fig. 59).

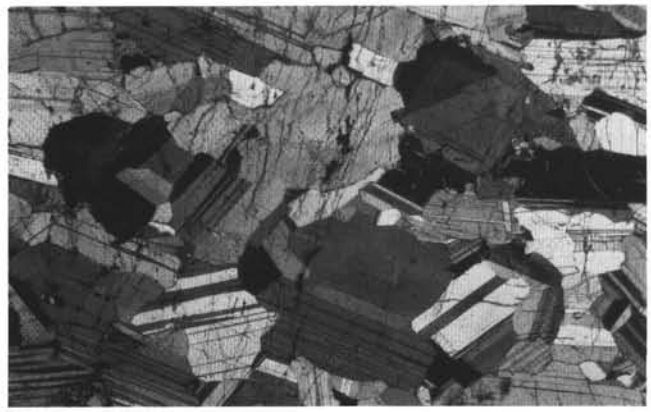

Figure 58. Photomicrograph of Sample 153-921B-4R-3, 7–10 cm (Unit 4). Plagioclase occurs as subhedral laths with a shape preferred orientation. Plagioclase twins are roughly parallel from grain to grain. Grains with conspicuously misoriented twins are generally equant. Most plagioclase grains show straight, simple albite twins; some grains also have deformation twins (Group 2 a microstructure). Field length is 8.6 mm.

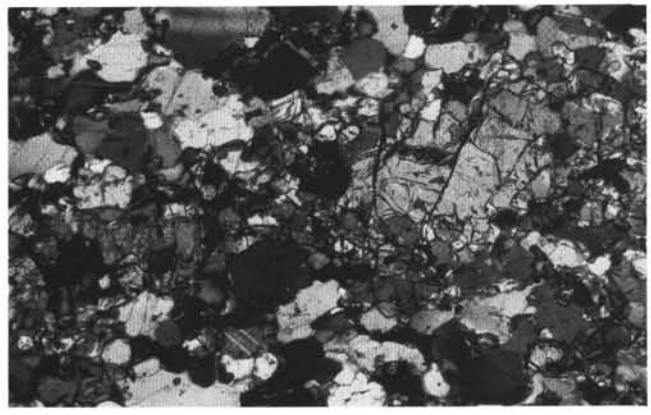

Figure 59. Photomicrograph of Sample 153-921C-2R-1, 125–134 cm, showing crystal-plastic microstructural fabric (textural Group 3; Fig. 17, "Explanatory Notes", this volume) from a lineated gabbro in Unit 3. Plagioclase occurs largely as a neoblast mosaic. Grain boundaries are sutured. Deformation twins are generally oriented parallel to the mesoscopic shape preferred orientation of pyroxene and olivine (i.e., parallel to long axis of the photo). An olivine porphyroclast with recrystallized tails and a thin trail of olivine neoblasts is also visible. Such elongated olivine grains (and pyroxene grains) define the strongly linear fabric on the mesoscopic scale. Field length is 3.4 mm.

Shear zones, discrete zones of high strain relative to surrounding rock, are defined by elongation of aligned minerals and are characterized by relatively fine grain size. The shear zones have deformation fabrics that range from moderately recrystallized to mylonitic (3 to 4 in intensity; Fig. 13, "Explanatory Notes," this volume). These zones are heterogeneously distributed throughout the core from Site 921. In thin section the minerals display crystal-plastic deformation features such as subgrains and neoblasts. The neoblasts are generally localized within relatively narrow (<2 mm) zones, in one case only with the width of only a few neoblasts (Fig. 60). The shear zones generally have sharp and well-defined boundaries and rock adjacent to the shear zones is commonly undeformed with no shape preferred orientation (Fig. 29). However, some shear zones have diffuse boundaries where the shape preferred orientation of plagioclase and pyroxene increases toward the middle of the zone. In Figure 20 the large elongate pyroxene grains are progressively deformed and rotated into parallelism with one side of the nearby shear zone, whereas pyroxene grains on

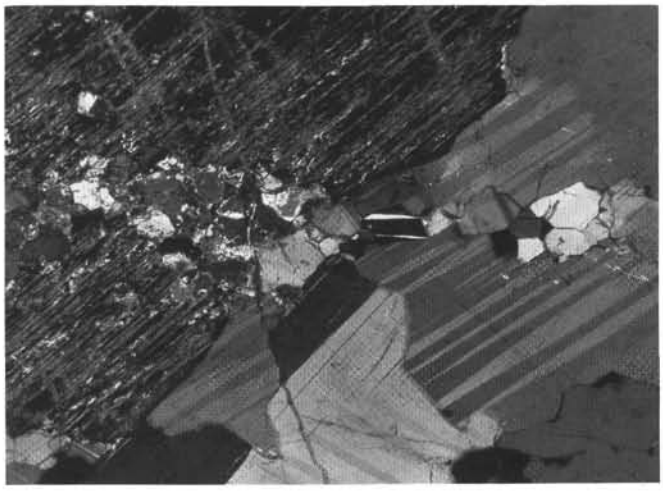

Figure 60. Photomicrograph of Sample 153-921B-3R-1, 134–137 cm showing thin (<500 µm) intercrystalline zone of recrystallization that cuts the entire width (5 cm) of the core. The zone is nowhere more than 3 neoblasts wide. Plagioclase neoblasts form in host plagioclase grains, and pyroxene neoblasts in pyroxene grains. Original grain boundaries show no offset across the zone. Field length is 3.4 mm.

the other side of the sharp boundary have random orientations right up to the shear zone edge. This curved shear zone in Sample 153-921E-3R-1, Piece 4, 25–36 cm (Fig. 20), has a sharp concave-side boundary but a relatively gradational convex side. Elongate pyroxene crystals show greater parallelism with the shear zone closer to the convex side. The iron oxide-rich shear zone in Piece 5 shows a narrowing and intensification of the shearing at 42 to 43 cm. In contrast to Piece 4 the boundaries of this shear zone are relatively sharp on both sides.

The orientation of shear zones is highly variable in the cores ranging from subhorizontal to subvertical, and anastomosing branches and splays with different dip angles and directions are common (Fig. 9). Shear zones also change in width along their trace (Fig. 18A, center of section).

Mixed Brittle and Crystal-plastic Fabrics

In the Site 921 holes there are several locations where localized brittle and crystal-plastic deformation are closely associated spatially. Mesoscopic and microstructural textural relations indicate that in some cases the brittle deformation overprints the crystal-plastic deformation, but in other locations they suggest that brittle failure either preceded or was synchronous with crystal-plastic deformation. During visual core description, the term "semi-brittle" was assigned to features where brittle and plastic structures coincide and their chronological relations could not be distinguished in hand specimen.

In Section 153-921B-2R-2 (Piece 5) distributed fracturing overprints crystal-plastic deformation. Fragmented plagioclase crystals are obliquely oriented to the sulfide mineral cataclastic zone that is located at a lithological contact. The fractures are most densely developed in the hanging wall of this shear zone and become less densely developed away from a contact between overlying gabbro and oxide gabbro beneath. The contact dips at about 50°. Although fracturing (characteristic of brittle deformation) and aligned elongate crystals with intra-crystalline strain (characteristic of crystal-plastic deformation) are both present, their textural relations suggest that crystal-plastic deformation was mainly overprinted by brittle deformation. The displacement across this shear zone is unconstrained but the textures do not suggest high shear strains.

In another example of microfracturing related to crystal-plastic shear zones, the pegmatitic gabbro at the top of interval 153-921E-2R-2 (Pieces 1–4) displays distributed microfractures that become increasingly closer spaced toward several shear zones (Pieces 4, 6, 7, and 8). Pieces 6, 7, and 8 are characterized by angular fragments of pyroxene crystals, embedded in a matrix of fine-grained polygonal plagioclase crystals. Some of them are fractured and the fractures are filled with plagioclase. Clinopyroxene crystals are not strongly bent or stretched. A similar fragmentation of pyroxene crystals is seen in Figure 21 (Sample 153-921E-2R-2, 50–60 cm) directly overlying a steeply-dipping oxide-mineral-rich shear zone. Section 153-921E-5R-1 (Piece 2), directly underlying a crystal-plastic shear zone in oxide-mineral-bearing gabbro has a similar texture.

Fractured crystals and a foliation defined by shape preferred orientation of pyroxene are present in a shear zone at the base of Piece 2 in Section 7R-2. This occurs within a weakly deformed to undeformed zone that spans Sections 5R-2 to 8R-1. The greatest volume of mixed brittle and plastic deformation is present in Section 8R-1 where a quartz diorite is underlain by several pieces (Pieces 5, 7, 9, and 10) of brecciated oxide gabbro (Fig. 9). Mafic mineral fragments in the oxide gabbro range in size from several centimeters to one millimeter. Elongate pyroxene crystals are aligned in narrow (<1 cm) shear zones. Within and adjacent to those zones, the crystals have an interlocking crystal texture with fractures between crystal fragments filled with fine-grained plagioclase. Thin sections show that the plagioclase matrix consists of small polygonal neoblasts, indicative of recrystallization.

Some brittle shear zones consisting of a dense mesh of fractures and veins, deform plagioclase and pyroxene into elongate grains by distributed microfracturing. These shear zones are evident along the margins of Pieces 3 through 6 of Section 153-921D-4R-1. The "sugary" texture of the plagioclase in hand specimen near the shear zones points to grain size reduction and suggests recrystallization.

Brittle Features

Brittle deformation at Site 921 is represented by variably developed distributed microfractures (described above), discrete faults, joint sets, cataclastic zones, and veins.

Faults and Joints

Discrete fault surfaces are rare in the Site 921 samples. The only brittle deformation evident in rocks from Hole 921A is a fault surface that dips about 50° with subhorizontal slickenlines (Section 153-921A-2R-1, Piece 1). Two vertical planar joints and an irregular joint are also present (Section 153-921A-2R-1, Pieces 1, 6, and 8).

In the core from Hole 921B, two small faults offset the foliation defined by aligned clinopyroxene grains (Section 153-921B-1W-1, Pieces 8 and 9; Fig. 61). Both faults have a reverse shear sense with a separation on the cut core face of 1 cm. The faults and associated intercrystalline cracks that penetrate the wall rock contain chlorite and actinolite. The only other possible fault surface in Hole 921B is represented by a strongly grooved surface with iron staining (Section 153-921B-1W-1, Piece 7). Fractures found in (Sections 153-921B-2R-2, Piece 3, and 153-921B-3R-1, Pieces 7 and 11) are lined with yellow and green clay minerals and are commonly iron-stained. None of these fractures has any slickenlines on their surfaces.

Jointing occurs along the tops and the bases of pieces from Hole 921D, with steeply dipping joints along mineralized surfaces. Iron staining and clay minerals are present on many of these surfaces showing that they are pre-existing veins or minor faults and not drilling induced features (e.g., Sections 153-921D-3R-1, Pieces 4 and 7, and 153-921D-5R-1, Piece 12B).

Cataclastic Zones

Rocks from the uppermost section of Hole 921B contain several cataclastic zones (Section 153-921B-1W-1, Pieces 3, 4, 5, 7, and 12; see Fig. 4) that are characterized by light green/brown, branching

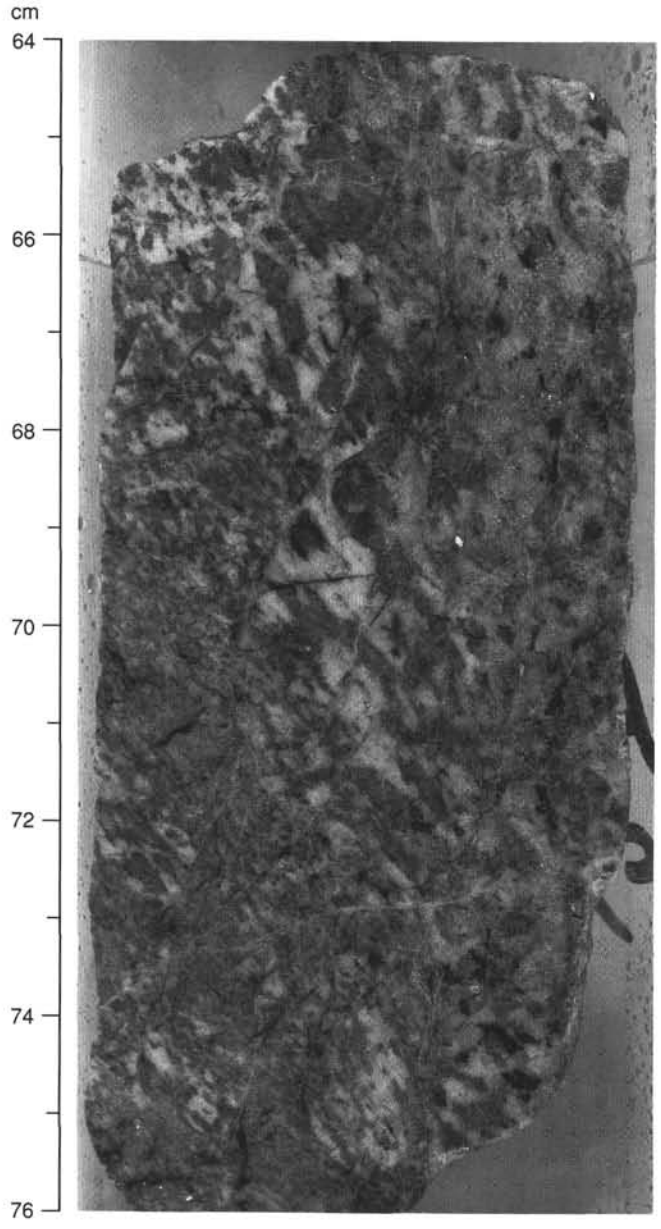

Figure 61. Lineated gabbro with small faults offsetting the crystal-plastic foliation defined by elongate minerals. Photograph of Sample 153-921B-1W-1 (Piece 9, 64–76 cm).

strands of variable thickness consisting of ultra-fine-grained fragments of fractured minerals (gouge). The minerals in these cataclastic strands include epidote, clinopyroxene that is partly altered to brown amphibole, actinolite, minor chlorite, and clay minerals. The strands are spaced at 0.1 to 2 cm, and their thickness varies mainly between 1 and 3 mm, with a maximum thickness of 6 cm (Fig. 4). Cataclastic zones have diffuse margins and typically have a shallow dip (subhorizontal to 20°). They locally deform an earlier crystal-plastic fabric that is preserved in lenses between the sheared cataclastic zone branches. Pieces without cataclastic shear zones in this section are deformed by moderately dense, distributed microfractures (e.g., Section 153-921B-1W-1, Pieces 9 and 14).

Also in Section 153-921B-1W-1, a subhorizontal cataclastic zone, 1 cm wide, is localized along the margin of a diabase dike, chilled against the medium-grained gabbro (Fig. 62) (Sample 153-921B-1W-1, 92–103 cm). The cataclastic zone overprints a steeply dipping crystal-plastic fabric in the gabbro that changes gradually to a lower

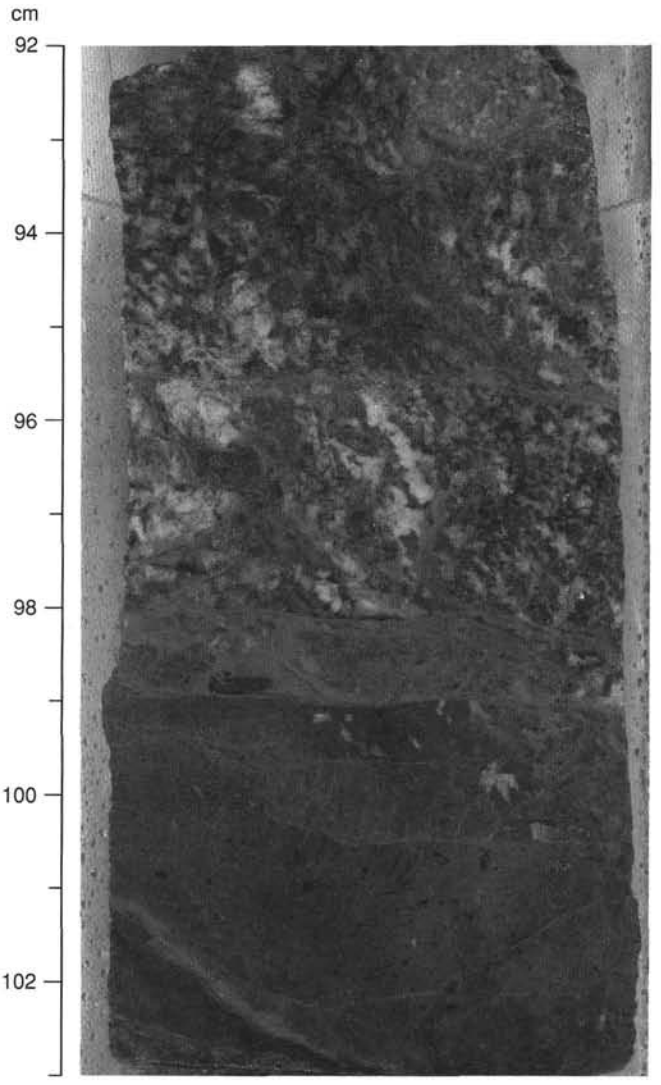

Figure 62. Sample 153-921B-1W-1, 92–103 cm. The chilled margin of a diabase dike against medium-grained gabbro is cut by thin subhorizontal cataclastic shear fractures.

angle, approaching the chilled contact. Within the cataclastic zone intense grain-size reduction is evident, but there are conflicting shear-sense indicators on the flat faces of the split core piece. This piece also contains sulfide minerals on either side of the cataclasites. The boundary between the cataclastic material and the country rock is very irregular. Another chilled margin lies below this zone where the crystal-plastic fabric is also distorted close to the margin but no cataclastic zone is present.

Cores from Hole 921C are also cut by closely spaced cataclastic shear zones (Section 153-921C-1W-1, Pieces 1–3). Each shear zone, defined by a high concentration of anastomosing, narrow (<1 mm) veinlets, is a few centimeters thick, with submillimeter horizons rich in submicroscopic fragments of altered pyroxene, chlorite, actinolite, and epidote. The shear zone orientation is predominantly subhorizontal but no unique shear sense could be determined.

Another form of brittle deformation, distributed microfracturing or microjointing, occurs in the medium-grained gabbro in the base of interval 153-921D-2R-1 (Pieces 5–10). The section displays moderately densely distributed microfractures with negligible displacements. Commonly the microfractures are filled and appear as networks of dark green chlorite and actinolite veins overprint crystal-plastic fabrics. Similar distributed fractures are present in interval 3R-1

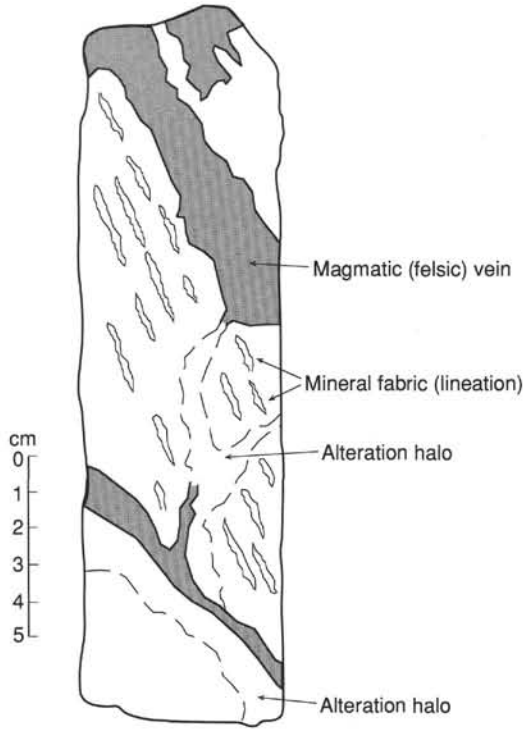

Figure 63. Line drawing of felsic magmatic vein cutting the lineated mineral fabric in Sample 153-921E-7R-2, 94–114 cm (Unit 2).

(Pieces 4–9) and in both sections of Core 2R of Hole 921E. In Section 153-921E-2R-1, distributed fractures weakly deform the gabbro (Pieces 1–8) and generally increase toward the contact with the underlying olivine gabbro that is relatively undeformed (Pieces 9–11). Pieces 4 and 5 have concentrations of plagioclase along the microfractures. Areas affected by distributed micro-fracturing are considered separately from the cataclastic zones described above because the latter show abundant evidence of shearing displacements and therefore frictional behavior.

Veins

The crystal-plastic deformation features and magmatic textures in Site 921 gabbroic rocks are cut by various types of veins. The main vein types in Site 921 rocks include felsic veins and chlorite ± actinolite veins. Veins are also associated with oxidized zones and with cataclastic zones where they fill fractures and microfractures.

Felsic Veins

These veins occur as submillimeter to centimeter-scale, planar to irregular, veins and pods with sharp to diffuse boundaries cutting across the deformation fabric (foliation and/or lineation) and the primary igneous texture in the rocks (Fig. 24). They commonly contain plagioclase + amphibole (replacement product after clinopyroxene) ± iron oxide minerals ± chlorite ± clay minerals and have alteration halos (see "Metamorphic Petrology," this chapter). Locally, they form dikelets with widths less than 1 cm that display sharp contact relations with the host rock or as several centimeter-wide zones with thin anastomosing veins (Fig. 63; Section 153-921E-7R-2, Piece 4). This second kind of felsic vein has irregular margins following the grain boundaries in coarse-grained gabbros. Their dips range from subhorizontal to subvertical although subhorizontal ones are more common (Sections 153-921E-4R-1, Pieces 1 and 6, and 6R-2, Piece 1). They are intersected and cut by chlorite ± actinolite veins (Fig. 64; Sections 153-921E-3R-1, Piece 12, -5R-2, Piece 6, and 921C-3R-3, Piece 3).

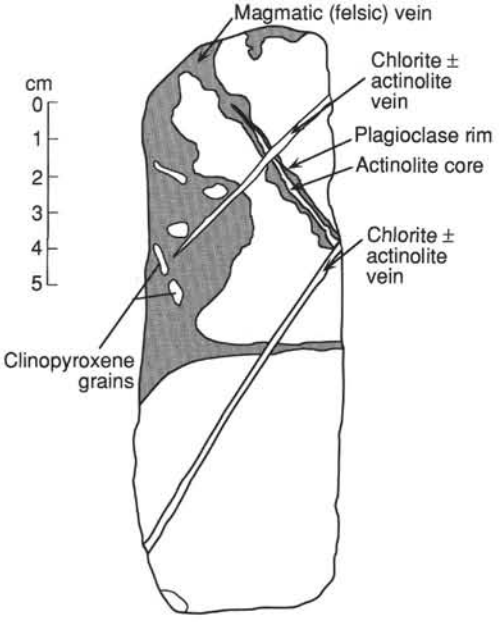

Figure 64. Line drawing of chlorite and actinolite veins cutting a felsic magmatic vein with an actinolite core of Sample 153-921E-3R-1 (Piece 15, 130–146 cm; Unit 2).

Chlorite ± Actinolite Veins

These veins are the most common types of veins in all cores from Site 921. They show varying widths, geometries, and orientations but commonly display sharp boundaries with the host rock and in some cases have symmetric alteration halos (Sections 153-921C-2R-3, Piece 8, and -3R-1, Piece 9). Some individual veins show en echelon segments and/or offsets along their trace (Sections 153-921E-2R-1, Piece 5, and 153-921B-2R-2, Pieces 1 and 3), whereas others are sheared along their margins (Section 153-921B-3R-1, Piece 4). They occur as subhorizontal to subvertical, individual, or subparallel veins (Fig. 65). In Section 153-921D-2R-1 (Piece 10) subhorizontal veins consistently cut the vertical ones. In lineated gabbros, the veins of chlorite and actinolite cut across the mineral fabric at high angles (Sections 153-921B-1W-2, Piece 4, -2R-1, Piece 5, and -2R-2, Piece 2), and the chlorite ± actinolite veins intersect and cut the felsic magmatic veins (Figs. 64 and 66).

Almost all chlorite ± actinolite veins occur as pure-extensional cracks with wall-perpendicular fibers (e.g., Section 153-921A-2R-1, Piece 12). Clinopyroxene, plagioclase, and olivine grains are split by these veins with no apparent lateral offset or displacement. Veins associated with oxidized zones in gabbros occur near or along the shear zones separating gabbros with different grain sizes. For example, the contact between a coarse- and medium-grained gabbro in Piece 6 (Section 153-921D-4R-1) is mildly sheared and is associated with sulfide-mineral-bearing veins dipping approximately 50° (i.e., parallel to the contact).

An aragonite + chlorite vein dipping steeply (72°) cuts across a chlorite ± actinolite vein in Piece 7 (Section 153-921D-3R-1), and the rock is fractured along the vein plane. This is the only vein with a different mineral assemblage that post-dates the formation of chlorite ± actinolite veins in Site 921 rocks.

Veins in Cataclasites and Shear Zones

Cataclasites and cataclastic zones in the gabbroic rocks display an extensive network of microfractures and veinlets associated with widespread alteration of the host minerals (Fig. 4). These submillimeter-scale veins commonly occur in anastomosing networks. They are subhorizontal in general and in some places are sheared along their

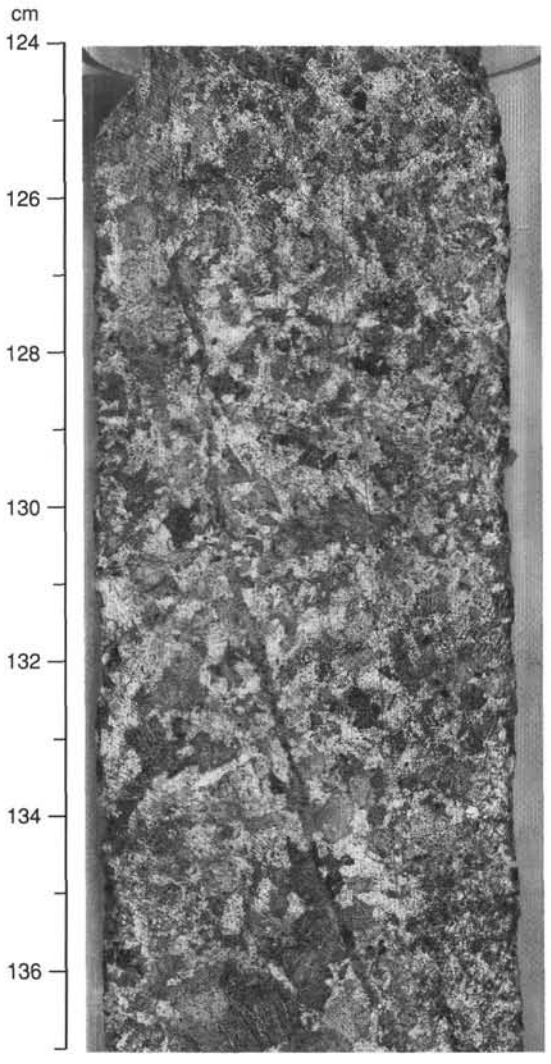

Figure 65. Series of steeply dipping en-echelon actinolite and chlorite hair line veins, and 1-mm-thick composite vein cutting diffuse compositional and grain-size variations in Sample 153-921B-4R-1, 124–137 cm, Piece 9 (Unit 4).

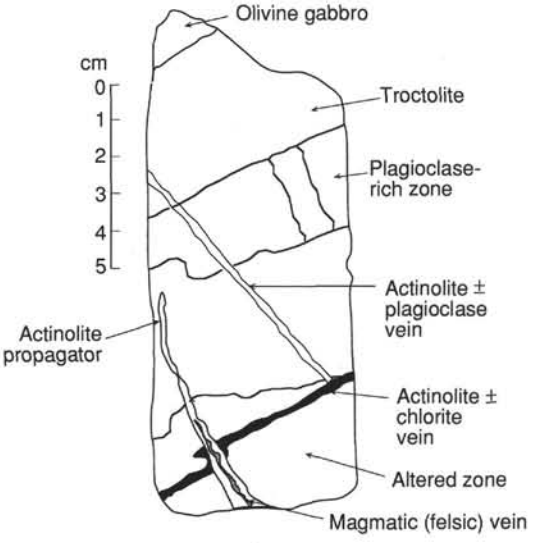

Figure 66. Line drawing of an actinolite and chlorite vein cutting both a felsic magmatic vein and an actinolite and plagioclase vein, Sample 153-921E-8R-1 (Piece 13C, 119–132 cm). Even though the felsic vein appears to offset the actinolite and chlorite vein, the actinolite and chlorite vein actually cuts the felsic vein and its thickness is much reduced where it traverses the felsic vein. This rock is also compositionally layered, with plagioclase-rich, troctolite and olivine gabbro bands.

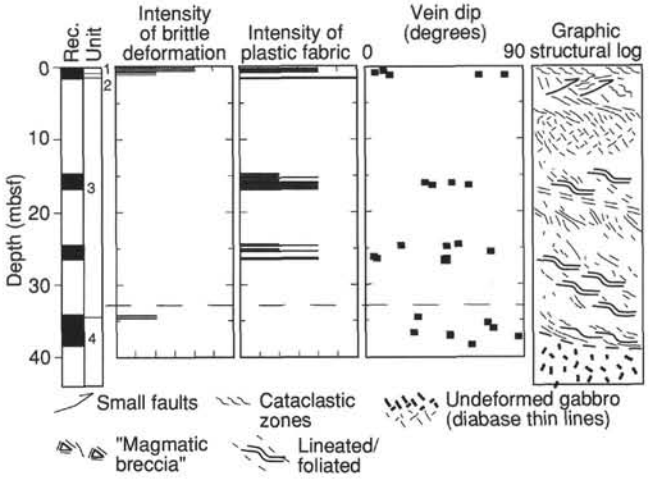

Figure 67. Core recovery, igneous units, structural features, and a structural summary plotted vs. depth for Hole 921B. Intensities are described in "Explanatory Notes" (this volume). "Magmatic breccia" refers to angular clinopyroxene clasts separated by plagioclase-rich net veins (e.g., Fig. 9).

boundaries. These veins, microfaults, and aggregates of the fine- to medium-grained host rock in the cataclastic zones are cut by undeformed veins and veinlets composed of chlorite + carbonate minerals ± zeolite minerals ± sulfide minerals (Fig. 4; Sections 153-921B-1W-1, Pieces 4 and 5, 153-921D-5R-1, Pieces 4 through 8, and -921C-1R-1, Piece 3). Some mylonitic shear zones include veins that are subparallel to the shear zone boundaries and that contain plagioclase + clinopyroxene ± iron oxide minerals (Sections 153-921E-2R-2, Piece 4, and -7R-2, Piece 2).

Vein Orientations and Generations

The variation of vein dip with depth does not seem to present any consistent pattern except in Hole 921D (Figs. 67, 68, and 69). In that hole, Core 2R has only shallowly dipping veins while Cores 3R and 4R have only steeply dipping veins. In Core 5R, veins cut the core at angles changing from shallowly to steeply dipping as in most of the core recovered at the other holes. However, the number of veins measured is low, especially in the top four cores of Hole 921D; thus, the consistency may be an artifact of the low core recovery (Fig. 68). The low recovery as well as relatively sparse occurrence of veins hampers reconstruction of an unambiguous sequence of vein generations. Few veins intersect other veins in the recovered core. The felsic magmatic veins were locally cut by chlorite ± actinolite veins and in the one case cited above, a chlorite ± actinolite vein was cut by a carbonate mineral + chlorite vein. The generational sequence is apparently very simple and consists of felsic veins followed by all other veins, concluding with late carbonate mineral-bearing veins.

Downhole Variations and Comparisons

Hole 921A is very shallow (17.10 mbsf) and a relatively small amount of core (3.10 m) was recovered. The only structural features of note are a minor fault near the top of the recovered hard-rock section and a few joints and veins. Total recovery of gabbro was 1.28 m. No shape-preferred orientation fabric, shear zones, or other defor-

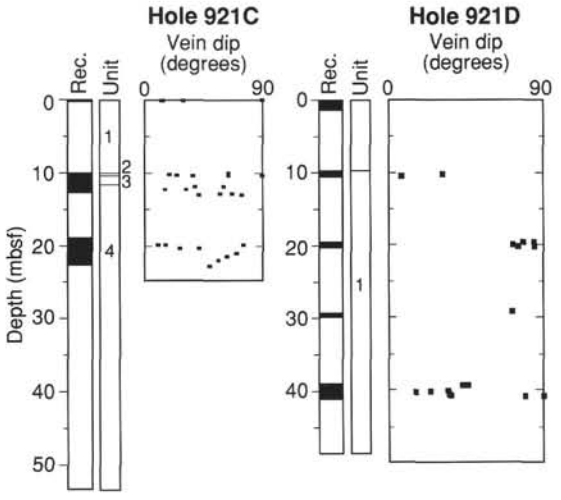

Figure 68. Vein dip vs. depth for gabbroic rocks from Holes 921C and 921D. Rocks from Hole 921D show the only systematic variation of vein dip vs. depth, with only steep dips in the middle two cores in contrast to gentle dips at the top and varied dips at the bottom.

mation features are present. Thin sections are all nearly devoid of crystal-plastic or brittle deformation (Table 8).

The brittle deformation features in rocks from Hole 921B are concentrated at the top of the hole with an overall reduction in deformation (brittle and plastic) as the contact with poikilitic olivine gabbro (Unit 4) in Section 4R-1 is approached (Piece 6). The topmost core from Hole 921B is structurally very complex. As indicated in Figure 67, within the first section is a moderately to highly deformed metagabbro with aligned mineral grains, cut by several cataclastic zones (Unit 1). Thin-section Sample 153-921B-1W-1, 64–67 cm, (Fig. 70) shows the brittle shear zones microveins cutting the porphyroclast and ending at the neoblast mosaic. In addition, the rock in this section exhibits several compositional and textural changes. Below this deformed metagabbro is a section of undeformed diabase (Unit 2). Downhole the next core contains a lineated fabric in most of the recovered pieces, defined by a preferred alignment of clinopyroxene grains. The lineation dips shallowly to steeply and is characteristic of most of Unit 3. This style of deformation continues in the next core and through the first five pieces of Section 4R-1, the bottom of igneous Unit 3. Group 3 and 4 crystal-plastic microstructures (Figs. 59, 71, and 72) dominate Sections 1W-2 to 3R-2. The occurrence of localized neoblasts (Group 4 microstructures) and strong strain-partitioning on the mesoscopic scale in Sections 3R-1 and 3R-2 corresponds to a zone that contains a higher frequency of compositional and textural variations. The contact between the two igneous units (Units 3 and 4) defined in this hole at Piece 6 of Section 4R-1, dips at about 35°, and shape-preferred orientation of plagioclase and clinopyroxene defines a foliation subparallel to the contact. The underlying poikilitic olivine gabbro unit that makes up the rest of core recovered from this hole is largely undeformed. The thin-section observations are consistent with this conclusion, as no intra- or intercrystalline deformation is evident, (Groups 1a and 1b) (Figs. 58 and 73, respectively).

Like Hole 921B, Hole 921C contains cataclastic zones in the small amount of rock recovered in the first section (Fig. 74; Sample 153-921C-1R-1, 29–32 cm). Apart from veins, there are no other significant brittle deformation features below the first section from Hole 921C (Unit 1). Core 2R recovered very different material, starting with an undeformed diabase (Unit 2) followed by a lineated gabbro similar to that in Hole 921B (Unit 3). A shear zone is also located in the top of this core. The lower sections of this core and the following core (Core 3R) show very little deformation of any kind. The variably lineated and weakly foliated fabrics diminish in intensity at the boundary of the overlying gabbros with an olivine gabbro in Unit 4 (poikilitic olivine gabbro) that has its top at Piece 4 of Section 2R-2. A lineation continues through several pieces into the top of Unit 4 before weakening. The thin sections show a change from pervasive crystal-plastic microstructures (Group 3) to random and shape preferred fabric without intracrystalline deformation (Groups 1a and 1b) near the boundary between the lineated gabbro (Unit 3) and poikilitic olivine gabbro (Unit 4; Table 8). Crude grain-size layering and textural variations are the obvious mesoscopic characteristics of the core in the bottom portions of this hole.

The uppermost section of Hole 921D contrasts with cores from Holes 921B and 921C in that no cataclastic zones were recovered. The first few sections of Hole 921D show few structural features except for a very subtle subhorizontal alignment of pyroxene grains in Section 2R-1 and a couple of semi-brittle shear zones in Section 4R-1. Core 5R of this hole was somewhat more complex and includes foliated rock (Pieces 6 and 10), compositional and texture variations, and several thin (~3 mm) brittle shear zones (Section 5R-1, Pieces 5 through 8). The brittle fabric observed in thin sections overprints the original magmatic (Group 1) fabric. The thin sections show very little development of small neoblasts except near brittle shear zones as seen in Sample 153-921D-4R-1 (59–62 cm).

More extensive recovery (17.65 m) was obtained in Hole 921E. Each core recovered in this hole exhibits at least some deformation fabric and many showed several kinds within the same section. In general, a foliation defined by the alignment of plagioclase, olivine and/or pyroxene crystals exists all the way down the hole with peak intensities in Cores 2R, 7R, and 8R, each of which is located within a different unit. Localized shear zones cut the core in Sections 5R-1 and 8R-1. These mixed brittle and crystal-plastic shear zones are associated with pieces that have angular igneous fragments separated by net veins of recrystallized material in Sections 5R-1, 7R-2, 8R-1, and 8R-2. Elongate mafic minerals are commonly aligned sub-parallel to the narrow (1 mm) brittle shear zones that generally cut material with this texture. The last core in this hole again shows a very subtle shape preferred orientation of elongate pyroxene.

The thin sections near the top of the hole show both undeformed magmatic textures and localized crystal-plastic (Groups 1 and 4) microstructures (Figs. 71 and 73). This characterization continues into the lithologic transition zone between igneous Units 1 and 2 from Section 3R-1 (Piece 4) to Section 5R-1 (Piece 3) (see "Igneous Petrology," this chapter). In general, ductile deformation is concentrated in the olivine-poor (<10%) lithologies, which are most similar to the pegmatitic olivine gabbro of Unit 1. The olivine-rich (>10%) lithologies are virtually undeformed in the lithologic transition zone. Most of igneous Unit 2 is characterized by undeformed magmatic textures (Group 1). Unit 3 again has microstructures from Groups 1 and 4 showing a combination of undeformed and locally deformed rocks (Table 8).

Gabbroic rocks from Holes 921B and 921C have the greatest similarities in both igneous composition and structural features. They both have undeformed diabase and a cataclastically deformed metagabbro at the top. Downhole from the diabase is gabbro that is commonly weakly to moderately lineated. Gabbroic rocks at the bottom of the core display a wide range of textural variation but little evidence of deformation in hand specimen. The change from lineated rocks to undeformed rocks occurs gradationally in Hole 921C, where a lineation can be seen into the first few pieces of igneous Unit 4, and relatively abruptly in Hole 921B where a more or less pervasive lineation ends at the top of igneous Unit 4.

Rocks from Hole 921D in general show fewer and more uniformly distributed deformation features than those of either Holes 921B or 921C. Both the deformation and igneous composition are heterogenous in all sections from Hole 921D. In terms of structural style, the differences between rocks of Hole 921D and those of either 921B or 921C are much greater than the differences between rocks from Holes 921B and 921C. The single igneous unit assigned to rocks from Hole 921D is a reflection of the relatively fine-scale heterogeneity of the structural elements as well as the variations in the igneous texture.

Table 8. Thin-section samples and textural grouping from gabbroic rocks from Site 921.

Core, section, interval (cm)	Lithology	Textural group
153-921A-		
2R-1, 18–25	Olivine gabbro	1a
2R-1, 34–38	Olivine gabbro	2a
2R-1, 119–124	Olivine gabbro	2a
153-921B-		
1W-1, 45–48	Cataclastic metagabbro	6
1W-1, 64–67	Cataclastic metagabbro	5b
1W-1, 97–100	Cataclastic metagabbro	6
1W-2, 5–8	Diabase	1a
1W-2, 26–29	Lineated gabbro	3b
2R-2, 16–19	Lineated gabbro	3a
2R-2, 113–116	Lineated gabbro	2a
3R-1, 16–20	Lineated gabbro	3b
3R-1, 33–36	Lineated gabbro	4a
3R-1, 134–137	Lineated gabbro	2a
3R-2, 33–37	Lineated gabbro	4a
4R-1, 40–44	Poikilitic olivine gabbro	2b
4R-1, 59–65	Poikilitic olivine gabbro	1b, 1a
4R-1, 137–140	Poikilitic olivine gabbro	1a
4R-2, 50–53	Poikilitic olivine gabbro	1a
4R-2, 89–96	Poikilitic olivine gabbro	1a
4R-3, 77–83	Poikilitic olivine gabbro	1b
4R-4, 16–19	Poikilitic olivine gabbro	1a
153-921C-		
1R-1, 29–34	Cataclastic metagabbro	5b
2R-1, 7–10	Diabase	1a
2R-1, 113–116	Lineated gabbro	3b
2R-1, 127–130	Lineated gabbro	3b
2R-2, 6–10	Lineated gabbro	3b
2R-2, 61–65	Poikilitic olivine gabbro	1b
2R-2, 114–117	Poikilitic olivine gabbro	1a
3R-1, 83–86	Poikilitic olivine gabbro	1a
3R-1, 86–89	Poikilitic olivine gabbro	1a
3R-1, 136–139	Poikilitic olivine gabbro	1a
3R-2, 55–58	Poikilitic olivine gabbro	1a
153-921D-		
2R-1, 57–60	Mixed-olivine gabbro	2a
2R-1, 83–85	Mixed-olivine gabbro	2a
2R-1, 74–77	Mixed-olivine gabbro	2a
4R-1, 28–31	Mixed-olivine gabbro	6
4R-1, 59–62	Mixed-olivine gabbro	5a
5R-1, 118–121	Mixed-olivine gabbro	2b
5R-1, 121–124	Mixed-olivine gabbro	2b
5R-2, 56–59	Mixed-olivine gabbro	2a
5R-2, 60–63	Mixed-olivine gabbro	1a
153-921E-		
1R-1, 34–37	Pegmetitic gabbro	4b
2R-2, 24–30	Pegmetitic gabbro	2a
2R-2, 78–81	Pegmetitic gabbro	4a
3R-1, 37–41	Pegmetitic gabbro	4b
3R-1, 107–113	Het. poikilitic olivine gabbro	2a
3R-1, 138–144	Het. poikilitic olivine gabbro	2a
4R-1, 44–50	Het. poikilitic olivine gabbro	1a
4R-2, 26–30	Het. poikilitic olivine gabbro	2a
5R-1, 0–3	Het. poikilitic olivine gabbro	4b
5R-2, 14–17	Het. poikilitic olivine gabbro	2a
5R-2, 125–131	Het. poikilitic olivine gabbro	2b
6R-1, 50–57	Het. poikilitic olivine gabbro	2a
6R-1, 97–101	Het. poikilitic olivine gabbro	1b
6R-2, 45–48	Het. poikilitic olivine gabbro	2a
7R-1, 25–29	Het. poikilitic olivine gabbro	6
7R-1, 52–53	Het. poikilitic olivine gabbro	1a
7R-1, 92–96	Het. poikilitic olivine gabbro	1a
7R-2, 4–7	Het. poikilitic olivine gabbro	1a
7R-2, 70–75	Het. poikilitic olivine gabbro	4b
7R-2, 77–83	Het. poikilitic olivine gabbro	1a
7R-3, 35–39	Het. poikilitic olivine gabbro	2a
7R-3, 83–86	Het. poikilitic olivine gabbro	2b
7R-3, 93–94	Het. poikilitic olivine gabbro	2a
7R-3, 99–104	Het. poikilitic olivine gabbro	1b
8R-1, 56–62	Varitex./olivine gabbro	4a
8R-1, 113–118	Varitex./olivine gabbro	1a
9R-1, 52–58	Varitex./olivine gabbro	2b

Notes: Classification based on criteria summarized in the "Structural Geology" section of the "Explanatory Notes" (this volume). Het. = heterogeneous, varitex. = varitextured.

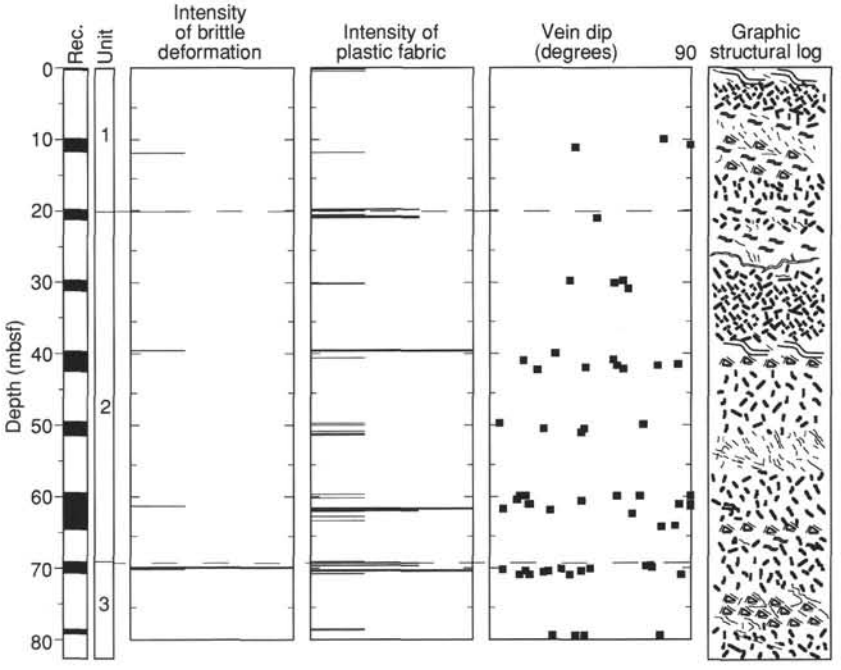

Figure 69. Core recovery, igneous units, structural features, and a structural summary plotted vs. depth for Hole 921E. Brittle shear zones apparently overprint crystal-plastic deformation in Cores 2R, 3R, 5R, 7R, and 8R. Symbols for the graphic structure column are shown in Figure 67. Intensities are described in "Explanatory Notes" (this volume).

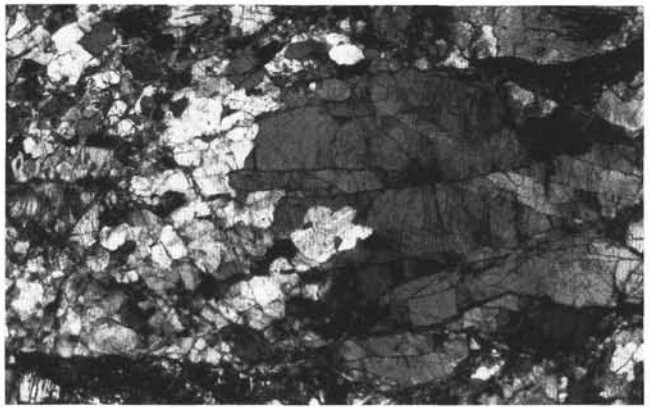

Figure 70. Large plagioclase porphyroclast in a cataclastic shear zone showing mixed crystal-plastic and cataclastic microstructures (textural Group 5; Fig. 17, "Explanatory Notes," this volume) (Sample 153-921B-1W-1, 64–67 cm). Field length is 5.4 mm. The microvein network in the porphyroclast ends in a neoblast mosaic.

Figure 71. Photomicrograph of Sample 153-921E-3R-1, 37–40 cm, shows heterogeneous dynamic recrystallization of plagioclase. (textural Group 4b; Fig. 17, "Explanatory Notes," this volume). Neoblasts are <100 µm and have sutured grain boundaries. The internal lattice strain in relict plagioclase is indicated by undulatory extinction and deformation twins. Field length is 3.4 mm.

The last core of Hole 921D contains lineated pieces, cataclastic shear zones, and other compositional and textural variations. This deepest core contains more features and more intense deformation than the upper parts; however, the sparse recovery in the other cores retrieved from this hole makes comparisons specious.

The core from the deepest hole, Hole 921E, contains deformation features of several types. Every core, and practically every section, contains pieces that exhibit either a foliation or contain shear or cataclastic zones. As shown in Figure 69, there is little systematic change of mesoscopic deformation type or intensity with depth. Mixed brittle and crystal-plastic shear zones cut Cores 2R, 5R, and 8R (Units 1, 2, and 3, respectively). Although not rigorously quantified, evidence of the greatest strain appears in Cores 7R and -8R, but few other generalizations can be made. The olivine-poor gabbroic rocks in igneous Units 1 and 3 of 921E are coarser grained but mineralogically similar to the lineated gabbro (Unit 3) in Holes 921B and 921C and can be loosely correlated (see "Igneous Petrology," this chapter). These olivine-poor lithologies are consistently the only ones where pervasive or localized crystal-plastic microstructures (Groups 3 and 4) are observed in all three holes.

Discussion

Penetrative crystal-plastic fabrics are concentrated in plagioclase in Holes 921B, 921C, and 921E, mostly in pyroxene-rich or olivine-poor gabbro (including gabbronorite and ferrogabbro). Most of the olivine-rich (troctolitic) gabbro are characterized by well preserved primary igneous textures. Crystal-plastic deformation in the more olivine-rich rocks is localized in relatively narrow shear zones, sometimes of microscopic size (for example, see Fig. 60).

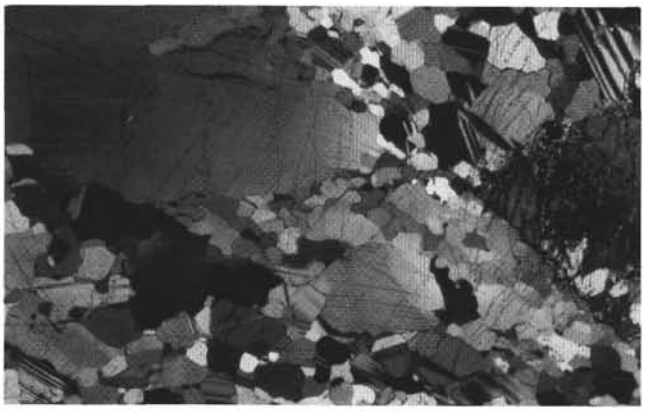

Figure 72. Photomicrograph of Sample 153-921B-3R-2, 33–35 cm, showing localized neoblasts of plagioclase (textural Group 4a; Fig. 17, "Explanatory Notes," this volume). The large relict plagioclase grain (upper left) is surrounded by polygonal neoblasts. The relict grain shows a faint patchy extinction. Field length is 3.4 mm.

Figure 73. Sample 153-921B-4R-4, 16–18 cm. Field of view: 8.6 mm. Plagioclase occurs as randomly oriented subhedral laths enclosed by subophitic olivine. Note optical continuity of olivine across the top of the photomicrograph and scarcity of equant anhedral plagioclase grains. Most plagioclase grains show straight, simple albite twins. This section displays a typical magmatic texture (Group 1a).

Mixed brittle and plastic structures (such as those described in Section 153-921E-8R-1) may occur because of the onset of deformation during the late stages of crystallization. The brecciated pyroxene crystals may have been hydraulically fractured by overpressuring of pockets of trapped melt in a crystal mush. Alternatively, magma may have been injected from an external source. Although overpressuring is not essential to form the observed textures, the suspension of fragmented pyroxene crystals in a fine-grained plagioclase matrix suggests brittle deformation, eventually followed by grain-size reduction attending crystal-plastic strain.

PALEOMAGNETISM

Paleomagnetic measurements were made on most archive half-rounds and a total of 52 minicores (approximately one sample per section) taken from Holes 921A through 921E. The remanent magnetization of these gabbro samples is complex and includes high-stability components of both normal and reversed polarity, although the latter is the dominant polarity. The complex magnetization history may preclude reorientation of structural features in the core; however, the multicomponent magnetizations provide a potentially powerful tool for examining the relative timing of remanence acquisition relative to magmatic and extensional processes. In addition, the presence of reversed polarity magnetizations provides a minimum age estimate (>0.78 Ma; geomagnetic polarity time scale of Cande and Kent, 1992) for these gabbroic exposures on the western flank of the median valley.

Whole-core Measurements

Whole-core susceptibility was measured at 3 cm spacing for most core sections from Holes 921A, 921B, 921C, 921D, and 921E. Olivine gabbros and poikilitic olivine gabbros have relatively low susceptibilities (10^{-3}–10^{-2} SI), as might be expected from the paucity of magnetite noted in both hand specimen and thin-section descriptions. The whole-core susceptibility data show a number of high-susceptibility intervals, which are directly correlatable with the presence of oxide gabbros or pegmatitic gabbros with significant amounts of oxide minerals (Fig. 75). The magnitude of these susceptibility peaks (e.g., Piece 1 in Section 153-921E-5R-1) are not as high as might be expected for samples with a significant volume (>2%) of magnetite. Thus, oxide-rich zones may be dominantly composed of ilmenite (as suggested by elevated abundances of TiO_2; see "Geochemistry," this chapter) or simply constitute a relatively minor volumetric proportion of the core sections identified as oxide gabbros.

Archive half-cores from Site 921 were measured at an interval of 3 cm with the pass-through cryogenic magnetometer, although the low percentage (~20%) of recovered material limits the utility of the downhole magnetic data. Approximately half of the cores, and particularly those sections with oxide-rich gabbros, have natural remanent magnetization (NRM) intensities that exceed the measurement range of the cryogenic magnetometer (i.e., >3–5 A/m). Reliable NRM data was obtained for the remaining cores, with magnetizations ranging from approximately 0.01 to 3.0 A/m and often with steep positive inclinations (60°–80°). Comparison with discrete sample demagnetization data suggests that these initial steep inclinations, in part, represent a drilling-induced remanence, which is typically removed by alternating field (AF) demagnetization at peak fields of 5 to 10 mT.

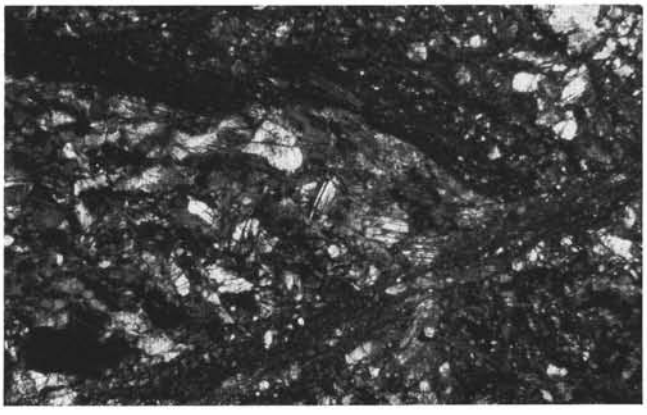

Figure 74. Photomicrograph of Sample 153-921C-1R-1, 29–31 cm, showing cataclastic (textural Group 6; Fig. 17, "Explanatory Notes," this volume) microstructures. The intersecting zones of cataclasis are composed of a cryptocrystalline fault gouge. Field length is 8.6 mm.

Half-core remanence data from Hole 921E illustrate that inclination values downhole are variable even after demagnetization at 20 mT (Fig. 76). The upper portions of the hole are predominantly of reversed polarity, with a mean inclination of approximately –30°. Remanence data from Cores 153-921E-5R to -8R are highly scattered, and the final core (-9R) obtained from this hole exhibits only shallow positive inclinations. Remanent intensities from Hole 921E cores after 20 mT demagnetization are approximately an order of magnitude lower in the middle portion of the hole. A similar pattern of inclination, and particularly intensity, variation is observed in Hole 921D (Fig. 77). The scattered remanence directions are probably an

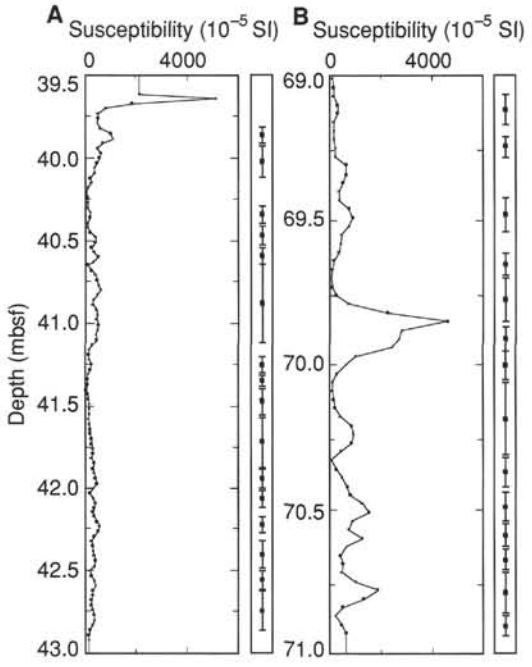

Figure 75. Susceptibility variations for representative cores from Hole 921E. **A.** Core 5R. **B.** Core 8R. The susceptibility peaks in both cores correspond to the oxide gabbro layers within the predominantly olivine gabbro core. Continuous core pieces longer than 7 cm (the length of the sensor response function for the Bartington susceptibility meter) are shown to the right of each core plot.

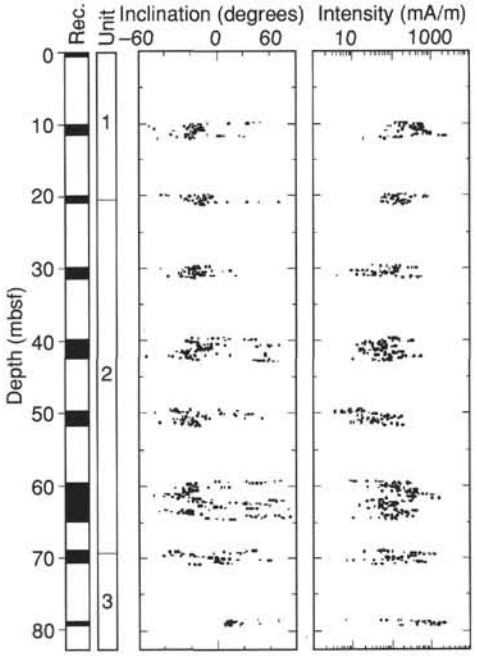

Figure 76. Downhole remanence data for Hole 921E archive half-cores after demagnetization at 20 mT. Inclinations are predominantly negative in the upper portion of the hole, highly scattered between 40 and 70 mbsf, and mostly shallow positive in the lowermost core. The intensities appear to be weaker in the central portion of the core than at the top and bottom.

expression of the complex remanence history of these gabbros, as documented below from analysis of the discrete sample data.

Results from Core 153-921D-4R (Fig. 78) illustrate the role of moderate coercivity overprints (i.e., exceeding the maximum fields achievable with the AF coils on the cryogenic magnetometer) in generating some of the scatter evident in the downhole inclination data. The NRM inclinations of the archive half-cores are typically steep (+60° to +90°), reflecting the presence of a drilling-induced remanence. Discrete sample NRM inclinations from this core are generally compatible with the pass-through remanence data. The somewhat shallower positive NRM inclinations of the discrete samples relative to the archive half-core data may reflect a smaller drilling-induced remanence in the center of the cores (Pinto and McWilliams, 1990). Demagnetization at peak fields of 20 mT results in a progression toward negative inclinations throughout most of the core, although there are several intervals with little inclination (or intensity) change. The highest stability component identified from AF demagnetized discrete samples is consistent with the pass-through data, even in intervals where the archive half-core inclination remains positive after 20 mT demagnetization (e.g., 37.8 mbsf in Fig. 78). These results suggest that a moderate coercivity component of normal polarity is present in addition to the magnetically softer (removed by ~10 mT), steeply inclined, drilling-related remanence. Thus, the apparent normal polarity in the lower portion of Core 153-921B-4R may represent either inadequate isolation of a reversed polarity magnetization or "true" normal polarity.

Discrete Sample Measurements

The natural remanent magnetization and initial susceptibility were determined for 52 discrete samples from Holes 921A, 921B, 921C, 921D, and 921E (Table 9). Although the number of samples is small, NRM intensities of discrete samples show an approximate log normal distribution (Fig. 79) with a geometric mean of 0.52 A/m ± 0.5 log units (arithmetic mean = 1.10 A/m). This probably constitutes a minimum estimate because the highest polarity magnetization component

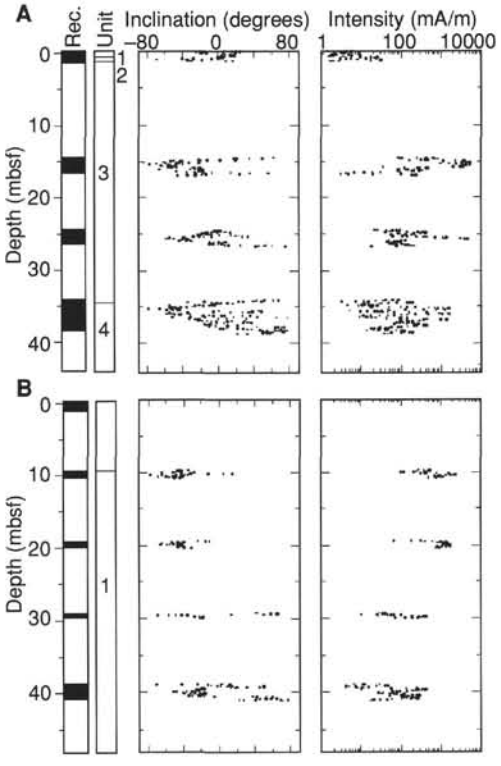

Figure 77. Downhole remanence data for Holes 921B (**A**) and 921D (**B**) archive half-cores after demagnetization at 20 mT. Note the similarity in downhole variations to those from Hole 921E.

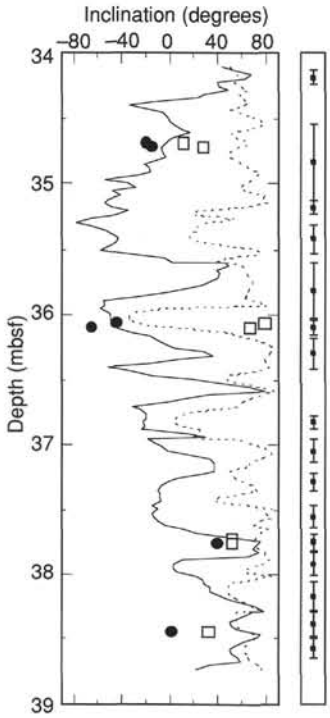

Figure 78. Correlation of archive half-core NRM (dotted line) and half-core demagnetized at 10 mT (solid line) inclination data, with discrete samples from Core 153-921B-4R. Discrete sample NRM (squares) and high-stability magnetization components (filled circles) agree reasonably well with the whole-core data.

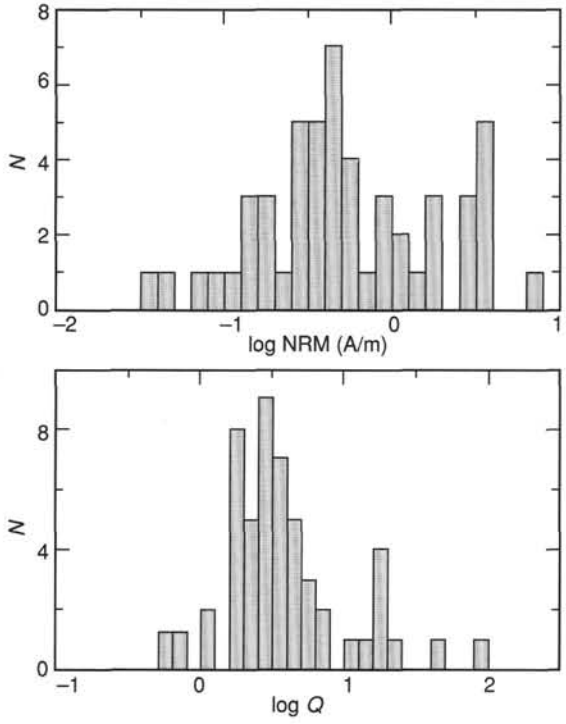

Figure 79. Histogram of NRM intensity and Koenigsberger ratio (Q) for Site 921 gabbros, showing log-normal distribution of samples.

is generally of reversed polarity and thus systematically will be reduced by the presence of normal polarity overprints (e.g., drilling-induced magnetizations). The mean NRM intensity is similar to that obtained for gabbros from Site 735B (1.6 A/m, excluding oxide gabbros; Kikawa and Pariso, 1991) and from dive samples at 15°N on the Mid-Atlantic Ridge (0.35 A/m; Wooldridge et al., 1990). No magnetic data are available for oxide gabbros since shipboard sampling was restricted to gabbros, olivine gabbros, and troctolites. Volume susceptibility for the discrete samples from Site 921 are typically 10^{-3} to 10^{-2} (SI units), similar to values previously reported from oceanic gabbros. The corresponding mean Koenigsberger ratio (the ratio of the remanent to induced magnetization, Q) for the gabbros is 3.89 ± 0.4 log units (arithmetic mean = 7.47), suggesting a significant (~20%) contribution from induced magnetization.

The majority of the discrete samples were stepwise demagnetized, primarily by AF treatment, and the best fit magnetization directions determined by principal component analysis (e.g., Kirschvink, 1980). Discrete sample magnetizations vary from univectorial to fairly complex, with up to three or four remanence components. There are examples of both normal and reversed polarity univectorial samples from Site 921 (Fig. 80A and 80B). The combination of moderate coercivity (e.g., Fig. 80B) and discrete unblocking temperatures near 575° (e.g., Fig. 80A) suggest fine-grained magnetite is the dominant carrier of remanence. Most samples have a drilling related remanence (removed by 5–10 mT) and one or more higher coercivity remanence components of either normal or reversed polarity (Fig. 80C to 80F). Final stable directions are not reached for approximately 40% of the samples, indicating the characteristic remanence direction has not been isolated. This interpretation is further supported by the broad distribution of inclinations for the high stability components identified (Fig. 81).

Anisotropy of magnetic susceptibility was also determined for the majority of the discrete samples. The degree of anisotropy, as defined by the ratio K_1/K_3, where K_1 and K_3 are the maximum and minimum principal axes of the susceptibility ellipsoid, respectively, is moderate to high (Fig. 82). Adjacent minicores exhibit very different anisotropy characteristics and values. For example, samples at 50.36 and 50.40 mbsf in Hole 921E have degrees of anisotropy of 1.328 and 1.164, respectively, exemplifying the heterogeneous nature of the magnetic properties within these gabbros. This high degree of small-scale variability precludes the identification of larger scale correlation downhole with any other characteristics. The three samples with the anomalously high anisotropy have strongly developed magmatic foliation (as defined by plagioclase preferred orientation seen in hand specimen and thin section). There is no obvious trend toward either oblate or prolate magnetic fabrics except in the three samples mentioned above that are oblate (Fig. 82).

Discussion of Paleomagnetic Results

Perhaps the most important paleomagnetic result from Site 921 is the identification of reversed polarity magnetizations, which constrain the age of this gabbroic block to be older than 0.78 Ma, the time of the last geomagnetic field reversal. Although the demagnetization behavior of samples from Site 921 is complex (see below), several observations provide convincing evidence for the presence of reversed polarity magnetizations. The final component may not have been adequately isolated in many cases; however, the majority of samples have high-stability components with negative inclinations with a mean (–35.5°, alpha 5.3, $n = 32$; McFadden and Reid, 1982), which is statistically indistinguishable from the expected reversed polarity dipole direction (–41°) at the site. In addition, most samples have a normal polarity overprint that is nearly antipodal to the high-stability magnetization direction. Finally, the generally high-stability to both AF and thermal demagnetization and the isolation of similar components by these two methods in closely spaced minicores (Fig. 83A and B) provide further support for the presence of primary reversed polarity magnetization.

Although the dominant reversed polarity of gabbros at Site 921 is well-established, discrete sample demagnetization studies have revealed a number of complexities that limit the usefulness of the remanence data for reorientation of structural features within the cores.

Table 9. Summary of magnetic properties of discrete samples from Site 921.

Core, section, interval (cm)	Piece	Rock type	Depth (mbsf)	NRM			*K* (SI)	AMS		
				Dec.	Inc.	Int.		P	L	F
1530-921A-										
2R-1, 102–105	10	Olivine gabbro	8.72	139.7	–47.2	7.57	0.02321	1.283	1.108	1.157
153-921B-										
1W-1, 64–67	9	Gneissic gabbro	0.64	30.3	9.5	0.05	0.00042	ND	ND	ND
1W-2, 15–18	3	Gabbro	1.57	57.2	10.3	0.43	0.01211	1.077	1.051	1.025
2R-1, 85–88	11	Gabbro	15.45	120.0	20.3	0.50	0.00760	1.099	1.063	1.034
2R-2, 16–20	1	Lineated gabbro	16.08	250.4	5.3	0.65	0.00465	1.031	1.023	1.008
3R-1, 133–136	13	Olivine gabbro	25.83	130.4	45.5	2.79	0.00105	1.054	1.052	1.002
3R-1, 134–137	13	Olivine gabbro	25.84	126.1	–37.6	3.29	0.00222	1.068	1.030	1.037
4R-1, 59–61	6B	Olivine gabbro	34.69	273.9	11.0	0.15	0.00204	1.183	1.111	1.065
4R-1, 62–65	6B	Olivine gabbro	34.72	257.6	27.3	0.15	0.00179	1.168	1.128	1.035
4R-2, 47–50	2	Olivine gabbro	36.07	7.8	79.1	0.30	0.00525	1.126	1.061	1.061
4R-2, 50–53	2	Olivine gabbro	36.10	356.1	–65.0	0.04	0.00250	1.159	1.108	1.046
4R-3, 77–80	8	Olivine gabbro	37.73	113.3	51.7	0.45	0.00394	1.252	1.037	1.207
4R-3, 80–83	8	Olivine gabbro	37.76	111.5	51.3	1.13	0.00926	1.188	1.072	1.108
4R-4, 16–19	1	Olivine gabbro	38.44	182.4	32.2	0.12	0.00571	1.134	1.070	1.061
153-921C-										
2R-1, 113–116	14	Lineated gabbro	11.13	152.4	56.9	1.16	0.01119	1.151	1.062	1.084
2R-2, 114–117	10	Olivine gabbro	12.54	96.7	62.0	0.26	0.00350	1.094	1.050	1.042
2R-2, 117–120	10	Olivine gabbro	12.57	71.9	34.3	0.50	0.00525	1.086	1.061	1.024
3R-1, 83–86	5B	Olivine gabbro	20.43	130.8	56.8	0.09	0.00158	1.149	1.112	1.033
3R-1, 86–89	5B	Olivine gabbro	20.46	121.0	63.2	0.08	0.00132	ND	ND	ND
3R-2, 136–139	13	Olivine gabbro	22.40	134.5	59.0	0.19	0.00322	1.123	1.102	1.019
153-921D-										
2R-1, 55–58	6	Gabbro	10.35	220.1	–44.1	3.69	0.00666	1.079	1.045	1.033
2R-1, 57–60	6	Gabbro	10.37	216.8	–44.5	3.97	0.00873	1.151	1.074	1.072
4R-1, 54–57	6B	Oxide gabbro	29.84	22.8	–17.0	0.59	0.00085	1.026	1.011	1.014
5R-1, 118–121	12C	Olivine gabbro	40.08	167.8	69.9	0.35	0.00444	1.164	1.129	1.031
5R-1, 121–124	12C	Olivine gabbro	40.11	113.3	59.9	0.13	0.00242	1.155	1.124	1.028
5R-2, 56–59	5	Olivine gabbro	40.91	59.2	60.0	1.99	0.00905	1.178	1.107	1.065
5R-2, 60–63	5	Olivine gabbro	40.95	53.1	64.3	1.94	0.00802	1.173	1.095	1.072
153-921E-										
2R-1, 6–9	1	Gabbro	9.96	106.3	63.5	0.97	0.00527	1.124	1.044	1.076
2R-2, 24–27	1	Pegmatitic melagabbro	11.39	246.8	0.6	1.70	0.00971	1.186	1.040	1.141
2R-2, 27–30	1	Pegmatitic melagabbro	11.42	254.5	–2.3	2.62	0.00432	1.110	1.035	1.072
2R-2, 83–86	8	Olivine gabbro	11.98	256.7	5.4	0.60	0.00711	1.050	1.023	1.027
3R-1, 138–141	15	Olivine gabbro	21.18	89.1	51.8	0.46	0.00366	1.084	1.024	1.059
3R-1, 141–144	15	Olivine gabbro	21.21	76.6	–2.6	0.43	0.00387	1.094	1.028	1.065
4R-1, 44–47	5	Olivine gabbro	30.14	122.8	56.3	0.22	0.00412	1.109	1.016	1.091
4R-1, 47–50	5	Olivine gabbro	30.17	46.8	–19.0	0.20	0.00196	1.070	1.015	1.055
4R-2, 36–39	1B	Olivine gabbro	31.31	49.4	39.6	0.20	0.00519	1.180	1.050	1.123
5R-2, 125–128	7	Olivine gabbro	41.89	214.8	56.2	0.29	0.00354	1.090	1.039	1.049
5R-2, 128–131	7	Olivine gabbro	41.92	230.5	59.5	0.59	0.00463	1.059	1.031	1.027
5R-3, 44–47	5	Olivine gabbro	42.57	249.4	55.5	0.26	0.00457	1.100	1.026	1.071
6R-1, 86–89	11A	Olivine gabbro	50.36	162.7	51.4	1.28	0.01162	1.328	1.083	1.226
6R-1, 93–96	11A	Olivine gabbro	50.43	94.6	70.5	0.37	0.00475	1.164	1.070	1.088
6R-2, 10–13	1B	Olivine gabbro	51.10	192.7	70.3	0.36	0.00366	1.111	1.054	1.054
7R-1, 92–95	9A	Olivine gabbro	60.32	12.9	16.4	0.30	0.00367	1.137	1.067	1.066
7R-2, 77–80	3	Olivine gabbro	61.58	84.3	–1.9	0.32	0.00513	1.092	1.060	1.030
7R-2, 80–83	3	Olivine gabbro	61.61	83.9	37.9	0.49	0.00830	1.078	1.042	1.034
7R-3, 51–54	1C	Olivine gabbro	62.66	75.0	60.4	0.97	0.00777	1.084	1.055	1.027
7R-3, 55–58	1C	Olivine gabbro	62.70	81.7	64.2	0.58	0.00827	1.083	1.057	1.024
7R-3, 83–86	2	Olivine gabbro	62.98	26.4	62.3	0.36	0.00440	1.141	1.068	1.068
8R-2, 18–21	2	Gabbro	70.50	193.4	59.8	3.77	0.02418	1.087	1.018	1.067
8R-2, 57–60	6	Olivine gabbro	70.89	204.3	–69.2	0.89	0.00965	1.107	1.026	1.079
9R-1, 52–55	4	Gabbro	79.12	356.1	23.0	3.57	0.00618	1.077	1.020	1.055
9R-1, 55–58	4	Gabbro	79.15	355.0	18.7	3.09	0.00606	1.065	1.018	1.046

Notes: Table includes volume susceptibility (*K*), natural remanent magnetization (NRM), magnetic fabric parameters (P, L, F; see caption for Fig. 82). Rock names (see "Igneous Petrology," this chapter) are defined for whole piece and may not be representative for minicore samples. ND = not determined.

For example, comparison of AF and thermal demagnetization results from one pair of minicore samples reveals distinct differences in the final magnetization components isolated by the two methods (Fig. 83C and 83D). The significance of the highest stability magnetization component is also ambiguous in some cases. Sample 153-921E-6R-1, 93–96 cm, illustrates a case in which isolation of distinct components during demagnetization was not possible (Fig. 84). Following removal of a drilling-induced remanence, demagnetization from 5 mT to 30 mT follows a great circle path from a normal polarity direction toward a reversed a reversed polarity direction. Further demagnetization (30–70 mT) follows a second great circle path, representing the interaction of this reversed polarity direction and an additional magnetization component. There is no evidence that the demagnetization of this sample has isolated the characteristic remanence by 70 mT.

It is unclear whether the presence of both normal and reversed polarity magnetizations at Site 921 reflects the high degree of small-scale heterogeneity of magnetic properties (and hence possibly different responses to the same physical and/or geomagnetic conditions) or whether it is related to distinct histories (e.g., local reheating, alteration, structural juxtaposition). Apparent polarity shifts occur both within and between pieces. The origin of such intimately associated normal and reversed polarity intervals will be the subject of shore-based studies.

The identification of reversed polarity high-stability intervals in these cores provides some age constraints on the area, as well as some limitations on the nature of asymmetric spreading in this region of the Mid-Atlantic Ridge. Recovery of reversed polarity material from this area is not an unexpected result given the sea-surface magnetic anom-

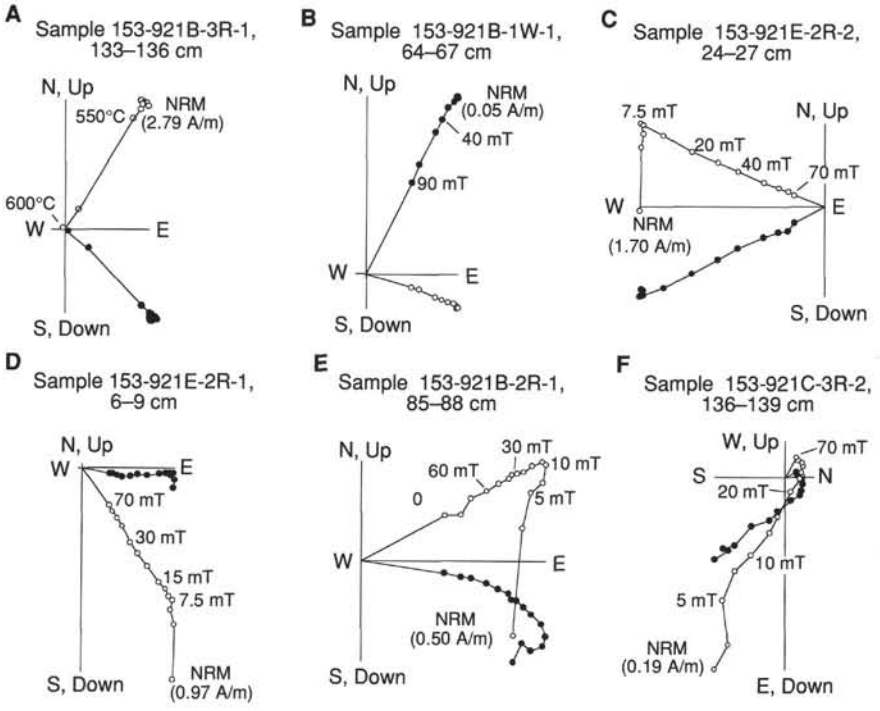

Figure 80. Vector endpoint diagrams for AF and thermal demagnetization of representative discrete samples. (**A**) and (**B**) show univectorial negative and positive inclination examples. (**C**) shows reversed polarity containing a drilling overprint that is removed by 7.5 mT. (**D**) is a multicomponent example with a drilling component and two normal components, one removed between 7.5 mT and 30 mT, the second from 30 mT to 70 mT. (**E**) shows a similar example with a drilling overprint and one or more reversed polarity components. (**F**) is a multicomponent sample typical of many of the complexly magnetized samples obtained, with a drilling remanence (<5 mT), a normal overprint removed between 5 mT and 50 mT, and the highest stability component isolated between 50 and 70 mT. This reversed polarity component does not tend toward the origin and hence is not considered to be the characteristic remanence direction. Filled (open) circles are projections of the vector onto the horizontal (vertical) plane. NRM intensity for each sample given in parentheses.

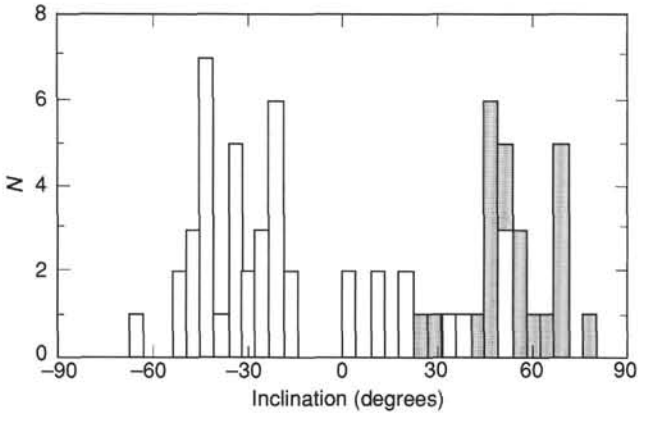

Figure 81. Inclinations of magnetization components from Site 921 discrete samples. The normal polarity overprint (shaded) has a mean value of 56.3° ± 6°, steeper than the expected geocentric axial dipole inclination (41°). The higher stability component shows two populations, one positive and one negative inclination group with mean values 27.5° ± 14° and –33.5° ± 5°, respectively.

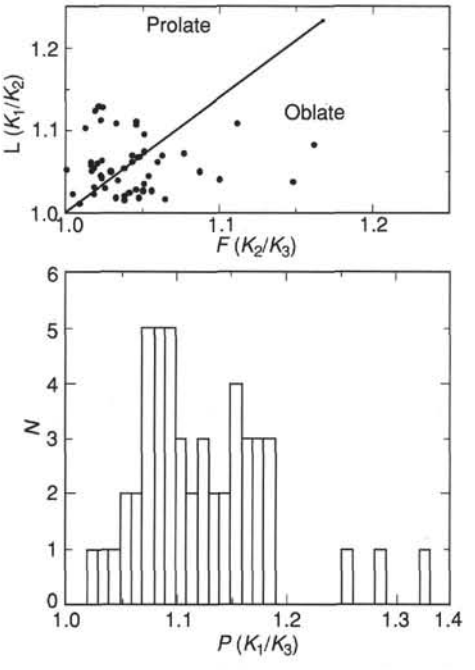

Figure 82. Magnetic fabric of gabbros from Site 921. Magnetic fabric lineation (L) vs. foliation (F), illustrating dominantly triaxial susceptibility ellipsoid shape. Anisotropy degree (P) for Site 921 gabbros.

aly data, which suggest the western flank of the median valley is reversely magnetized (Schulz et al., 1988). Also the observation of an apparent reversal within Hole 921E, together with the complex nature of the remanence, makes any reorientation of the magmatic or structural features within the cores difficult.

PHYSICAL PROPERTIES

Minicores were sampled from 44 locations representative of rock types cored at Site 921. These were analyzed for horizontal compressional wave velocity (V_p), resistivity, and a determination of index properties (bulk density, grain density, water content, porosity, and dry density; Table 10). Thermal conductivities were determined from 28 half-round archive sections of core (Table 11). Bulk whole-core densities were also measured using the gamma-ray attenuation porosity evaluator (GRAPE) component of the multisensor track. Descriptions of experimental methods are provided in the "Physical Properties" section of the "Explanatory Notes" (this volume) and in the "Explanatory Notes" of the Leg 147 *Initial Reports* (Gillis, Mével, Allan, et al., 1993).

Comparative analysis of bulk densities determined from GRAPE and discrete sample methods for Site 920 material ("Physical Properties" section, "Site 920," this volume) shows that trends in density variations downhole are also represented by GRAPE measurements when coring recovers long (>15 cm), continuous intervals. However,

Table 10. Index properties, horizontal compressional-wave velocities (V_p), resistivities, and water contents of the crystalline rocks recovered from Site 921.

Core, section, interval (cm)	Piece	Depth (mbsf)	V_p (m/s)	Resistivity (Ωm)	Wet-bulk density (g/cm^3)	Dry-bulk density (g/cm^3)	Grain density (g/cm^3)	Void ratio	Porosity (%)	Water content (%)	Alteration estimate (%)	Rock type	Unit
153-921A-													
2R-1, 102–104	10	8.72	4996	130.0	2.9431	2.9341	2.9604	0.009	0.8877	0.3093	*	OG	1
153-921B-													
1W-1, 64–66	9	0.64	5429	149.2	2.893	2.877	2.923	0.0161	1.582	0.562	62	CMG	1
1W-2, 15–17	3	1.57	5521	609.7	2.969	2.966	2.975	0.0030	0.297	0.102	11	G	3
2R-1, 85–87	11	15.50	6028	155.1	3.021	3.017	3.029	0.0041	0.407	0.138	22	G	3
2R-2, 16–18	1	16.10	5344	120.3	2.974	2.966	2.990	0.0082	0.818	0.282	7	LG	3
3R-1, 134–136	13	25.80	5609	203.9	3.001	2.995	3.013	0.0059	0.588	0.201	2	OG	3
4R-1, 59–61	6B	34.70	5832	248.4	2.980	2.975	2.989	0.0045	0.449	0.154	35	OG	3
4R-1, 62–64	6B	34.70	5758	448.0	2.994	2.989	3.003	0.0046	0.461	0.158	35	OG	3
4R-2, 50–52	2	36.10	6516	220.5	2.959	2.952	2.974	0.0077	0.759	0.263	3	OG	4
4R-3, 77–79	8	37.70	5306	231.8	2.792	2.783	2.808	0.0089	0.883	0.324	21	OG	4
4R-3, 80–82	8	37.80	5289	263.8	2.848	2.840	2.862	0.0076	0.759	0.273	21	OG	4
4R-4, 16–18	1	38.40	5374	84.1	2.875	2.867	2.888	0.0073	0.726	0.259	2	OG	4
153-921C-													
2R-1, 113–115	14	11.10	5264	*	2.980	2.978	2.984	0.0021	0.213	0.073	48	LG	3
2R-2, 114–116	9	12.50	5038	*	3.025	3.020	3.034	0.0049	0.485	0.164	4	OG	4
2R-2, 117–119	10	12.60	5459	246.4	2.996	2.990	3.006	0.0051	0.509	0.174	4	OG	4
3R-1, 83–85	5B	20.40	5513	1765.5	2.977	2.974	2.983	0.0031	0.307	0.106	11	OG	4
3R-1, 86–88	5B	20.50	5548	1181.1	2.985	2.982	2.991	0.0030	0.297	0.102	11	OG	4
3R-2, 136–138	13	22.40	5475	364.1	2.944	2.939	2.954	0.0052	0.517	0.180	14	OG	4
153-921D-													
2R-1, 55–57	6	10.40	5124	808.7	2.959	2.952	2.972	0.0067	0.669	0.232	25	G	1
2R-1, 57–59	6	10.40	5277	200.3	2.915	2.905	2.935	0.0103	1.023	0.360	25	G	1
4R-1, 54–56	6B	29.80	5073	58.9	3.033	3.016	3.065	0.0161	1.588	0.538	19	OXG/G	1
5R-1, 121–123	2C	40.10	6012	317.6	2.942	2.935	2.954	0.0065	0.647	0.225	0	AB	1
5R-2, 60–62	5	41.00	5656	500.5	2.865	2.859	2.876	0.0058	0.577	0.206	2	OG	1
153-921E-													
2R-1, 6–8	1	9.96	4976	595.5	2.970	2.961	2.987	0.0087	0.859	0.296	6	G	1
2R-2, 27–29	1	11.40	5336	239.2	2.963	2.954	2.978	0.0081	0.804	0.278	9	PG	1
2R-2, 83–85	8	12.00	6330	344.7	3.033	3.026	3.046	0.0066	0.653	0.221	17	OG	1
3R-1, 141–143	15	21.20	5835	921.8	2.992	2.986	3.004	0.0062	0.620	0.212	(16–30)*	OG	2
4R-1, 44–46	5	30.10	5727	1000.5	2.904	2.900	2.910	0.0033	0.325	0.114	7	OG	2
4R-1, 47–49	5	30.20	5542	197.0	2.850	2.844	2.861	0.0061	0.603	0.217	7	OG	2
4R-2, 36–38	1B	31.30	5607	153.5	2.954	2.949	2.964	0.0048	0.475	0.165	5	OG	2
5R-2, 125–127	7	41.90	5889	63.5	2.857	2.851	2.869	0.0063	0.630	0.226	1	OG	2
5R-2, 128–130	7	41.90	5520	136.9	2.882	2.878	2.888	0.0036	0.361	0.128	1	OG	2
5R-3, 44–46	5	42.60	5399	258.8	2.884	2.878	2.895	0.0057	0.569	0.202	1	OG	2
6R-1, 93–95	11A	50.40	5740	141.4	2.942	2.936	2.953	0.0059	0.588	0.205	5	OG	2
6R-2, 10–12	1B	51.10	5741	241.8	3.001	2.996	3.011	0.0050	0.497	0.170	2	OG	2
7R-1, 92–94	9A	60.30	5398	181.9	3.087	3.079	3.101	0.0072	0.714	0.237	21	OG	2
7R-2, 77–79	3	61.60	5403	329.0	2.938	2.926	2.962	0.0124	1.229	0.429	13	OG	2
7R-2, 80–82	3	61.60	5801	228.6	2.971	2.966	2.982	0.0055	0.543	0.187	13	OG	2
7R-3, 55–57	1C	62.70	5485	143.4	2.864	2.861	2.870	0.0029	0.286	0.102	6	OG	2
7R-3, 83–85	2	63.00	5663	347.4	2.921	2.916	2.929	0.0044	0.437	0.153	6	OG	2
8R-2, 18–20	2	70.50	5535	1276.8	2.932	2.931	2.933	0.0007	0.074	0.026	20	G	3
8R-2, 57–59	6	70.90	5567	864.4	2.963	2.962	2.966	0.0014	0.136	0.047	6	OG	3
9R-1, 52–54	4	79.10	5640	1189.1	2.998	2.995	3.002	0.0022	0.217	0.074	2	G	3
9R-1, 55–57	4	79.20	5253	1462.8	2.981	2.977	2.988	0.0036	0.362	0.124	2	G	3

Notes: * = not measured in this sample (nearby value). Definitions: G = gabbro, OG = olivine gabbro, PG = pegmatitic gabbro, CMG = cataclastic metagabbro, LG = lineated gabbro, OXG = oxide-rich gabbro, AB = aphyric basalt.

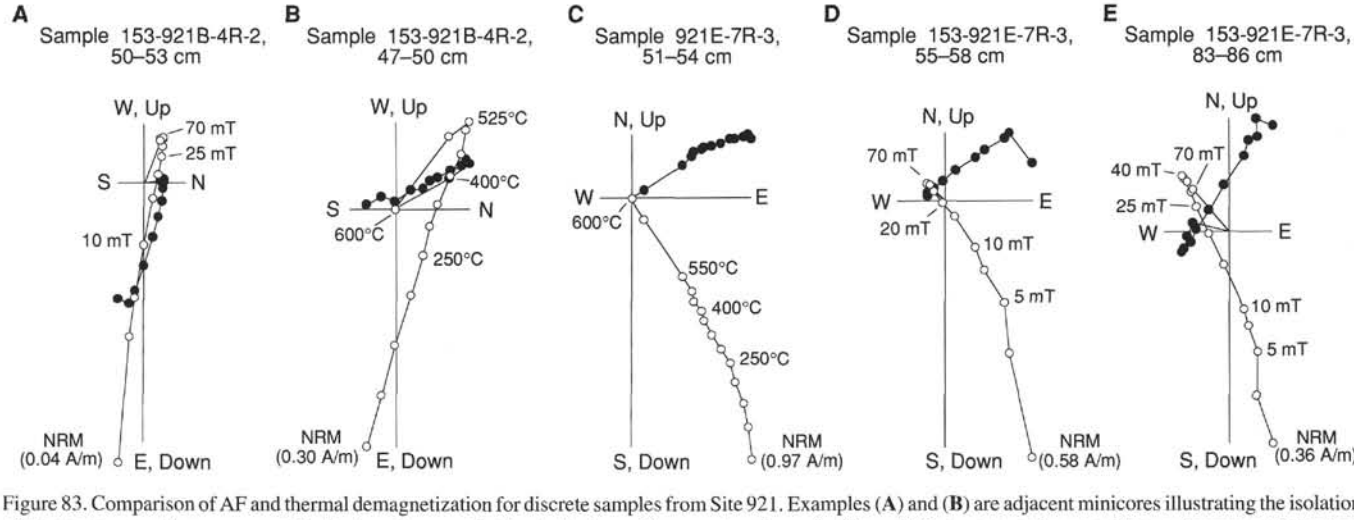

Figure 83. Comparison of AF and thermal demagnetization for discrete samples from Site 921. Examples (**A**) and (**B**) are adjacent minicores illustrating the isolation of the same magnetic components by the two demagnetization techniques. The samples shown in (**C**) and (**D**) are also adjacent minicores, however, the highest stability components are of opposite polarity. Note also that the final component in (**C**) corresponds to an intermediate direction in (**D**). An additional sample (**E**) from the same section suggests a possible downhole progression toward more pronounced reversed polarity final directions. NRM intensity for each sample given in parentheses.

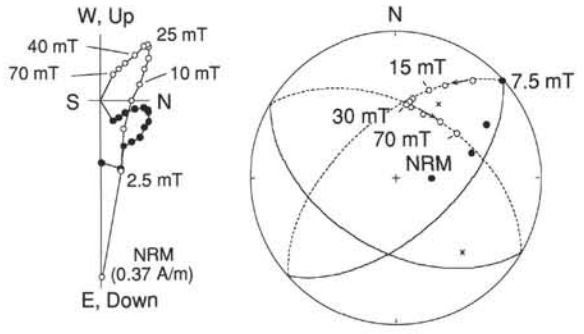

Figure 84. Vector endpoint diagram and equal area plot for Sample 153-921E-6R-1, 93–96 cm, which was AF demagnetized. Filled (open) circles are projections of the vector onto the horizontal (vertical) plane. The demagnetization path follows two great circle paths after the removal of the drilling remanence acquired. This sample has at least three components of remanence and a characteristic remanence direction has not been isolated.

this analysis additionally resolves a large discrepancy in values determined by these two methods. Due to the rather limited nature of core recovery at Site 921, GRAPE data have not been included in the comparative analysis of physical properties presented below. The following discussion incorporates a summary of index properties for this site, an examination of downhole variations in these properties for Holes 921B, 921C, 921D, and 921E (the single measurement from Hole 921A precludes its inclusion in downhole analysis), and consideration of relationships between various physical properties examined at this site. While the measurements are believed to characterize accurately the samples studied, it must be kept in mind that the coarse grain-size and variability inherent of gabbroic rocks does limit the extent to which results from the analysis of small samples can be extrapolated to larger scale downhole characteristics at each location.

Summary of Index Properties for Site 921

Bulk densities, porosity, water content, and void ratio have been determined (with salt volume corrections for a salinity of 0.032) from wet and dry mass and volume measurements of minicores sampling the predominantly gabbroic rock recovered at Site 921 (Table 10). Bulk densities range from 2.79 to 3.08 g/cm^3 with a median value of 2.96. Grain densities are only slightly higher (2.81 to 3.10 g/cm^3 with a median value of 2.97 g/cm^3), reflecting the characteristic low porosity (0.07% to 1.59% with a median value of 0.57%) of these rocks. V_p ranges from 4976 to 6516 m/s in these rocks, with a median value of 5520 m/s. The densities and velocities of these rocks are similar to those observed in metagabbroic rocks exposed in fracture zones of the Atlantic (e.g., compilation of Christensen, 1982). The rocks display thermal conductivities ranging from 2.23 to 3.1 W/m°C with a median value of 2.7 W/m°C, which is within the range of variability observed in gabbroic material by Clark (1966).

Downhole Variations

Hole 921B

Variations in rock resistivity, V_p, porosity, density, thermal conductivity, and alteration as a function of depth for Hole 921B are shown within panels of Figure 85 adjacent to bars indicating core recovery and unit boundaries determined from considerations of primary mineralogy and texture (see "Igneous Petrology," this chapter).

Resistivities of the gabbroic rock recovered from Hole 921B fall in the 10–10^3 Ωm range (Fig. 85). A rapid increase in resistivity with depth from 0.64 to 1.6 m corresponds with a change from highly altered (62%) to relatively fresh (11% alteration) gabbro in Units 1 and 2, respectively (Fig. 85 and Table 10). Lower resistivities (120–155 Ωm) observed at 15.5–16.1 mbsf in Unit 3 are from somewhat

Table 11. Thermal-conductivity data of samples from Site 921.

Core, section, interval (cm)	Piece	Depth (mbsf)	Thermal conductivity (W/m°C)	Rock type	Alteration (%)
153-921B-					
1W-1, 63–76	9	0.63	2.342	CMG	62
1W-2, 13–24	3	1.55	2.485	G	11
2R-2, 1–21	1	15.93	2.927	FG	7
2R-2, 94–108	7	16.86	2.415	FG	10
3R-1, 131–147	13	25.81	2.684	OG	2
4R-2, 45–57	2	36.05	2.769	OG	3
4R-4, 1–20	1	38.29	2.234	OG	2
153-921C-					
2R-1, 110–125	14	11.1	2.741	LG	48
2R-2, 112–126	10	12.52	2.622	OG	4
3R-1, 22–35	4	19.82	2.690	OG	10
3R-1, 93–109	5C	20.53	2.902	OG	(11)*
3R-2, 124–142	13	22.28	2.239	OG	14
153-921D-					
2R-1, 49–62	6	10.29	2.865	G	25
4R-1, 53–68	6B	29.83	3.100	OXG/G	19
5R-1, 115–126	12C	40.05	2.800	OG	16
5R-2, 52–64	5	40.87	2.262	OG	2
153-921E-					
2R-2, 82–93	8	11.97	2.533	OG	17
3R-1, 129–145	15	21.09	2.539	OG	16
4R-1, 37–52	5	30.07	2.714	OG	7
5R-3, 37–48	5	42.50	2.430	OG	1
6R-1, 84–97	11A	50.34	2.727	OG	5
6R-2, 7–19	1B	51.07	2.834	OG	2
7R-2, 76–92	3	61.57	2.710	OG	13
7R-2, 94–113	4	61.75	2.393	OG	25
7R-3, 50–65	1C	62.65	2.675	OG	6
7R-4, 36–56	3	63.88	2.249	OG	27
8R-1, 70–86	10	69.70	2.932	LG	25
9R-1, 40–57	4	79.00	2.633	G	2

Notes: * = not measured in this sample (nearby value). Definitions: G = gabbro, FG = foliated gabbro, CMG = cataclastic metagabbro, LG = lineated gabbro, OG = olivine gabbro, OXG = oxide-rich gabbro.

altered (22%) gabbro and less altered (7%) foliated gabbro. Underlying olivine gabbro from Units 3 and 4 show resistivities of 200–400 Ωm, with the relatively unaltered (2%) olivine gabbro at the base of Unit 4 showing the lowest resistivity (84 Ωm) measured in this hole.

V_p (right curve, first panel, Fig. 85) appears to generally increase downhole with common offsets to lower velocities at two depths. The first apparent decrease in velocity corresponds to the transition from gabbro to foliated gabbro at about 16 mbsf. Beneath this, V_p again increases with depth until about 37 mbsf in Unit 4. At greater depth several observations support a velocity drop to near 5300 m/s at the base of Unit 4.

Porosity (Fig. 85) is highest in rock recovered from the top of Hole 921B; it then decreases sharply to less than about 1% for the remaining samples. A modest increase from 0.5% to 1% occurs near 16 mbsf and corresponds with the observed velocity decrease in the first panel. Porosity appears to decrease with depth in Unit 3 and then increases somewhat within Unit 4.

Density (Fig. 85) variations with depth are generally inverse to those described for porosity, with a density increase corresponding to the transition from Unit 1 to Unit 2 and a significant reduction in density associated with Unit 4.

Thermal conductivity (Fig. 85) varies greatly with depth. The most apparent features are a large decrease in thermal conductivity from about 2.9 to 2.4 W/m°C between 15.9 and 16.9 mbsf in Unit 3 and another large decrease from about 2.8 to 2.2 W/m°C between 36 and 38.3 mbsf in Unit 4.

Estimates of alteration with depth (corresponding to most of the physical property sample locations) from visual core descriptions (see "Metamorphic Petrology," this chapter) are shown in Figure 85. Alteration of the gabbro is greatest at the top of the hole and fluctuates from moderately low to very low values. The variations at 16 mbsf within Unit 3 and 36 mbsf within Unit 4 are also observed in the previously described physical properties measurements.

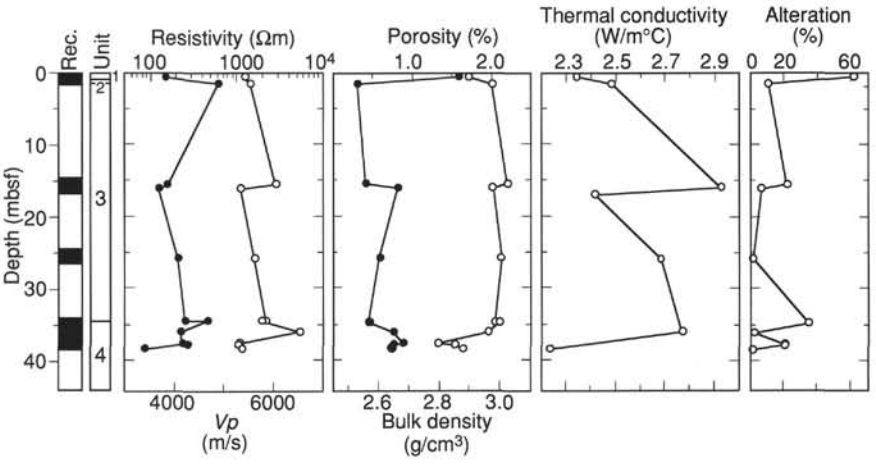

Figure 85. Physical property determinations, core recovery, and unit identification as functions of depth for Hole 921B. Circles represent locations of physical properties determinations. First panel from left: left curve is resistivity (filled circles), right curve is velocity (open circles). Second panel: left curve is porosity (filled circles), right curve is density (open circles).

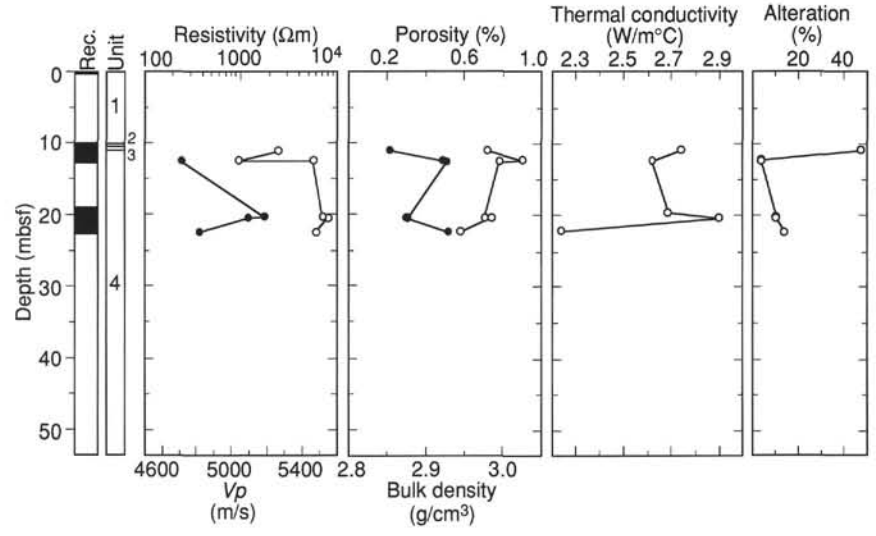

Figure 86. Physical property determinations, core recovery, and unit identification as functions of depth for Hole 921C. Circles represent locations of physical properties determinations. Format follows style of Figure 85.

Hole 921C

Downhole diagrams of physical properties measurements from Hole 921C are shown in Figure 86, with bars indicating core recovery and unit identification. Obviously the very limited recovery also limits downhole interpretations, but some information can be extracted. Units 1 and 2 were not sampled by minicores, but the transition from Unit 3 to Unit 4 at 11.64 mbsf is clearly supported by the large variations observed in velocity, porosity, bulk density, thermal conductivity, and alteration observations from 11.1 to 12.5 mbsf (samples from this depth were too narrow to measure resistivity). Another change appears between 20.5 and 22.4 mbsf in Unit 4, characterized by consistent decreases in resistivity, V_p, and thermal conductivity, and an increase in porosity.

Hole 921D

Variations in resistivity, V_p, porosity, bulk density, thermal conductivity, and alteration as a function of depth in Hole 921D are shown in Figure 87. The main feature in this single unit hole of limited core recovery is the oxide gabbro occurring at about 30 mbsf, characterized by relatively low resistivity and velocity and high porosity, bulk density, and thermal conductivity. The olivine gabbro from the base of the hole is characterized by relatively high resistivity, velocity, and bulk density and very low porosity, thermal conductivity, and alteration.

Hole 921E

Figure 88 shows the variations in resistivity, velocity, porosity, bulk density, thermal conductivity, and alteration as a function of depth in Hole 921E. Unit 1 is characterized by an increase in velocity, bulk density, and alteration, and a reduction in resistivity and porosity with depth as rock type changes from gabbro to pegmatitic melanogabbro and then olivine gabbro with depth. Resistivity, velocity, porosity, bulk density, alteration, and thermal conductivity (questionable) generally decrease slightly with depth in the underlying olivine gabbro of Unit 2 to about 42 mbsf; beneath this level, bulk density, thermal conductivity, and alteration show slight to moderate increasing trends whereas resistivity, velocity, and porosity remain relatively constant to about 60 mbsf.

The moderately altered (about 20%) gabbro and lineated gabbro constituting Unit 3 from 69 mbsf to the base of Hole 921E show slightly higher resistivities and lower porosities overall, while velocity and bulk density remain approximately constant. Thermal conductivity is high in the somewhat altered (25%) lineated gabbro at the top of Unit 3 and declines to lower values with decreased alteration in olivine gabbro.

Considerable variation in porosity, bulk density, thermal conductivity, and alteration is observed in the thickest core recovery interval (about 59–65 mbsf); these parameters vary nearly as much in this interval as through the entire remaining core and raise concern as to whether the highly variable nature of this rock precludes meaningful

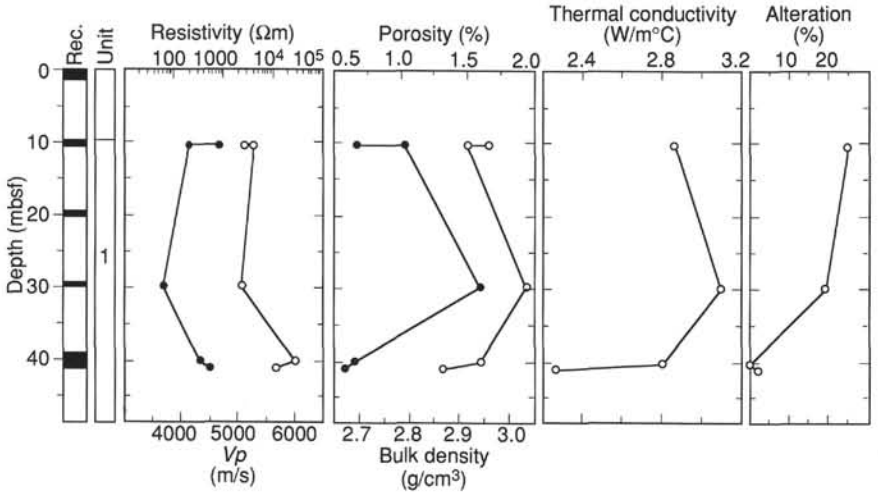

Figure 87. Physical property determinations, core recovery, and unit identification as functions of depth for Hole 921D. Circles represent locations of physical properties determinations. Format follows style of Figure 85.

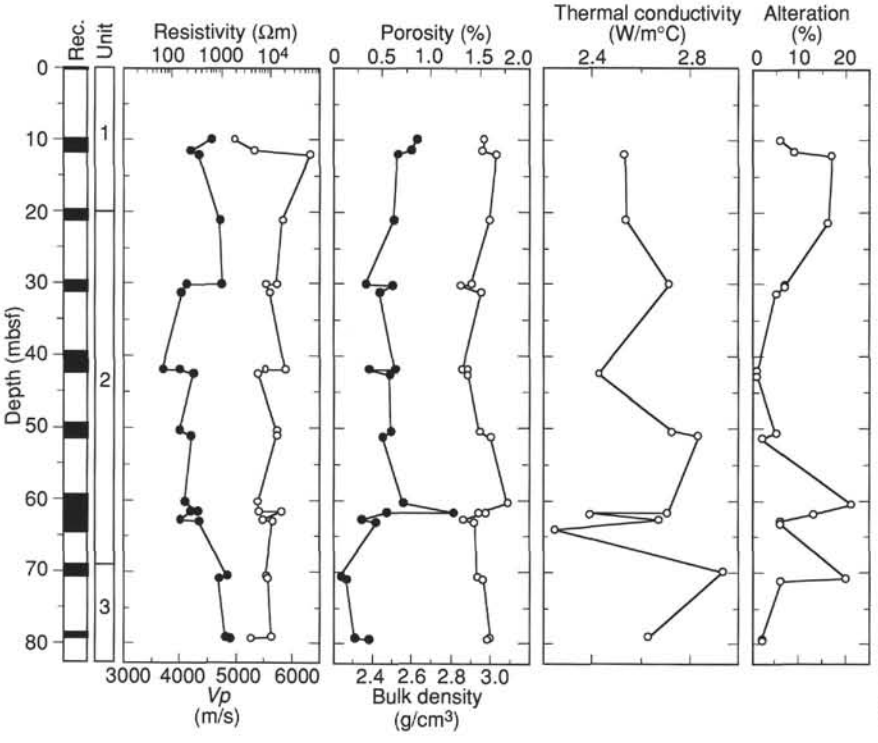

Figure 88. Physical property determinations, core recovery, and unit identification as functions of depth for Hole 921E. Circles represent locations of physical properties determinations. Format follows style of Figure 85.

downhole analysis from minicore sampling. While it remains possible that limited sampling is biasing downhole interpretations it appears more likely that the longer wavelength trends are probably real and a downhole investigation of these characteristics is appropriate for the intended overview nature of shipboard physical properties analysis. Many of the trends recovered from the successive minicore analysis in this interval are smoothly varying and are likely to represent characteristics that vary downhole. For example it is evident that resistivity and velocity analyses in this interval yield a narrow range of values that could have been recovered from even fewer samples.

Comparative Analysis of Site 921 Physical Properties Measurements

The uppermost oceanic crust at this location is composed of variably altered and deformed gabbro that was probably emplaced in an extensional tectonic regime at a slow-spreading mid-ocean ridge. It is characterized by seismic Layer 2 compressional-wave velocities and shows moderate to somewhat high thermal conductivities. Fluctuations in conductivity appear to mostly reflect variations in rock lithology and extent of deformation; the oxide mineral-rich gabbro in Unit 1 of Hole 921D shows the highest conductivity (3.1 W/m°C), and foliated and lineated gabbro are less conductive than the bulk of the remaining gabbro and olivine gabbro.

The bulk densities of the crust at this site are moderately high, clustering at about 2.95 g/cm^3 (Fig. 89), and associated velocities cluster around 5500 m/s. Slightly altered (11%–25%) olivine gabbro appears to be somewhat more dense than fresher (2%–6% alteration) olivine gabbro showing similar velocity characteristics. Oxide gabbro is characterized by relatively high density but low velocity, as was also observed at Hole 735B (Robinson, von Herzen, et al., 1989). The gabbroic suite of rocks displays a general increase in velocity with increasing density, while such a trend is absent from the olivine gabbro samples considered separately. Similarly, the gabbroic suite

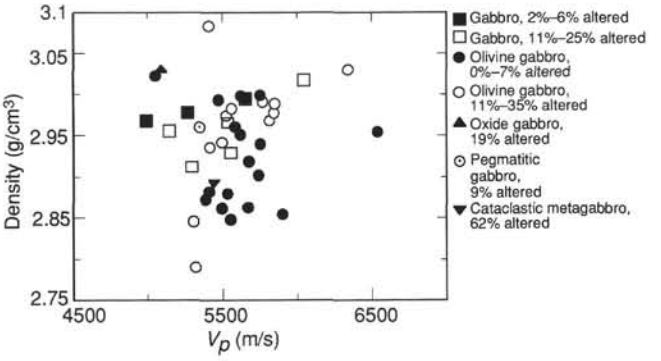

Figure 89. Velocity (V_p) vs. density for rocks recovered at Site 921.

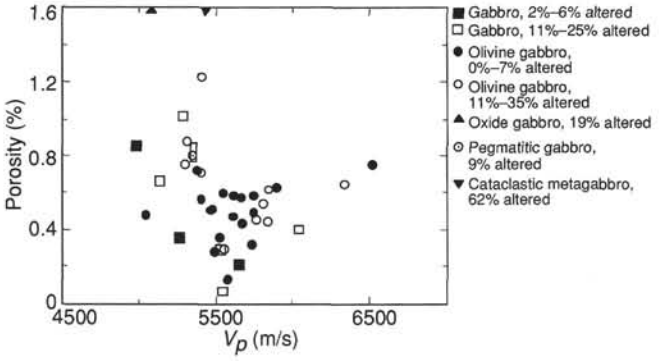

Figure 90. Velocity (V_p) vs. porosity for rocks recovered at Site 921.

displays a general decrease in velocity with increasing porosity (Fig. 90), while olivine gabbro samples show only a weak trend of decreasing velocity with increasing porosity. Two moderately porous (0.8%) olivine gabbro samples show higher velocities (6300–6500 m/s) than any of the less porous gabbro or olivine gabbro samples. The somewhat altered (19%) oxide gabbro and moderately altered (62%) cataclastic metagabbro show the highest porosities (1.6%) of all samples.

While the densities and velocities observed at this site are within the range of observations from similar rocks exposed in fracture zones of the Atlantic (e.g., Christensen, 1982), the absence of a clear velocity-density trend for the entire set of gabbroic samples suggests that variations in modal mineralogy may be the predominant factor responsible for the observed variations in sample V_p. The observation that altered olivine gabbro is frequently denser than fresh olivine gabbro (Fig. 89) may be further evidence that important modal and/or compositional variations occur within this group. The velocities measured in the rocks of Site 921 are generally 1000 m/s slower than similar density, low to moderate porosity gabbroic rocks recovered from Hole 735B in the Southwest Indian Ocean (Robinson, Von Herzen, et al., 1989) or from the Hess Deep area (Gillis, Mével, Allan, et al., 1993a).

Resistivities measured in gabbroic rock from Site 921 are shown in Figure 91 in terms of the formation factor (ratio of rock and pore-water resistivity) and porosity (shown as a ratio of rock volume corrected for salt). The samples display a roughly linear trend in the log-log plot, supportive of the interpretation that electrolytic conduction in pore spaces is the dominant conduction mechanism in many of these rocks (Pezard et al., 1991). Lower resistivities (300 Ωm) are observed in relatively unaltered (0–7%) gabbroic rocks and a somewhat altered (19%) oxide gabbro (Sample 153-921D-4R-1, Piece 6B, 54–56 cm). However, even these low resistivities are an order of magnitude higher than resistivities observed in fresh oxide gabbro obtained at Hole 735B (10 Ωm), which Pezard et al. (1991) interpret

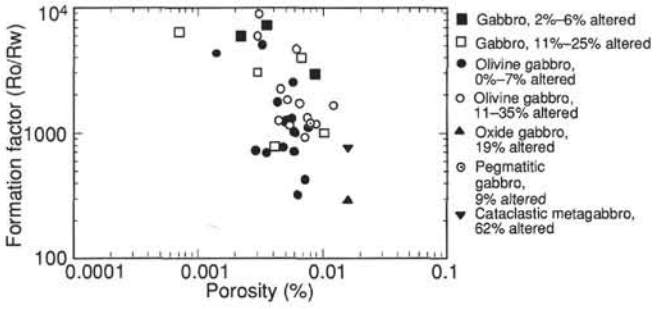

Figure 91. Formation factor (ratio of rock and pore-water resistivity) vs. porosity (corrected for salt) relationships for rocks recovered at Site 921.

as evidence for electronic conduction in metallic grains of the matrix. The higher resistivity observed in the oxide gabbro sample at Site 921 suggests that even moderate alteration can change the dominant conduction mechanism in these rocks.

REFERENCES*

Auzende, J.M., Cannat, M., Gente, P., Henriet, J.P., Juteau, T., Karson, J.A., Lagabrielle, Y., and Tivey, M.A., 1993. Deep layers of mantle and oceanic crust exposed along the southern wall of the Kane Fracture Zone: submersible observations. *C.R. Acad. Sci. Ser. 2,* 317:1641–1648.

Bryan, W.B., Thompson, G., and Ludden, J.N., 1981. Compositional variation in normal MORB from 22°–25°N: Mid-Atlantic Ridge and Kane Fracture Zone. *J. Geophys. Res.,* 86:11815–11836.

Bryan, W.F., Humphris, S., Thompson, G., and Casey, J.F., 1994. Comparative volcanology of small eruptive centers in the MARK area. *J. Geophys. Res.,* 99:3013–3029.

Cande, S.C., and Kent, D.V., 1992. A new geomagnetic polarity time scale for the Late Cretaceous and Cenozoic. *J. Geophys. Res.,* 97:13917–13951.

Christensen, N.I., 1982. Seismic velocities. *In* Carmichael, R.S. (Ed.), *Handbook of Physical Properties of Rocks:* Boca Raton, FL (CRC Press), 2:1–228.

Clark, S.P. (Ed.), 1966. *Handbook of Physical Constants.* Mem.—Geol. Soc. Am., 97.

Gillis, K.M., Mével, C., Allan, J.F., et al., 1993. *Proc. ODP, Init. Repts.,* 147: College Station, TX, (Ocean Drilling Program).

Humphris, S.E., Bryan, W.B., Thompson, G., and Autio, L.K., 1990. Morphology, geochemistry, and evolution of Serocki volcano. *In* Detrick, R., Honnorez, J., Bryan, W.B., Juteau, T., et al. *Proc. ODP, Sci. Results,* 106/109: College Station, TX (Ocean Drilling Program), 67–84.

Karson, J.A., and Dick, H.J.B., 1983. Tectonics of ridge-transform intersections at the Kane Fracture Zone. *Mar. Geophys. Res.,* 6:51–98.

Kikawa, E., and Pariso, J.E., 1991. Magnetic properties of gabbros from Hole 735B, Southwest Indian Ridge. *In* Von Herzen, R.P., Robinson, P.T., et al., *Proc. ODP, Sci. Results,* 118: College Station, TX (Ocean Drilling Program), 285–307.

Kirschvink, J.L., 1980. The least-squares line and plane and analysis of palaeomagnetic data. *Geophys. J. R. Astron. Soc.,* 62:699–718.

Klein, E.M., and Langmuir, C.H., 1987. Global correlations of ocean ridge basalt chemistry with axial depth and crustal thickness. *J. Geophys. Res.,* 92:8089–8115.

Liou, J.G., Kuniyoshi, S., and Ito, K., 1974. Experimental studies of the phase relations between greenschist and amphibolite in a basaltic system. *Am. J. of Sci.,* 274:613–632.

McFadden, P.L., and Reid, A.B., 1982. Analysis of paleomagnetic inclination data. *Geophys. J. R. Astron. Soc.,* 69:307–319.

Miyashiro, A., and Shido, F., 1980. Differentiation of gabbros in the mid-Atlantic ridge near 24°N. *Geochem. J.,* 14:145–154.

Pezard, P.A., Howard, J.J., and Goldberg, D., 1991. Electrical conduction in oceanic gabbros, Hole 735B, Southwest Indian Ridge. *In* Von Herzen, R.P.,

*Abbreviations for names of organizations and publications in ODP reference lists follow the style given in *Chemical Abstracts Service Source Index* (published by American Chemical Society).

Robinson, P.T., et al., *Proc. ODP, Sci. Results,* 118: College Station, TX (Ocean Drilling Program), 323–332.
Pinto, M.J., and McWilliams, M., 1990. Drilling-induced isothermal remanent magnetization. *Geophysics,* 55:111–115.
Purdy, G.M., Rabinowitz, P.D., and Schouten, H., 1979. The Mid-Atlantic Ridge at 23°N; bathymetry and magnetics. *In* Melson, W.G., Rabinowitz, P.D., et al., *Init. Repts. DSDP,* 45: Washington (U.S. Govt. Printing Office), 119–128.
Robinson, P.T., Von Herzen, R., et al., 1989. *Proc. ODP, Init. Repts.,* 118: College Station, TX (Ocean Drilling Program).
Schouten, H., Cande, S.C., and Klitgord, K.D., 1985. *Magnetic Anomaly Profiles 22°–38°N in Ocean Margin Drilling Program Regional Data Synthesis Series, Atlas II, Mid-Atlantic Ridge between 22° and 38°N:* Woods Hole, MA (Marine Science International).
Schulz, N.J., Detrick, R.S., and Miller, S.P., 1988. Two- and three-dimensional inversions of magnetic anomalies in the MARK area (Mid-Atlantic Ridge, 23°N). *Mar. Geophys. Res.,* 10:41–57.
Spear, F.S., 1981. An experimental study of hornblende stability and compositional variability in amphibolite. *Am. J. Sci.,* 281:697–734.
Sun, S.-S., and McDonough, W.F., 1989. Chemical and isotopic systematics of oceanic basalts: implications for mantle composition and processes. *In* Saunders, A.D., and Norry, M.J. (Eds.), *Magmatism in the Ocean Basins.* Geol. Soc. Spec. Publ. London, 42:313–345.
Tiezzi, L.J., and Scott, R.B., 1980. Crystal fractionation in a cumulate gabbro, Mid-Atlantic Ridge, 26°N. *J. Geophys. Res.,* 85:5438–5454.
Wooldridge, A.L., Haggerty, S.E., Rona, P.A., and Harrison, C.G.A., 1990. Magnetic properties and opaque mineralogy of rocks from selected seafloor hydrothermal sites at oceanic ridges. *J. Geophys. Res.,* 95:12351–12374.

Ms 153IR-103

NOTE: For all sites drilled, core-description forms ("barrel sheets"), and core photographs can be found in Section 3, beginning on page 277. Thin-section data are given in Section 4, beginning on page 665. The CD-ROM (back pocket, this volume) contains the complete set of spreadsheets with piece-by-piece data for all structural features identified and measured. A set of summary spreadsheets that are linked to the igneous and metamorphic spreadsheets are also contained on the CD-ROM. Keys, summary tables, checklists, and thin-section summaries and notes are also archived. Compressed versions of the figures created for this volume, compatible with Macintosh computers, are located in the directories labeled REPT92X in the "Structure" directory. Scanned TIFF images of all the SVCD drawings are archived in the "STRCDRAW" file. Apparent dip data and true strike and dip data for all measurable features are contained in the "STR_DIP" subdirectory. This directory also contains the LinesToPlane documentation and program that converts the apparent dip data to true strike and dip in an archived form. GRAPE, MST, and index properties are also reported on the CD-ROM.